batteries

MDPI

Review

Review on Advancements in Carbon Nanotubes: Synthesis, Purification, and Multifaceted Applications †

Anil Kumar Madikere Raghunatha Reddy [1], Ali Darwiche [2], Mogalahalli Venkatashamy Reddy [3] and Karim Zaghib [1,*]

[1] Department of Chemical and Materials Engineering, Concordia University, 1455 De Maisonneuve Blvd. West, Montreal, QC H3G 1M8, Canada; anil.mr@concordia.ca
[2] SOLiTHOR, Ondernemerslaan 5429, 3800 Sint-Truiden, Belgium
[3] Nouveau Monde Graphite (NMG), Saint-Michel-des-Saints, QC J0K 3B0, Canada; reddymvvr@gmail.com
* Correspondence: karim.zaghib@concordia.ca
† In memory of Christian Collette from Arkema France.

Abstract: Since their discovery over two decades ago, carbon nanotubes (CNTs) have captivated researchers due to their exceptional electrical, optical, mechanical, and thermal properties, making them versatile candidates for various advanced applications. CNTs have transformed numerous scientific domains, including nanotechnology, electronics, materials science, and biomedical engineering. Their applications range from nanoelectronics, robust nanocomposites, and energy storage devices to innovative materials, sensors, conducting polymers, field emission sources, and Li-ion batteries. Furthermore, CNTs have found critical roles in biosensing, water purification, bone scaffolding, and targeted gene and drug delivery. The chemical reactivity and functional versatility of CNTs are profoundly influenced by their structural and physicochemical properties, such as surface area, surface charge, size distribution, surface chemistry, and purity. This review comprehensively explores the current state of CNT research, focusing on widely used synthesis, purification, and characterization techniques alongside emerging applications. By highlighting recent advancements and addressing unresolved challenges, it aims to present a novel perspective on the transformative potential of CNTs, fostering innovation across diverse scientific and technological fields.

Keywords: carbon nanotubes; LIBs; synthesis; purification; diverse applications

check for updates

Academic Editor: Wei Lv

Received: 29 December 2024
Revised: 25 January 2025
Accepted: 27 January 2025
Published: 8 February 2025

Citation: Madikere Raghunatha Reddy, A.K.; Darwiche, A.; Reddy, M.V.; Zaghib, K. Review on Advancements in Carbon Nanotubes: Synthesis, Purification, and Multifaceted Applications. *Batteries* **2025**, *11*, 71. https://doi.org/10.3390/batteries11020071

Copyright: © 2025 by the authors. Licensee MDPI, Basel, Switzerland. This article is an open access article distributed under the terms and conditions of the Creative Commons Attribution (CC BY) license (https://creativecommons.org/licenses/by/4.0/).

1. Introduction

Remarkable scientific advances were achieved in the 20th century, the most fruitful hundred years for scientific research on material technology and nanotechnology. By its very nature, it is a multidisciplinary field involving a wide variety of biological, physical, and chemical techniques in the fabrication of different materials at the nanoscale. While nanotechnology itself is a well-established area of study, carbon nanotubes represent relatively new nanomaterials, their existence having been known for more than twenty years. The first identification of the crystal structure of graphite was made by Bernal in 1924, while the first report of the development of carbon fibers was by Radushkevich and Lukyanovich in 1952 [1]. The single or double-walled CNTs were then observed by Oberlin et al. in 1976 [2]. Iijima [3] was often credited with the discovery and confirmation of fullerenes before identifying multi-walled carbon nanotubes (MWCNTs) in 1991. For more details about the discovery of different forms of carbon, readers can consult the recent review on carbon nanotubes by Terrones [4].

Graphite, the most stable crystalline form of carbon, consists of layers of carbon atoms held together by weak Van der Waals forces, allowing the layers to slide over one another easily. Carbon nanotubes (CNTs) are derived from this structure and are classified based on the number of concentrically rolled-up graphene sheets into single-walled (SWCNT or SWNT), double-walled (DWCNT), and multi-walled CNTs (MWCNTs) [5]. These cylindrical nanostructures, which can be open-ended or closed-ended, are seamless cylinders formed from one or more graphene sheets and exhibit unique mechanical, electrical, and thermal properties, making them significant in various applications (Figure 1a–c).

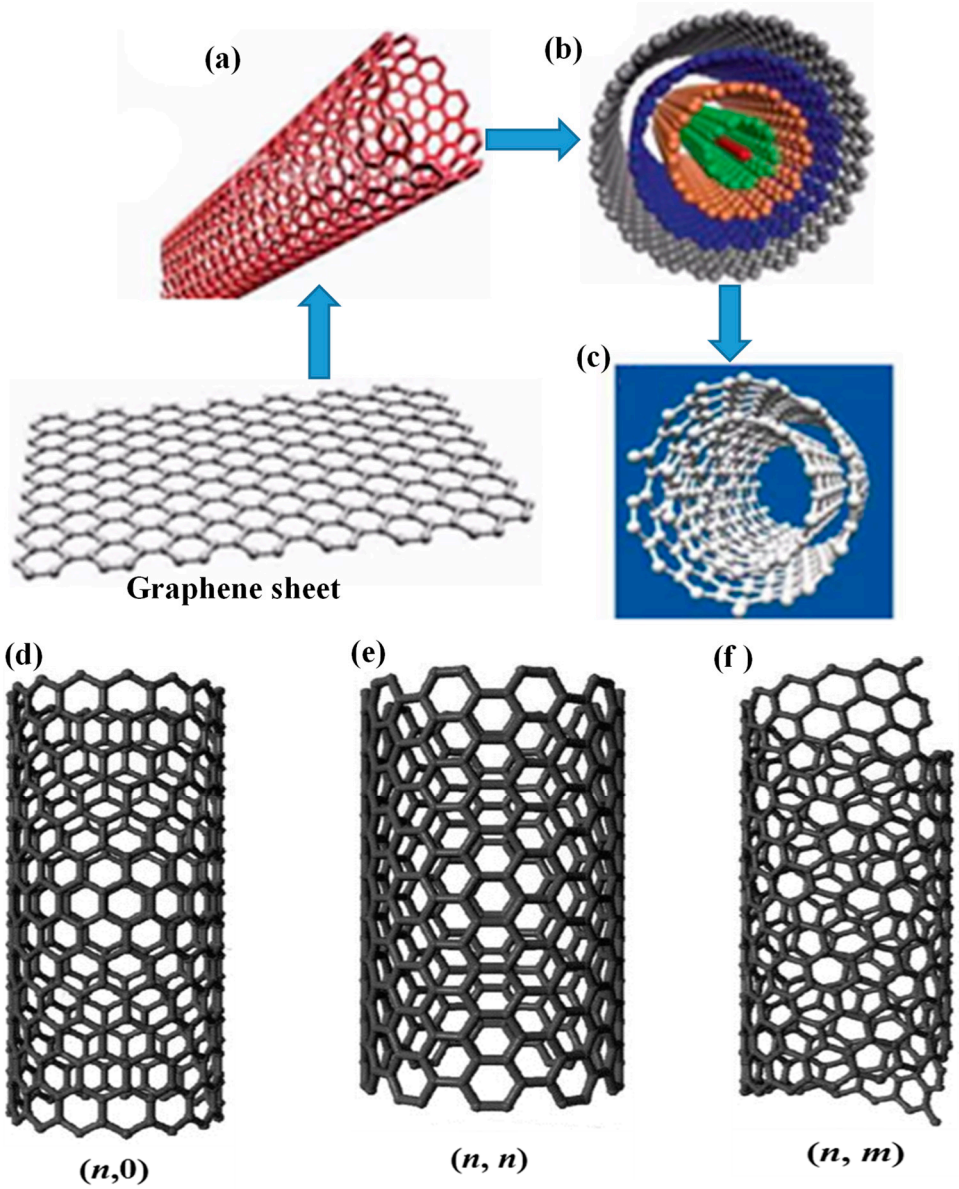

Figure 1. Wrapping of graphene sheet to form (**a**) SWCNTs, (**b**) DWCNTs, and (**c**) MWCNTs. Schematic illustrations of SWCNT structures, reproduced with permission [5]. (**d**) Zigzag arrangement, (**e**) armchair configuration, and (**f**) chiral conformation, reproduced with permission [4].

MWCNTs comprise several to tens of concentric cylinders with uniform periodic interlayer spacing around a hollow core. The inner diameter varies from 0.4 nm to a few nanometers, while the outer diameter generally falls from 2 nm up to 20–30 nm. In contrast, SWCNTs have diameters from about 0.4 to 2–3 nm and can reach lengths in the micrometer range. The robust Van der Waals interactions along SWCNT sidewalls lead to the formation of densely packed hexagonal bundles [6,7].

The properties of SWCNTs change with the orientation, or chirality, of the rolled graphene sheet, giving them either metallic or semiconducting characteristics. The chiral vector described by a pair of indices (n, m) characterizes the SWCNT's electrical, mechanical, optical, and other properties. SWCNTs have been classified into three forms: zigzag with m = 0, armchair with n = m, and chiral with n, m, as shown in Figure 1d–f. Zigzag and armchair types have high symmetry, but most SWCNTs are chiral and occur in two enantiomeric (mirror-image) forms. Each (n, m) configuration exhibits distinct optoelectronic properties due to quantum confinement, which stems from the properties dependent on chirality [8].

MWCNTs are composed of many graphene layers with variable chiralities; therefore, their electronic properties are difficult to predict. They come in two major structures: the Parchment and the Russian Doll models. In the case of the Russian Doll model, there is a nanotube inside another nanotube, and this one on the outside is easily larger in diameter than that inside it. In contrast, the Parchment model is formed by repeatedly rolling one graphene sheet like a paper scroll. Many characteristics of SWCNTs and MWCNTs are similar; the multilayer structure of the walls constitutes the principal difference between MWCNTs. The outer walls protect the inner nanotubes from external chemical interaction and provide superior tensile strength compared to SWCNTs [9]. With their unique properties and enormous potential applications in electronics such as transistors, memories, sensors, and displays; photonics; energy such as fuel cells, solar cells, supercapacitors, and Li-ion batteries; separation membranes; filtration; clothing; drug delivery; and biomedical applications, these nanomaterials have been the focus of much attention by material scientists and engineers [10–12].

In 2012, Liu et al. [13] reported that CNTs are superior in electrical, mechanical, and thermal properties compared to carbon-based materials. The sp^2 bonds between each carbon atom provide excellent tensile strength to the CNT, up to 1.2 TPa, much more significant than steel or Kevlar. These sp^2 bonds are even stronger than those of diamonds. They are also elastic; the elastic modulus (Young's modulus) for CNTs usually lies in the 50–200 GPa range, as determined in many TEM measurements [14]. Within a relatively short period, CNTs have become one of the hot topics in scientific research, with over 10,000 publications annually.

This review is structured as follows: Section 2 discusses the synthesis techniques of carbon nanotubes (CNTs), including methods such as chemical vapor deposition and arc discharge. Section 3 covers purification strategies and characterization techniques essential for achieving desired CNT properties. Section 4 highlights the emerging applications of CNTs across fields such as nanoelectronics, energy storage, and biomedical engineering. Section 5 delves into the challenges and opportunities associated with CNT research, offering insights into future directions. Finally, Section 5 provides concluding remarks summarizing the transformative potential of CNTs.

2. Synthesis

CNTs are synthesized by various techniques, most of which are based on gas-phase processes. The general methods widely used in CNT production include the following: (1) carbon arc discharge [3], (2) laser ablation, and (3) chemical vapor deposition (CVD) [15,16]. Liu et al. were the only group to explore the flame pyrolysis technique for mass-producing CNTs using simple equipment and conditions [17]. Other synthesis methods that have been reported in the literature include bottom–up organic routes [18–23], hydrothermal synthesis [24], electrolysis [25], and ball milling [26].

The synthesis methodology is essential since every application requires CNTs of a particular property and nature. Arc discharge and laser ablation require high temperatures

(>1700 °C). Yet, these have essentially given way to low-temperature CVD techniques at less than 800 °C due to the possibility of precise control over parameters such as length, diameter, orientation, purity, density, and alignment of CNT [27,28].

Purity remains one of the critical concerns in CNT synthesis. Due to the catalysts involved in the synthesis, many impurities are familiar, like nano-crystalline graphite, amorphous carbon, fullerenes, and the metals most often used are Fe, Co, Mo, or Ni. These impurities are detrimental to the properties of CNTs. Hence, developing efficient, easy, and inexpensive purification methods has been one of the leading research challenges in the last decade [29,30]. It should be noted that these purification methods can create defects in CNTs and thus affect their properties and further applications.

2.1. Arc Discharge

In 1991, Iijima successfully synthesized highly crystalline multi-walled carbon nanotubes (MWCNTs) using the arc discharge method [3]. This high-temperature technique is also widely employed for the mass production of fullerenes [31]. The process involves creating an arc between graphite cathode and anode electrodes within a vacuum chamber filled with an inert gas, such as helium or argon. These electrodes typically have an optical density (OD) of 6–10 mm and are spaced about 1 mm apart. A direct current of 80–100 A, driven by a voltage of approximately 20 V, generates a high-temperature arc discharge. The arc temperature exceeds 3000 °C, sufficient to vaporize carbon atoms into plasma [32–34]. During the process, a carbon deposit accumulates on the cathode (negative electrode) while the anode (positive electrode) is gradually consumed. This method was pivotal in the initial production and identification of carbon nanotubes (CNTs) [35]. A schematic of the arc discharge setup is shown in Figure 2a [36].

The large-scale production of high-quality carbon nanotubes primarily relies on precise control of several factors, including the uniformity of the plasma arc between the electrodes, the current density, the pressure of the inert gas, and the cooling mechanisms for both the electrodes and the chamber [37]. Two main approaches for synthesizing CNTs are (i) using various catalyst precursors and (ii) without catalyst precursors. Typically, MWCNTs are synthesized without catalyst precursors, while SWCNTs use a transition metal catalyst such as Fe, Co, Ni, Y, or Mo.

The synthesis of MWCNTs by an arc discharge method can be comparatively easy if the growth conditions are well controlled. Ebbesen and Ajayan [32] succeeded in the large-scale synthesis of MWCNTs in He gas, which is the best inert gas because of its high ionization potential [33,37]. DC arc discharge methods between graphite electrodes were also employed for synthesizing MWCNTs in many works with different atmospheres and carbon precursors [38–42]. For example, Parkansky et al. [43] and Tsai et al. [44] used pulse techniques for the synthesis of MWCNTs, which were deposited on Ni/glass substrates in ambient air, forming nanotube walls of 5 to 15 nm with lengths up to 3 μm.

The arc discharge technique was also applied to liquid solutions, including liquid N_2, deionized water, and aqueous solutions of various salts such as $NiSO_4$, $CoSO_4$, $FeSO_4$, H_3VO_4, and NaCl [45–49]. More recently, Belgacem et al. synthesized boron- and nitrogen-doped MWCNTs using the arc discharge technique [50]. The synthesis of DWCNTs is more complicated than that of MWCNTs or SWCNTs, although several successful attempts have been reported [51–55]. In 2001, Hutchison et al. [51] first synthesized DWCNTs using a mixture of argon and hydrogen in the arc discharge method.

Metal catalysts are indispensable for synthesizing SWCNTs. Several metal catalysts have been attempted, including Fe, Co, Ni, and mixtures of these metals with other metals like Pt, Ru, and Cu [5,9,36,56–62]. In 1993, Iijima and Ichihashi [5] first reported the production of SWCNTs using Fe-graphite electrodes in a methane–argon atmosphere. Other

studies, as conducted by IBM researchers [56], have obtained high yields of SWCNTs using mixtures of Fe-Co-Ni-graphite in a helium atmosphere. Mixtures such as Ni-Y-graphite have, for instance, become standard for producing SWCNTs of an average diameter of about 1.4 nm [63]. Other high-purity techniques developed to produce SWCNT include the FH arc discharge method, where hydrogen DC arc discharge evaporates carbon anodes containing 1% Fe catalyst in an H_2-Ar mixture [64,65]. An interesting study was carried out on the influence of Mo on yield and the quality of SWCNTs in both Ni/Y-He and Fe-Ar/H_2 systems by Wang et al. [66]; a remarkable increase in the soot yield was noticed in the presence of Mo. However, improvement in the purity of SWCNTs was realized only in the Fe/Mo-Ar/H_2 system and not in the Ni/Y/Mo-He system. Li et al. [67] prepared SWCNTs, 1.5–2 nm in diameter and several micrometers long, by pulsed-arc discharge in air. Maria and Mieno [68] prepared SWCNTs of better quality by bipolar pulsed arc discharge than the standard DC arc discharge method. This suggests that even better quality SWCNTs may be prepared by further optimization of the pulsed arc technique. Overall, the production efficiency of SWCNTs via arc discharge can be significantly improved by fine-tuning various factors such as the optical plasma conditions, inert gas type, and catalyst used during the synthesis process.

In the arc discharge technique of CNTs synthesis, several process parameters are vital in determining the size and purities of the CNTs. According to Arora et al. [36], critical parameters include chamber temperature, promoter addition, composition of catalysts, concentration, grain size, type of atmosphere, chamber pressure, electrode design, power supply type, and the nature of the carbon precursor [36]. Nevertheless, one of the most significant advantages this method presents is the ability to produce CNTs in large sizes. Compared to the other CNT production methods, the high temperature involved in the arc discharge gives the product crystallinity, yielding a high quality and quantity [47]. On the downside, only limited control over the chiral vector of the nanotubes is allowed by the arc discharge method, a factor very influential on their physical properties and hence ultimately their applications. This requirement for high-purity graphite electrodes, metal powders, and inert gases like helium and argon adds to the cost of both SWCNTs and MWCNTs. SWCNTs are more costly due to the utilization of metallic catalysts, adding an extra requirement in their synthesis for a purification step. Although many purification methods have been developed, the overall costs remain high in the large-scale industrial production of CNTs.

2.2. Laser Ablation Method

Laser ablation was first applied by Kroto et al. [69] to synthesize fullerenes. Later, the same method was extended by Guo et al. [70] in 1995 to produce CNTs by introducing a metal catalyst inside the carbon target. High-power laser vaporization combined with high-temperature furnaces (commonly of the YAG type) constitutes another synthesis route for SWCNTs and MWCNTs. For instance, the laser vaporization of pure graphite block sealed in a quartz tube heated up to 1200 °C in an Argon atmosphere yields MWCNTs [71]. The schematic diagram of the laser ablation setup is shown in Figure 2b. This temperature is remarkably lower than the arc discharge method [72,73].

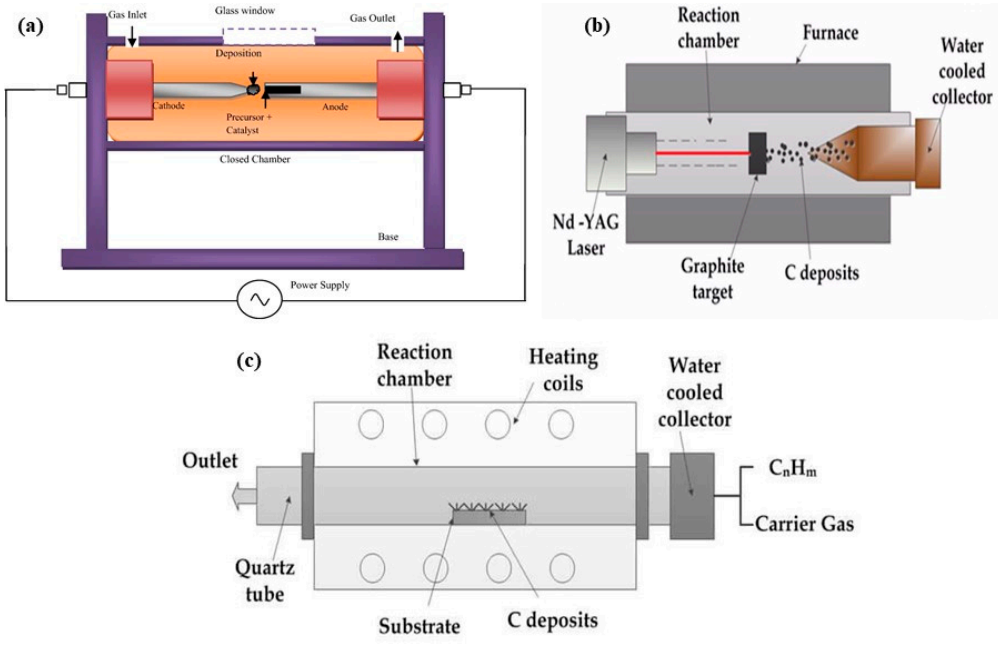

Figure 2. (**a**) An arc discharge setup. Adopted with permission from [36]. Copyright © 2014 Elsevier. (**b**) A laser ablation setup. Adopted with permission from [74]. (**c**) Chemical vapor deposition method. Adopted with permission from [74].

Various parameters affecting the quantity and quality of CNTs by laser ablation are target material, characteristics of the laser including peak power, beam energy, wavelength of oscillation, continuous-wave/pulsed nature, repetition rate, substrate material, ambient temperature, chamber pressure, chemical composition, buffer gas flow, and buffer gas pressure along with target substrate distance conditions [75,76]. On the other hand, just like in the arc-discharge method, SWCNT growth demands metal catalysts to promote their development. Smalley et al. [70] showed that the basic principles of the laser ablation process are essentially identical to the arc-discharge method, except that its energy is supplied through the action of a laser beam impinging on a graphite target containing catalyst materials, which are usually in the form of either cobalt or nickel. Further studies showed that the diameter of the CNTs decreases with laser power increase [77,78]. The use of ultrafast laser pulses or bimetallic graphite containing Ni/Y catalysts Ni > Y or Ni/Co in equal atomic ratio yields a higher amount (up to 1.5 g/h) of SWCNTs [75]. Lasers generally used in this process are Nd: YAG [79] and CO_2 lasers [80,81]. However, other groups have successfully produced SWCNTs using UV lasers, for instance, KrF excimer [73], XeCl excimer lasers [72], or Tm: Ho: LuLF lasers [82]. The laser ablation technique has been used to produce high-quality SWCNTs with controlled diameters. Among other factors, diameter variations could be changed by oven temperature, catalytic metals, and gas flow rate. The yields of SWCNTs by this technique are very high with relatively low impurities because the metallic atoms from the catalyst tend to evaporate from the closed end of the nanotube. A major problem with laser ablation is that many-branched nanotubes are generated along with straight CNTs.

As for the commercial aspects, large-scale production of CNTs by laser ablation has not yet been commercialized because of the use of high-purity graphite rods, high-power lasers, and the nanotube production rate per day which is still lower than that obtained by using the arc-discharge technique. Although both methods can result in a relatively high yield of CNTs of high quality, each method faces some specific problems: (1) both methods require a high-temperature and vacuum condition, the scaling up of which is highly costly; (2) there are some purification and separation processes to clean the by-products and impurities

within the CNT; and (3) these processes are highly costly relative to the overall production cost because the graphite electrodes and targets must be replaced all the time during the synthesis process, hence limiting the continuous production of CNTs [83].

2.3. Chemical Vapor Deposition (CVD)

Chemical vapor deposition (CVD) is predominantly used for large-scale carbon nanotube (CNT) production among the various synthesis methods. This is mainly due to its ability to utilize fluidized bed reactors, which ensure uniform gas diffusion and efficient heat transfer to the metal catalyst nanoparticles [84–86]. The technique is quite versatile as it can be used to synthesize millimeter-long aligned CNT forests among various other kinds of CNT structures [86]; aside from that, the technique also synthesizes other types of CNT-related materials such as nanohorns and nanocoils [87]. Among various techniques, CVD is preferred owing to its simplicity, low cost, and scalability for commercial applications [76,88]. There are several reports on various types of CVD techniques in the literature, each being fitted for multiple applications, including plasma-enhanced oxygen-assisted CVD (PECVD) [3], water-assisted CVD [59,89–91], microwave plasma CVD (MPECVD) [32], radio-frequency CVD (RF-CVD) [16], hot-filament CVD (HFCVD) [92,93], as well as fixed-bed reactors [45], fluidized bed reactors [45], laser-assisted CVD [45], aerosol-assisted CVD [45], floating catalyst techniques [45], and catalytic/thermal chemical vapor deposition CCVD [9]. CCVD is one of the most popular techniques for synthesizing CNTs, wherein hydrocarbon vapors undergo thermal decomposition in the presence of metal catalysts. In this technique, the hydrocarbon vapor is passed through a tube furnace at an elevated temperature of 600–1200 °C for 15–60 min with the help of the catalyst, which prompts the decomposition of hydrocarbons, as depicted in Figure 2c.

Generally, various factors that commonly affect CVD synthesis include carbon feedstock type, catalyst, carrier gas, flow rate, pressure, growth time, temperature, reactor geometry, substrates, and consumption of power [88,94]. Different carbon feedstock materials have been tried with CNT synthesis during the last two decades. The tested feedstock materials include all petroleum-based hydrocarbons like methane, ethylene, naphthalene, and acetylene, whereas the liquid carbon feedstock sources include alcohols, benzene, xylene, toluene, and cyclohexane. Research groups have tried different feedstocks in the last 20 years to optimize the synthesis process [95]. Several groups also tested other carbon feedstocks (e.g., polymers, carbon monoxide). In addition, renewable and eco-friendly botanical materials such as camphor, oiled petroleum wastes (de-oiled asphalt, eucalyptus oil, and turpentine oil), bamboo charcoal, waste rice husk, vulcanized scrap rubber, wood sawdust [96] and rice straw, vegetable oils including coconut [97], neem, and palm oil were used as carbon sources in CNTs production [95]. The metal nanoparticle catalysts used include Fe, Ni, Co, Mo, Pt, and Pd [98,99] and their combinations [100], which are usually various on different substrates like SiO_2, MgO, Al_2O_3 [85,100] $CaCO_3$ [101]. However, some recent research involved the use of a non-metallic catalyst because the purification process is easier than conventional metal catalysts. The first non-metallic synthesis was reported in 1997 by Kusunoki et al. [102], which involved the decomposition of SiC. Another ceramic of interest is porous alumina, where no metallic catalyst was used in CNT synthesis [103–105]. The carrier gases are often nitrogen, hydrogen, or ammonia. Carbon filaments grown by the pyrolysis of hydrocarbons with metal catalysts have been under intense debate for several years. Recently, three main mechanisms have gained wide recognition in the scientific community:

1. Carbon diffusion from the top through catalytic particles [106,107];
2. Carbon diffusion from the top on catalytic particles [2,108];
3. Carbon diffusion from the bottom through catalytic particles [2,107,109].

Another critical process parameter is the size of the metallic catalyst particles since it greatly influences the final diameter of both MWCNTs and SWCNTs. When the catalyst particles are a few nanometers in size, the usual result is SWCNTs, while larger particles of the order of tens of nanometers result in MWCNTs [110]. The other crucial parameter is temperature, which changes the root of the CNTs in terms of diameter, length, and alignment. The temperature increase also raises the diameter of the CNTs [111,112]. Usually, the SWCNT synthesis occurs at a high temperature in the 900 to 1200 °C range, whereas most of the MWCNTs are produced in a relatively low-temperature range of 650 to 900 °C. This temperature range reflects that SWCNTs have higher formation energy than MWCNTs due to their smaller diameters and thus higher strain energy and curvature. Consequently, MWCNTs more readily grow from a broader range of hydrocarbons, whereas only hydrocarbons that can retain stability at higher temperatures of 900–1200 °C—like CO and CH_4—are suitable for producing SWCNTs.

Among the standard methods for synthesizing carbon nanotubes (CNTs), chemical vapor deposition (CVD) is the most extensively studied and widely used for large-scale production. It offers higher yields and a simpler setup than arc discharge and laser ablation techniques. This technique is also suitable for preparing longer nanotubes, which are desirable for composite fibers. The main advantage of CVD is its ability to synthesize aligned CNT arrays in controlled diameter and length. The growth of nanotubes in CVD is in parallel alignment with each other. The growth direction of carbon nanotubes (CNTs) is typically perpendicular to the substrate surface and guided by catalyst–surface interactions and Van der Waals forces between the tubes. However, large-scale chemical vapor deposition (CVD) methods often introduce contaminants, which can significantly impact the properties of the CNTs. Such impurities are typically removed through time-consuming and expensive heat annealing or chemical treatment. For instance, metallic residuals within CNTs used in lithium-ion composite high-voltage cathodes degrade the capacity and active material cycling stability [113,114].

The CNTs synthesized by CVD are typically MWCNTs and generally more defective. Hence, their tensile strength is roughly an order of magnitude lower than that obtained using the arc discharge method [113,114]. Current commercial CNT synthesis is mainly obtained using CVD, with various techniques as discussed in the Yan et al. review [45,115], including (1) Multi-wall carbon nanotube production by the Hyperion Company; (2) The Endo process at Shinshu University; (3) The "CoMoCAT Process" from SWeNT at the University of Oklahoma; (4) The "HiPCo Process" at Rice University; (5) The "Nano Agglomerate Fluidized" process by Tsinghua University; (6) The "Baytube" process by Bayer Company; (7) Methods on super growth of SWCNT arrays; (8) Graphistrength® multi-walled carbon by Arkema; (9) Super-aligned CNTs for yarn preparation.

2.4. Other Methods

This section discusses non-standard techniques for synthesizing CNTs. Different research groups proposed liquid pyrolysis, a bottom–up organic approach, electrolysis, low-temperature solid pyrolysis, or using solar energy to produce CNTs with well-defined properties. Liquid pyrolysis, also sometimes called flame pyrolysis, was first proposed for mass production of CNTs using this new technique by Lui et al. [116–118]. The equipment used in this process is very simple, and the conditions involved in the synthesis are not very complex. This process produced CNTs with high yields with fewer impurities. The diameters of the nanotubes were between 10 and 20 nm, while their lengths reached up to several microns. Carbon monoxide was the carbon source, while heat was supplied through the combustion of an acetylene/air-premixed gas mixture. Penta-carbonyl was

used as the catalyst, and hydrogen and helium-premixed gas were used as the protective gases. The effect of these chemicals on the growth of CNTs was also studied.

The bottom–up organic approach was reported for the first time by Li et al. [119]. This process produced homogeneous CNTs with definite structures. The technique is based on the template use of carbon macrocycles such as -cycloparapheylene or -cyclacene, thus allowing controlled chirality. For instance, a (5, 5) armchair CNT was obtained by bridging libraries to -cycloparaphenylene, while a (10, 10) zigzag CNT was obtained from 10-cyclacene. Indeed, other groups have also successfully yielded CNTs with selective chiralities using similar techniques, including different hoop-shaped carbon macrocycles: and cycloparaphenylenes and cyclo - paraphenylene 2, 6 naphthylene -19]. Recently, Liu et al. [120] further advanced the synthesis of SWCNTs with chirality defined by this bottom–up approach.

It Is based on the electrolysis method using graphite electrodes immersed in molten LiCl under argon with an applied voltage between the two electrodes. The technique was introduced by Hsu et al. in 1995 [121,122] and can yield MWCNTs. Under proper experimental conditions, 20–40% of the carbon material formed is CNTs. Salts such as KCl, NaCl, and LiBr were tried, and all showed the formation of CNTs. The molten salt's nature and the electrolyte's temperature strongly influence the formation of CNTs [123]. Despite its relatively inexpensive process, some limitations include the inability to adequately control the nanotube yield, diameter, and length and the difficulty of producing SWCNTs.

Whatever the synthesis method followed, temperature remains one of the significant critical variables affecting the production of CNTs. Laplaze et al. [124] first proposed a method to synthesize CNTs using solar energy. Concentrating solar radiation in a flux of 500 W/cm^2 on a graphite–metal target in an inert atmosphere led to a vaporization temperature of ca. 2800 K [125]. After a few years, they developed a more powerful solar furnace, reaching temperatures of ca. 3400 K and largely improving the yield of CNTs [126,127]. In another publication, they reported on synthesizing fullerenes and nanotubes with a yield as high as 2 g/h [128]. Other groups have also used solar energy for the pyrolytic synthesis of MWCNTs [129]. Although relatively cheap and available everywhere, solar energy has seldom been utilized commercially for the synthesis of CNTs due to the sensitivity of the process to pressure, carrier gas, carbon/metal ratio, slow production rates, and the fact that the obtained nanotubes have random lengths [130].

Meng et al. [131] employed low-temperature solid pyrolysis in a simple, effective, and high-yield process to produce oriented CNTs with MOFs at temperatures as low as 430 °C. Within this process, MOF (ZIF-67) crystals served as a single precursor to provide both the catalyst and carbon source for CNTs. By changing the corresponding MOFs, they established various oriented CNT-assembled structures through this approach. The formed CNTs were homogeneously doped with heteroatoms like nitrogen; the formed architectures possessed a large specific surface area, optimal pore size distribution, effective doping, interior voids, and robust frameworks. The consequences of these properties are high electrochemical activity, fast mass transport, and excellent strain accommodation.

3. Carbon Nanotube Purification

Generally, purification is defined as obtaining one desired product from a mixture. In the case of CNTs, it is a process of separation of nanotubes from other by-products, considering impurities such as carbon nanoparticles, amorphous carbon, residual catalysts, and other undesirable products that result from the synthesis process. The pure attainment of CNTs involves different purification techniques depending on the intended applications of the CNTs. Some of the most common purification methods include (a) physical, (b) chemical, and (c) physical–chemical.

The physical purification methods involve filtration, centrifugation, and high-temperature annealing. All these depend on the differences in properties such as magnetism, solution gravity, aspect ratio, and physical size to separate CNTs from contaminants. Physical methods have certain advantages in that they are quite effective for removing impure graphitic sheets from CNTs, so that, without using chemicals, the integrity of the original CNTs is preserved. However, most techniques are comparatively inefficient since time-consuming and complicated procedures are typically required.

The chemical methods are mainly oxidation processes that concern the removal of impurities, including gas-phase oxidation, liquid-phase oxidation, and electrochemical oxidation. These methods take hold by oxidizing carbon-based impurities and dissolving metal catalysts into acids. Compared with physical methods, these chemical methods are more efficient but have disadvantages in that they always introduce some degree of structure compromise by creating defects in the CNTs. Because of this, a hybrid approach has often been used that embodies both physical and chemical methods. This combined treatment enhanced the purification yield and quality of the CNTs by preserving their essential morphology and structure while attaining the desired level of purity.

Other purification techniques reported include microfiltration and chromatography for size separation and removal of amorphous carbon clusters [132]. However, optimizing the purification parameters of CNT samples has not yet been fully comprehended.

3.1. Oxidation Method

High purification of CNTs is possible by oxidative treatment in the liquid or gas phases. MWCNTs are one of the most oxidation-resistant carbon forms and thus exhibit thermal stability: thermogravimetric investigations confirm that the weight loss starts noticeably only at about 700 °C, much higher than for C_{60} and amorphous carbon. Ebbesen et al. [133] were among the first to report a successful procedure for purifying arc-discharge-produced CNTs. It is based on breaking MWCNTs into polyhedral, graphite-like particles; however, the process has several drawbacks, such as only a moderate purity achieved, more than 95% of the starting soot consumed, and the fact that nanotubes are highly reactive due to the formation of dangling bonds (unsatisfied valence) that require neutralization at high-temperature annealing at ~2800 °C [133,134].

The liquid-phase oxidative treatments generally involve the use of such oxidizing agents as boiling concentrated nitric and sulfuric acids, mixtures of hydrogen peroxide and sulfuric acid (piranha solution), gaseous oxygen, ozone, and potassium permanganate [135]. However, this method destroys the CNT structure [136], creating carboxylic acid and oxygen-containing groups at the ends and defect sites of the SWCNT framework [137–140]. These functional groups encourage CNT bundle exfoliation, which could seriously affect the interfacial adhesion of CNTs when used as reinforcement in composite materials [141].

3.2. Microwave Heating

Park et al. [142] used microwave heating under an air atmosphere to purify SWCNTs synthesized by arc discharge. In this technique, microwaves interact with residual metal catalysts and rapidly elevate their local temperature. This leads to the oxidation and breakdown of carbon layers surrounding the catalyst particles. A mild acid wash with 4M HCl is carried out for 1–2 h to remove the metal catalyst after treatment in a microwave. This method inflicts only minimal damage on the SWCNTs compared to the other purification methods [142,143]. Microwave-assisted purification also reduces the processing time by about one hour from several hours with conventional methods [144].

3.3. Filtration and Chromatography

Filtration-based separation exploits the physical size, aspect ratio, and solubility differences among SWCNTs, metal particles, and polyaromatic carbons. The nanotubes and particles are rendered as colloidal suspensions in water with surface-active agents like surfactants, polymers, or other colloidal particles to avoid CNT agglomeration or aggregation. This technique generally does not affect the SWCNT structure, with minimal sample loss or damage and no apparent chemical change upon purification [142]. Nevertheless, several filtration steps are usually necessary for high purification, and the method may not effectively produce the number of nanotubes required [145]. Bandow et al. [146] demonstrated the single-step purification of SWCNTs using microfiltration in an aqueous solution that contained a cationic surfactant: benzalkonium chloride. SEC with porous filters was employed by Brown et al. [147] to separate SWCNTs from amorphous carbon and catalyst particles along with ultrasonic-assisted microfiltration [148]. Huang et al. [149] separated the semiconducting and metallic SWCNTs using SEC. Other workers have separated SWCNTs based on particle diameter by employing techniques such as density-gradient ultracentrifugation [150]. Other techniques include gel permeation chromatography (GPC) and high-performance liquid chromatography combined with SEC (HPLC-SEC) [15].

3.4. Other Purification Methods

Ago et al. [151] first applied an oxygen plasma treatment for MWCNT purification identically to HOPG, taking 400 W for 15 min. This treatment seriously damaged the MWCNTs, significantly giving them rough surfaces and changing their electronic structure. Felten et al. [152,153] functionalized MWCNTs by treating them in an oxygen plasma and studied changes in their electronic properties.

Acid reflux represents one of the most popular methods for eliminating impurities from CNTs. However, it often creates functional groups like -COOH and -OH on sidewalls and at the tips of the CNT. Various changes in acid type, concentration, duration, and temperature when purifying CNTs have been performed by different researchers [2,5,69,154–160]. Another approach to purify CNTs is to rely on a washing treatment with strong acid combined with sonication at room temperature. Such a procedure also effectively separates CNTs from amorphous carbon and metal catalysts [161].

Despite this, no single technique has yet been developed to provide good-quality and low-cost CNTs on an industrial scale. Most methods include problems concerning reproducibility, eco-friendliness, and poor scalability. Single-step purification methods that do not degrade the intrinsic properties of CNTs are therefore desirable because these help produce “clean” nanotubes, reducing market costs. Other challenges in CNT purification include [162] the following:

- Elaboration of large-scale purification techniques, which result in CNTs having selected diameter, chirality, or thickness.
- Retaining conductivity of CNTs because most of the chemical purification methods result in the oxidation of the CNT frame.
- Development of value-added, purified CNT-based technologies.
- Scaling-up process to obtain uniform CNTs.
- Characterization techniques must be newly developed to assess CNTs uniformly.
- Standardized procedures should be developed to describe purity, impurity content, defects, etc.

Well-defined chemical and physical properties must be used to evaluate CNTs for commercial or standardized uses. High-resolution transmission electron microscopy (HRTEM) plays a crucial role in determining various physical properties, including the length, diame-

ter, and structure of both multi-walled carbon nanotubes (MWCNTs) and single-walled carbon nanotubes (SWCNTs). It can also disclose other features such as tube openings, orientation, defects, connectivity, and impurities. Other main techniques include SEM, which gives a general overview of the morphology of CNT powder and its structure. At the same time, STM and AFM are used to correlate structural defects with electronic properties [163–166]. These techniques allow for the identification of chiralities by measuring angles between hexagonal patterns and tube axes. Other methods used in CNT characterization include band-gap fluorescence, near-IR fluorescence spectroscopy, Raman and micro-Raman spectroscopy, and X-ray diffraction. Novel techniques have also been proposed for the characterization of CNTs, such as near-field optical microscopy, nanoscale optical imaging, and phonon spectroscopy.

4. Applications

CNTs offer remarkable advantages, including high surface area, unique hollow structure, hydrophobicity, optical properties, catalytic activity, ease of surface modification, exceptional electronic conductivity, substantial mechanical strength, and excellent thermal conductivity. These make them valuable in diverse fields such as electronics, medicine, energy storage, construction, manufacturing, and nanotechnology. In the next section, we explore some of these applications, focusing on their role in lithium-ion batteries.

4.1. Biomedical Applications

Since a big part of the human body is composed of carbon, CNTs are generally treated as one primary biocompatible material. The unique photosensitive, mechanical, optical, and electrical properties have drawn many researchers' attention in nanomedicine and nanotechnology [45]. However, for biomedical applications, CNTs should overcome three barriers: functionalization, pharmacology (dispersion, solubility), and toxicity. Kumar et al. [45] reviewed many of the desirable properties of CNTs that led to the expansion of their use in the medical field. They compared each CNT property and the corresponding biomedical application [45,167,168].

4.1.1. CNTs as Biosensors

Applications involving biosensors and medical devices comprising CNTs are of great interest due to their potential compatibility with other biological entities such as DNA and proteins [169–174]. The benefits and advantages yet to be realized in healthcare, environmental surveillance, food safety, and even military uses have consequently geared up several thrusts in research and development [175,176]. This indeed facilitates fast electron transfer, enhancing the sensitivity of transducers, hence making CNTs useful in the detection of viral diseases [177] while at the same time allowing for rapid identification of the pathogens affecting both humans and animals [178]. According to the type of analyte, CNT-based biosensors encompass enzyme biosensors (glucose [179,180], fructose [181]), targeting glucose, fructose, neurotransmitters [45,182–187], amino acids, insulin, cancer biomarkers [188–193], DNA [194–196], gene biosensors, and immunosensors. The approach for the quantification and optimization of selectivity and sensitivity of neurotransmitter sensors is described as follows: Candidate sensors are synthesized from single-walled carbon nanotubes and DNA oligonucleotides, and their responses toward neurotransmitters like dopamine, epinephrine, and norepinephrine are quantified. Central to the performance of these sensors is the ability to distinguish between various yet chemically very similar neurotransmitters [184]. In this work, a set of different DNA-oligonucleotides is tested as an organic phase, and corresponding sensor properties, such as Kd-values, are evaluated to find the most selective and robust sensors, as shown in Figure 3.

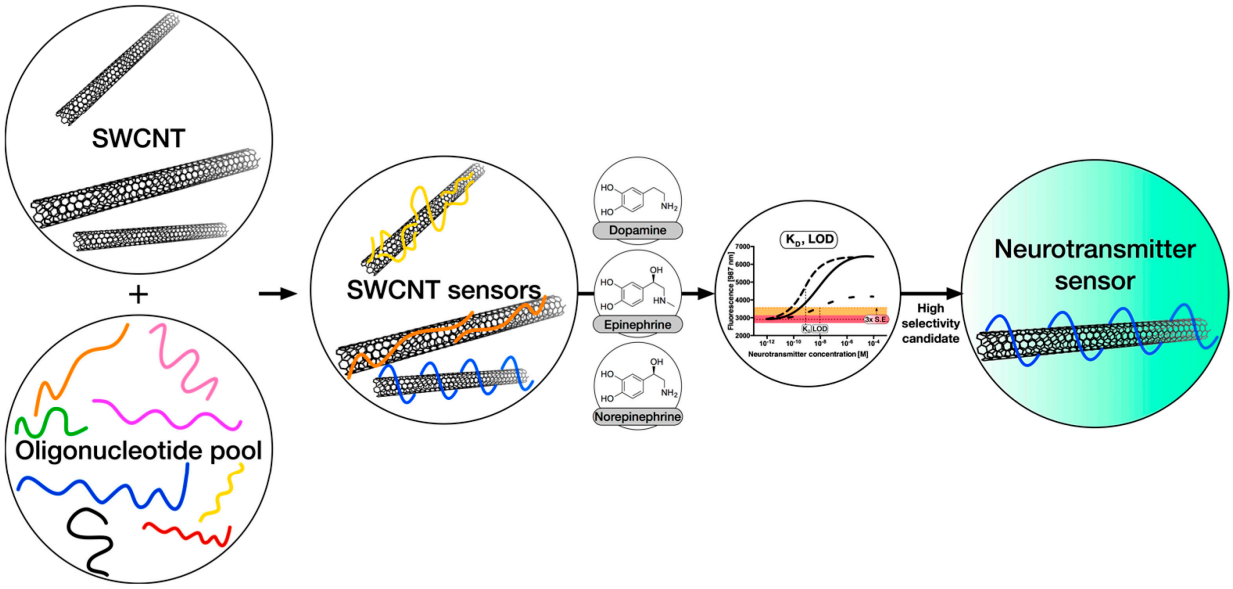

Figure 3. Strategy to measure and optimize selectivity and sensitivity of neurotransmitter sensors. Candidate sensors are synthesized from single-walled carbon nanotubes (SWCNTs) and DNA oligonucleotides, and their responses to neurotransmitters such as dopamine, epinephrine, and norepinephrine are quantified. Crucial for the success of these sensors is the discrimination between different but chemically very similar neurotransmitters, Adopted with permission from [184].

CNT-based biosensors hold immense promise for cancer therapy, detection, and diagnosis. Cancer originates due to abnormal and uncontrolled cell division, which results in the impairment of organs, leading to death. Each cancer cell expresses distinctive CBAs, which are distinctive of a particular cancer type. Several biomarkers are overexpressed, usually in cancer cells, and can indicate various diseases [45]. These biomarkers contain helpful information for early diagnosis, prognosis, postsurgical monitoring, advanced disease therapy assessment, and treatment response prediction. Biomarkers such as prostate-specific antigen (PSA), carcinoembryonic antigen (CEA), carcinoma antigen 125 (CA125), human chorionic gonadotropin, and alpha-fetoprotein (AFP) can be detected by CNT-based systems [16,45,191,192].

4.1.2. CNTs as Probes

Many researchers have explored CNTs as probes in understanding unknown regions or cavities and hence have been used in different manners in nanosensors such as pulse, temperature, blood glucose, and disease diagnosis [110,197–199]. High-resolution structural imaging [200–202], nano-lithography, field emission, and nanoelectrodes are other areas where probes based on CNTs are used since they exhibit better conductivity. Notably, CNTs represent ideal materials for AFM probes [202,203] because of their mechanical strength, flexibility, and low buckling force. Compared to conventional silicon or silicon nitride probes, the resolution is higher because their cylindrical shape and narrow tube diameter allow imaging within confined, deep cavities–for example, visualizing protein filaments [204]. Wong et al. [205] demonstrated, for the first time, high-resolution imaging of amyloid-β protofibrils using SWCNTs and MWCNTs. MWCNT scanning probe tips are commercially available from Seiko Instruments (Chiba, Japan) and Daiken Chemical Company (Decatur, AL, USA).

4.1.3. CNTs as Carriers for Drugs, Genes, Proteins, or Peptides

The ideal target of drug delivery systems is transporting therapeutic molecules directly to tumor sites, with minimal effects on healthy cells. Functionalized CNTs are currently being

developed as tumor-targeting vectors of drugs. Researchers have tested various systems to overcome problems regarding selectivity, toxicity, solubility, cell distribution, and cellular barrier permeation. Some platforms now under evaluation for drug delivery include polymers, quantum dots, emulsions, liposomes, micelles, molecular conjugates, dendrimers, and silica nanoparticles [206]. CNTs are highly suitable for drug loading and delivery due to their large surface area-to-volume ratio and hollow structure [16,167,168,207,208], where drugs penetrate cell nuclei without hindrance. The hydrophobic nature of CNTs also offers a stable vehicle for transducing biomolecules such as DNA, RNA, and proteins across cellular membranes [16,45,167,168]. One of the first approaches that demonstrated genetic material delivery was shown by Lu et al., in which RNA polymer poly(rU) was absorbed into SWCNTs through nonspecific interactions [209]. Genetic material could pass through both cellular and nuclear membranes in MCF7 breast cancer cells.

The use of CNTs for anti-cancer drug delivery has dramatically increased, and most studies have concerned functionalized SWCNT and MWCNT as drug nanocarriers. Kumar et al. [45] summarized these functionalized CNTs for anti-cancer drug delivery. They underlined that all these nanovesicles can cross cell membranes without developing cellular defense mechanisms owing to their nanoscale dimensions [167,168,210–213].

4.1.4. Other Applications in the Biomedical Field

Single- and multi-walled CNTs are being researched as implant material, such as artificial joints, due to their minimal possibility of rejection by the host. Proteins and amino acids are attached to CNTs further to minimize rejection. With their outstanding tensile strength, the CNTs may be used as replacements for bones by filling them with calcium and structuring them in a form to mimic the growth of the bone [214]. In tissue engineering, CNTs represent the link between biological sciences and material sciences. There are four significant fields of application: for the monitoring of cellular behavior; as tissue matrix enhancers; cell tracking and labeling; and inducing cellular behavior [168,215]. CNTs were shown to enhance cell adhesion, proliferation, and differentiation [216,217], and mixtures of SWCNTs with collagen were advantageous in muscle cell growth [218–222].

They are also excellent for separating biomolecules such as DNA and proteins due to its selective protein adsorption properties [223,224]. The high antimicrobial activity of CNTs was revealed by Kang et al. [225] for the first time, in which it was also stated that functionalization enhances this effect while reducing the toxicity against mammalian cells [226]. Moreover, individual SWCNTs are more toxic against bacteria than agglomerated CNTs [227]. Recently, Kumar et al. [45] reviewed the advances in CNT-based antimicrobial strategies so far developed for the treatment of diseases, including

- In vivo cancer treatment by drug therapy [228,229];
- Photoacoustic therapy, which selectively destroys cancer cells [230,231];
- Photothermal therapy wherein the NIR light absorption induces heat that can ablate the cancerous cells [232,233];
- Photodynamic therapy [234].

The primary factor that affects the applications of CNTs is their long-term toxicity. The safety of nanomaterials in any medical applications is an important consideration and the very small size of the CNTs (1–100 nm) raises health concerns. Toxicity from CNTs has been widely tested both in vitro and in vivo; however, studies provide inconclusive and sometimes conflicting results. As reviewed, several parameters are usually mentioned to affect cytotoxicity: CNT size, target organ exposure, CNT type and functionalization, product purity, degree of dispersion, surfactant type and concentration, cell culture conditions, type of cells, and interaction time [235–237]. The lungs, skin, and heart are possible target organs for CNT exposure. If CNTs evade phagocytic defenses, they may cause

structure–activity changes to proteins, create inflammatory reactions, and potentially be redistributed internally [168,238]. Kolosnjaj et al. [239] even considered whether CNTs themselves are directly carcinogenic or act simply as vectors for harmful pollutants such as polycyclic aromatic hydrocarbons, a subject on which debate continues. In all this research, the toxicological risks of CNTs are weighed against their benefits.

Recent works investigated the biodegradability of CNT: Chen et al. reported on microbial and enzymatic breakdown of carbon nanomaterials, which summarized general studies in this respect [240]. It was concluded that living organisms can reduce the toxicity of CNT and enhance their environmental removal. For instance, degradation of MWCNTs to CO_2 and several intermediates like 2-methoxy naphthalene, 2-naphthol, cinnamaldehyde, and isophthalic acid was possible by bacteria like Burkholderia kururiensis, Delftia acidovorans, and Stenotrophomonas maltophilia. These bacteria are common in soil, surface water, and groundwater environments [241]. There are reports of CNT degradation by MnP from *P. chrysosporium*, too [242].

4.2. Water and Air Filtration

Safe and clean water availability is decreasing and may further deteriorate in the following decades. This shortage is closely related to global food and health security, economic growth, social development, and political stability [243]. To address this problem, different water purification methods have been used or are in use [244]. CNT-based technologies are recognized for their singular combination of properties, including high surface area and aspect ratio, chemical reactivity, low cost, and environmental benignity [245]. In such systems, the CNTs are commonly packed closely enough to allow water to pass through while rejecting bacteria, biological materials, and other contaminants due to their nanoscale dimensions.

Some of the CNT-based approaches to water purification attempt at the removal of three major classes of pollutants, namely organic, inorganic, and biological [246,247]:

- Adsorption: Surface forces act to adsorb pollutants onto the sheets of CNTs.
- Hybrid Catalysis:
    - Photocatalysis: Photocatalysis decomposes pollutants at an augmented rate using light-driven reactions using the conducting and charge-transfer properties of CNTs;
    - Catalytic Wet Air Oxidation (CWAO): Although CWAO has been employed commercially for several decades, it remains one of the most efficient water-purifying techniques;
    - Nanobiohybrid Catalysis: Useful in pollutant sensing, monitoring, and degradation in water.
- Desalination.
- Disinfection: Eliminates biological contaminants such as bacteria and viruses.
- Sensing and Monitoring: Tracks the pollutants present in the water in real time.

The high emission rates of air pollutants worldwide, especially in developing countries like China, have become a severe health problem [248]. For instance, Deng et al. showed that exposure to indoor and outdoor pollutants in early life is associated with childhood asthma, and ambient pollution is highly associated with health risks [249]. Among air pollutants, PM and ozone are generally regarded as the two air pollutants that raise public concern since they appear visibly as haze and smog [250,251]. While HEPA and activated carbon filters are standard methods for indoor PM and ozone removal, an improved approach is still desired. Recently, CNTs have shown promise in PM and ozone removal for air filtration applications. Thus far, the research has been conducted using air filters with different CNT designs for PM capture [252], such as CNT coatings [253], freestanding

CNT films [254], aligned CNT sheets [255], hierarchical structures, and fluidized beds with agglomerated CNTs [256].

Concerning ozone filtration, CNT/quartz fiber films perform superior to traditional granular AC and KI solution filters of comparable weight [257]. Yang et al. tested the PM and ozone filtration by CNTs grown on ACF via chemical vapor deposition. They concluded that CNTs on ACF enhanced the material from a medium level to H11 for PM filtration, increasing the quality factor by 48%. The CNT/ACF filter exhibited more than 99% ozone removal. At the same time, ACF alone showed a similar value and was proven to be of a much higher quality factor than other CNT-based filter media due to its high ozone removal efficiency, mid-to-high PM filtration efficiency, and reduced pressure resistance [253,255,258–260].

4.3. Microelectronics and Field Emission

As a result of the high electronic conductivities of both SWCNTs and MWCNTs, electron emission from carbon nanotube tips under an applied voltage between the nanotube surface and an anode is relatively standard. It has resulted in the development of various prototype electronic devices using CNTs [261–263], some of which are flat panel displays, field emitters in FEDs [264,265], polarizers for LCDs, transparent electrodes [266,267], and TFTs that are used in OLEDs [268–271], incandescent displays [272,273], thermochromic displays [274,275], flexible fiber displays, bright light sources or lamps [276,277], and X-ray emitters [200,276–279]. Carbon nanotube lamps, thought to be low-cost to make, have shown excellent performance with lifetimes as long as 8000 h at high efficiency, particularly for the green color [280,281]. The readers are referred to the extensive chapter by Jiang [261] for recent work on carbon nanotube field-emission devices.

4.4. Molecular Sensors

Owing to unique physicochemical characteristics, nanomaterials—particularly carbon nanotubes (CNTs)—-have played a central role in various scientific, engineering, and interdisciplinary areas of research since the discovery of CNTs by Iijima [3]. Among them, the CNT-based gas sensor has attracted broad interest because of its advantages of fast response, higher sensitivity, and lower operating temperature [282]. Dai et al. [283] first performed experimental work concerning detecting toxic gases using SWCNTs. That work demonstrated the exceptional sensitivity of SWCNTs to ppm concentrations of NO_2 and NH_3 by measuring significant transport responses in SWCNTs at room temperature. To date, researchers have prepared sensors from SWCNT and MWCNTs for the detection of a large variety of gases such as NOx, O_2, NH_3, CO, CO_2, H_2O, H_2, organic vapors, VOCs, and SF_6 decomposition gas [245,282–290].

Various CNT-based sensors have been described in the literature, including the following: (1) sorption gas sensors [291], (2) ionization gas sensors [292], (3) capacitance gas sensors [175,293], and (4) resonance frequency shift gas sensors [294,295]. Recently, Zhang et al. [282] reviewed CNT-based sensors' adsorption mechanisms and applications for SF_6 decomposition products such as SO_2, H_2S, SO_2F_2, CF_4, and SOF_2. Both theoretical and experimental findings identify that, though CNTs exhibit very low sensitivity to SF_6, they have relatively high sensitivity and selectivity toward its decomposition products.

With their peculiar structural and functional features, CNTs and modified CNTs represent ideal active sensor elements for the detection of a wide range of chemical species, from gases to organic compounds. Their high electrocatalytic activity, fast electron transfer capabilities, and stable integration of nanotubes with redox polymers make them highly suitable for use as electrochemical biosensors.

More importantly, CNT-based sensors contribute to the safety of food by detecting substances such as cholesterol in milk powder, *E. coli O157:H7 DNA* in beef, Sudan I in chili powder and sauces, Salmonella typhimurium in milk, and *E. coli O157:H7*, Campylobacter, and Salmonella in milk [284,296]. Wang et al. [284] have presented a very comprehensive review of nanoscale sensors for food safety with an emphasis on fundamental investigations of nanosensor technology for food testing and the most recent advances in nanosensor design and application.

4.5. Ceramic and Polymer Composites

During the last two decades, CNTs have attracted significant attention because of their unique combination of highly high longitudinal elastic modulus, excellent thermal and electrical conductivity along their axis, and low density for use as toughening agents in various polymer, ceramic, and metal matrix composites. The axial stiffness of a single CNT is comparable to the best carbon fibers, nearing 1 TPa, while its strength is much higher and reaches about 50 GPa [297].

Most efforts have been concentrated on polymer-based CNT composites; however, several ceramic/CNT composites have also been processed to exploit unique properties provided by the CNTs. Although ceramics possess high stiffness, superior thermal stability, and relatively low density, their brittle nature restricts their application in structural uses [298,299]. The remarkable resilience of the CNTs can considerably improve their brittleness; therefore, CNTs are potentially beneficial reinforcing agents in ceramics. One of the central problems when processing nanotube composite materials is the disaggregation of the individual nanotubes into a uniform dispersion in a matrix where all the nanotubes are separated [300]. Thus, ceramic/CNT composites show promise for high-temperature stability and improved toughness and creep resistance [299]. For instance, the mixtures of hot-pressed SiC nanoparticles with ten wt.% carbon nanotubes prepared a composite SiC/MWCNT showing 10% strength and fracture toughness improvement over the bulk SiC [301].

The studies associated with CNT-based metal or metal–oxide composites have been continued by investigating Ti/MWCNT, Al/MWCNT, Al_2O_3/MWCNT, Ni/MWCNT, and Fe/MWCNT composites [4,302–304]. These composites with enhanced hardness and Young's modulus are compared to their bulk counterpart. For instance, Al-MWCNT composites reach strengths as high as stainless steel (0.7–1 GPa) at a much lower density of 2.6 g/cm^3 and lower cost than Al-Li alloys. Using acid-treated MWCNTs and following the method of spark plasma sintering, the composites of MWCNT/alumina were successfully fabricated, which exhibited excellent mechanical properties: a bending strength of 689.6 $\pm$ 29.1 MPa and a fracture toughness of 5.90 $\pm$ 0.27 MPa·m$^{1/2}$, as reported by Yamamoto et al. [305]. Other MWCNT-Al_2O_3 composites were studied by Kasperski et al. [304], who observed crack-bridging only for non-covalent functionalization; this agreed with higher fracture toughness seen in the case of longer CNTs (>10 μm) compared to shorter CNTs (<1.5 μm). Recently, 35 vol% CNT-reinforced CNT-SiCN ceramic composites were fabricated by infiltrating liquid-phase polymeric precursor into a CNT-preform followed by pyrolysis and demonstrated higher fracture energy than non-reinforced ceramics despite the reduced hardness [306].

Reinforcement of polymeric fibers with CNTs improved physical structure, tensile properties, thermal shrinkage resistance, chemical resistance, electrical and thermal conductivity, and an increase in thermal transition temperature [307–309]. Khan et al. [245] compared different fiber reinforcements such as carbon, S-glass, aramid, boron, quartz, SiC, and CNTs, considering properties like diameter, density, tensile strength, and elastic modulus. Among these, CNTs presented the most minor diameter, in the 0.001 to 0.1 μm range, low density of ~1.33 g/cm^3, high tensile strength of up to 50 GPa, and the highest elastic modulus of up to 1000 GPa.

CNT-reinforced polymer fibers have been prepared by melt and solution spinning and electrospinning [310–318]. A variety of different types of polymer/CNT fibers were reviewed in Andrews et al. [319], Spitalsky et al. [320], and Liu et al. [308]. Ajayan and coauthors pioneered the field of polymer resin–CNT composites [321], and four years later, it was demonstrated that multi-wall nanotube matrix composites exhibit stress-transfer efficiency at least an order of magnitude better than conventional fiber composites [322]. Energy density in strain increased by 150%, whereas flexibility increased by 140% [323], adding a mere one wt.% of randomly dispersed MWNTs in ultra-high molecular weight polyethylene film. Regarding aligned SWNT/epoxy composites, tension–tension fatigue strength was twofold over typical carbon fiber/epoxy composites [324]. In addition, the elastic modulus of polystyrene can be increased by 42% for 1–5 wt% MWCNTs, whereas break stress can improve by 25% [325].

To enhance CNT dispersion, concentration, and alignment in polymers, Wu et al. [326], using PVA as the matrix, developed a technique called "layer-by-layer deposition" to create CNT/polymer composite fibers and presented a schematic diagram for layer-by-layer deposition of SWCNTs. This approach allows in situ mixing at a molecular level, enhancing the dispersion of CNTs and the infiltration of PVA into the fiber structure, as depicted in Figure 4a–d.

Wu et al. [326] reported that the reinforcement of CNTs significantly improved the PVA matrix, with the strength value increasing from about 50 MPa to 1255 MPa and electrical conductivity improving from about 0 to 1948 Scm^{-1}. Their technique also yields excellent control over the dispersion and concentration of CNTs in the polymer matrix. It has some flexibility in creating composite fibers of different polymers and may be scaled up for industrial processing. More recently, El Moumen et al. [309] further demonstrated through indentation tests that a small addition of CNTs significantly improves the elastic modulus, fracture toughness, and crack resistance in the CNT–polymer composites. Adding only 1% CNTs increased the composite's stiffness by approximately 3.5%. The properties of CNT-polymer composites depend on various factors, including the type of polymer, CNT weight fraction, processing conditions, and other key parameters. These composites exhibit a diverse range of advantageous characteristics, such as lightweight structure, enhanced mechanical strength, and superior electrical and thermal conductivity. Optimizing these properties is crucial for developing advanced materials tailored for applications in aerospace, automotive, electronics, biomedical, and materials science industries, among others. This is illustrated by some exciting examples of applications that include high-performance structural components, flexible electronics, advanced sensors, and next-generation energy storage devices [327].

4.6. Hydrogen Storage

Hydrogen is considered the most promising fuel for fuel cell vehicles. Over the past two decades, carbon-based materials such as carbon nanotubes (CNTs), carbon fibers, and high-surface-area activated carbon have been extensively studied and utilized in various research applications [328,329]. Due to their vast surface area and huge pore volume, CNTs become effective adsorbents, particularly for hydrogen storage. Both SWCNTs and MWCNTs have hollow cores that can store various gases, mainly hydrogen. Dillon et al. reported that, for the first time in 1997, SWCNTs exhibited remarkable reversible hydrogen storage capabilities with an adsorption capacity of about 5–10% [330]. The short, open-ended SWCNTs were observed to adsorb hydrogen at room temperature in minutes of 3.5 to 4.5 wt%. Using a specific opening and cutting procedure for the nanotubes, they could store approximately 7 wt% at 0.07 MPa and room temperature after heating their samples to 900 K under a high vacuum. It was subsequently realized that hydrogen release

now appeared at much higher temperatures than reported before, from one single peak at 300 K to two at 450 and 600 K.

Since then, many groups have examined hydrogen storage on CNTs, especially SWCNTs. However, reported capacities range from 0.1 to 70%, and this considerable variation likely owes to the wide variability of sample purity, characterization, and possible hydrogen contamination. Dillon et al., for example, measured a few mg of SWCNTs and found a capacity of roughly 4.5 wt% hydrogen storage [330]. It was achieved by opening the tubes through ultrasonic treatment in nitric acid with a corrosion-resistant titanium alloy, Ti-6Al-4V, which also proved promising for hydrogen storage. Most of the hydrogen uptake was due to particles of titanium alloy and contaminants introduced during sonicationas was found later by Hirscher et al. [331]. There are still disagreements on whether hydrogen adsorption occurs inside or outside the tubes, between tubes in "bundles" or "ropes", or between the layers in MWCNTs.

Following Dillon's original report, work on SWCNT hydrogen storage has been extended [8,328,329,332–341]. Ghosh et al. conducted studies of molecular dynamics that assessed the effects of defects and separation distances of the individual nanotubes in SWCNT bundles on hydrogen capacity at 80 and 298 K, and it was observed that hydrogen uptake showed better storage for more considerable separation distances and higher temperatures; thus, bundles outperformed the isolated SWCNTs [338]. In other work, Zhao et al. indeed reported a reduction in hydrogen storage capacity with increasing temperature in SWCNTs, which may relate to the "hydrogen spillover" mechanism: a process involving H_2 dissociation on metal catalysts, surface diffusion of atomic hydrogen onto the carbon surface, and finally recombinative formation of the H_2 molecule, as schematically shown in Figure 4e [342].

SWCNTs were prepared using KCl and the Ni-Co alloy catalysts by the TC-AD method at 600 °C by Zhao et al. [339]. The as-synthesized SWCNTs were tested for hydrogen storage. Testing of CNTs without further treatment was attempted; however, results by several groups suggest that pure CNTs are unlikely for practical application in hydrogen storage [343]. The functionalization of CNTs with specified molecules, atoms, or ions increases the hydrogen binding energy and storage capacity due to the provision of multi-adsorption sites. It helps the electron charge transfer between metal and carbon atoms. For instance, Vasu et al. functionalized SWCNTs with metals, metal hydrides like BH_3, and metal oxides like SnO_2, WO_3, and TiO_2 for hydrogen storage applications [344]. They demonstrated that BH_3-functionalized SWCNTs grant a promising hydrogen storage capacity, reaching 4.7 wt%, and show very low desorption temperature ranges from 90 to 125 °C. Such material has shown excellent reproducibility with no more than a 2.4% degradation rate.

A few years after the early reports on SWCNTs, investigations focused on hydrogen storage in multi-walled carbon nanotubes. Indeed, improvements in the MWCNT hydrogen storage capacity have been published after doping with light heteroatoms such as boron, fluorine, sodium, and lithium [337,345–356]. These doping elements cause electron deficiency and increase the polarity of the carbon framework, inducing strong interactions with hydrogen molecules and improving storage capacity. For example, 1.2 wt.% Li-doped MWCNTs showed a reversible hydrogen storage capacity of 3.9 wt.% at 77 K and 0.1 MPa, way above undoped CNTs [353,357]. Capacity improvement is considered because of enhancement in the interaction between H_2 molecules and Li-doped MWCNTs and due to the charge isolation state of lithium.

It has also been realized that decorating CNTs with metals represents another efficient way to enhance hydrogen storage at room temperature, mainly due to the spillover effect. Chen et al. [358] presented that the alkali–metal-doped MWCNTs, synthesized by catalytic decomposition of CH_4, have enhanced hydrogen storage characteristics. At moderate tem-

perature and ambient pressure, the storage capacities of unmodified and KOH-treated CNTs attained 0.71 wt.% and 4.47 wt.%, respectively. Besides being responsible for structural defects, the presence of metals like cobalt in the CNTs has been used to demonstrate the ability of metals to enhance hydrogen adsorption by promoting dissociation of hydrogen, a critical process involved in the hydrogen spillover mechanism. The ability of many metals, including Ca, Co, Fe, Ni, Pt, Ag, Cu, Mg, and Pd, to promote the hydrogen dissociation process has been used to credit their role in enhancing storage [289,290,350–352,359,360].

Hydrogen storage in Pd-decorated MWCNTs prepared by laser ablation and chemical reduction processes was recently studied by Merhabi et al. [350]. The group performed volumetric measurements and observed a significant difference between the two preparation techniques. The Pd decoration significantly enhanced the storage capacity due to the enhancement of hydrogen trapping compared to bare MWCNTs, the storage capacity increasing proportionally with Pd loading. In laser ablation, long exposures resulted in better Pd anchoring and higher hydrogen uptakes. Still, eventually, the excess loading caused structural damage to the MWCNTs and limited the capacity to 1.2% hydrogen uptake. In contrast, chemical reduction did not destroy the practical surface. Thus, hydrogen uptake increased linearly with Pd loading to as much as ten times higher than the laser ablation, reaching 12%. Nevertheless, neither of these methods achieved the U.S. DOE pre-2017 storage targets of 5.5 wt.% and a volumetric density of 40 kg/m^3 [340].

Further studies and computational analyses are also needed to realize the potential of nanotubes for hydrogen storage. It is also interesting to note that MWCNTs were studied for other types of gas storage, like argon [332] and nitrogen [361].

4.7. Energy Conversion and Storage

Rapid technological development and population expansion have raised the energy demand by manifold in the world [362]. To fulfill this demand, new emerging technologies in nanotechnology and new advanced materials are promising drives of new innovative energy systems with high performance [363]. Among all these technologies, carbon nanotubes are one of the most extensively researched for renewable energy conversion and storage applications. CNTs have unique size and surface-dependent properties such as high electrical conductivity, excellent electron mobility, significant electro-catalytic activity, good optical transparency, and inexpensiveness crucial for energy-related applications [276]. Some of the critical roles that have been played by CNTs in solar cells [364–366], supercapacitors [367–370], and lithium-ion batteries are discussed in the following section.

4.7.1. Solar Cells

Grätzel [371] invented the solar cell concept, after which academic and industrial research in solar cells has been widely developed based on their simple, sustainable, and eco-friendly applications. Solar cells can be made into different forms depending on the materials and fabrication methods. Such new systems include dye-sensitized solar cells (DSSCs) [372], inorganic and organic OSCs [317,364,366,373], and many hybrid systems [364,365,374,375]. Carbon nanotubes provide a large electron storage capacity and electronic conductivity to metals. Because of their one-dimensional nanostructure and remarkable electrically conductive properties, CNTs have been helpful for electron transport and can enhance photoelectric conversion efficiency in solar cells.

CNTs are incorporated into various layers of DSSCs, including the dye-soaked working electrode film on a transparent conducting oxide, the electrolyte, and the counter electrode also on the TCO. Kumar et al. [363] reviewed the use of CNTs in DSSCs by explaining how SWCNTs and MWCNTs are used worldwide to improve performance. The addition of CNTs in moderate quantities to the working electrode maintains its transparency while

increasing the power conversion efficiency in DSSCs due to improved charge-transport properties, as illustrated in Figure 4f [376,377]. However, the major challenge is to avoid the loss of transparency when CNTs are incorporated into the electrode.

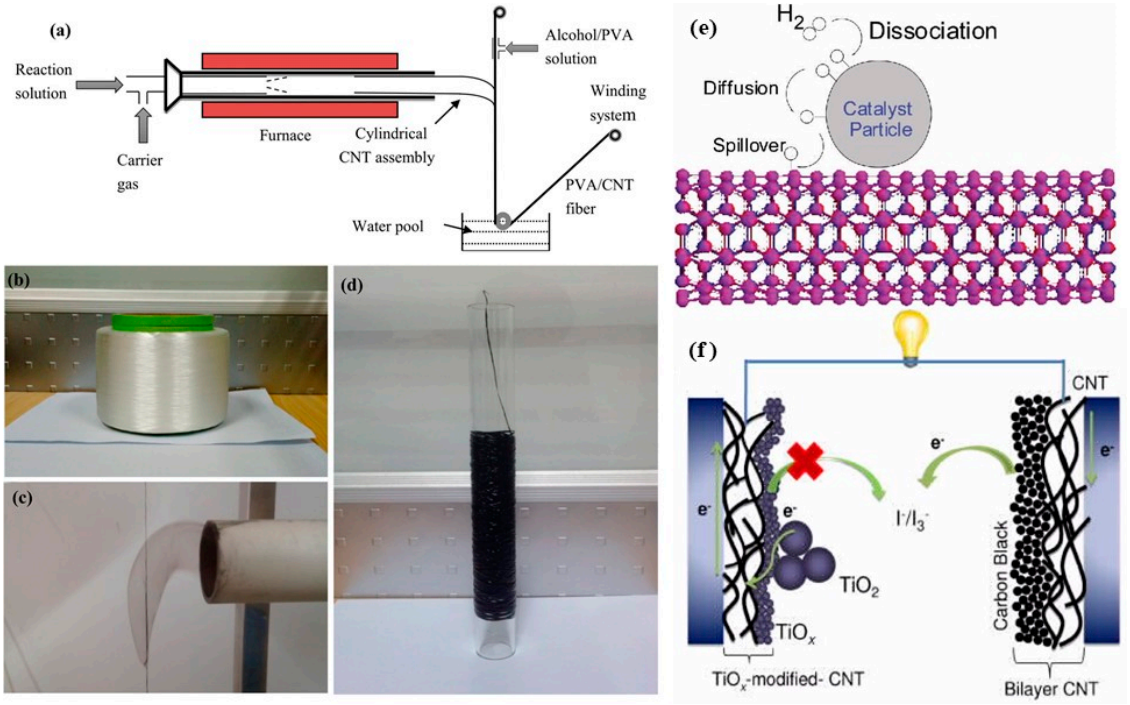

Figure 4. (**a**) Schematic of deposition process: a substrate wire wetted with alcohol/PVA solution is fed to the reactor for deposition of CNT assembly and finally wound up. (**b**) Vinylon wire is used as a substrate for depositing the first layer of CNTs. (**c**) Hollow cylindrical CNT assembly shrinking and depositing on the substrate wire wetted with alcohol/PVA solution. (**d**) CNT/PVA composite fiber wound on a glass tube. Adopted with permission from [326]. (**e**) The proposed atom hydrogen spillover mechanism of SWCNTs. Adopted with permission from [339]. (**f**) Schematic of DSSC with a pair of CNTs-based electrodes. Adopted with permission from [376].

The electrolyte in dye-sensitized solar cells (DSSCs) is essential for ensuring the ionic conductivity of the bulk solution while also maintaining a potential barrier that is suitable for energy conversion. It significantly influences the incident photon-to-current efficiency (IPCE) and the long-term stability of the cell. CNTs help enhance charge carrier diffusion within the electrolyte and between the electrodes. Recent works, such as that by Kumar et al. [363], have concentrated on CNT usage in ionic liquid electrolytes, where they take active participation in charge transport along with catalyzing I^3- reduction. I-/I^{3-} electrolytes are extensively used in DSSCs due to their high conductivity, low vapor pressure, significant diffusion coefficient, and excellent flowability [378].

The counter electrode in DSSCs is responsible for transporting the photogenerated electrons at the photoanode to the electrolyte; platinum is considered the ideal material since it exhibits efficient transport with high electrocatalytic activity [379]. The significant drawback is that platinum is costly and rare. Furthermore, although platinum is quite adequate, questions about its stability in different chemical and electrochemical applications may limit its use. A promising alternative to platinum is represented by carbon nanotubes illustrated in Figure 4f [376,380–382], which present several advantages, including low fabrication cost depending on the synthesis method, excellent thermal stability, a large active surface area, high catalytic activity, outstanding electrical conductivity, and strong corrosion resistance [372,383].

Even though much promising research on CNTs in DSSCs has been conducted, commercialization of these devices has not yet been considered. This technology still needs further development to make it viable for extensive applications in rooftop installations, window glass, and home intelligent sensors, among other things. However, all that needs to be ensured is excellent environmental stability. Data that outline the advantages of using CNTs for DSSCs would be more convincing.

4.7.2. Supercapacitors

The supercapacitor is an essential device in electronics and a substitute power source; it offers rapid charge/discharge with minimal heat, safety, and minimum maintenance for the longevity of its performance. While supercapacitors are well known for high power density, which allows them to be charged up and then discharged within an extremely short time, the amount of energy stored is generally low compared to batteries. High energy density in supercapacitors indicates that these devices can store substantial energy but still support fast charge/discharge rates. In such a device, two non-reactive porous electrodes are submerged in an electrolyte, across which the collectors have a voltage drop. Generally, supercapacitors are considered to fall into two categories: (1) pseudocapacitors, which store charge through the reversible oxidation/reduction on the electrode surface, also called Faradaic charge transfer, and (2) electric double-layer capacitors, a non-Faradaic process in which no charge is transferred across the electrode interface in energy storage, which is electrostatic [384]. The essentials concerning the material for supercapacitor electrodes are said to be three in number: high capacitance, low resistance, and stability.

Most research has focused on carbon nanomaterials, particularly carbon nanotubes (CNTs) and graphene, as practical electrode materials for supercapacitors. This is due to their large surface area, excellent electrical conductivity, impressive mechanical strength [385], and ability to endure volume changes during charge–discharge cycles [386]. Among others, Niu et al. first proposed using CNTs in supercapacitors [387]. Generally, the CNT-based supercapacitors are divided into three types: (1) bare CNTs [369,388], (2) CNT/polymer composites [326], and (3) CNT/metal oxide (MeOx) hybrid electrodes [389]. Kumar et al. summarized significant works that have used CNTs in supercapacitor electrodes based on the categories shown in Figure 5a [363].

Supercapacitors made from pure carbon nanotubes (CNTs) still struggle to achieve high energy density without compromising power density. To improve performance, modifications to the CNTs are essential. Reported values for specific capacitance range from 11 to 180 F/g, for energy density from 0.5 to 94 Wh/kg, and for power density from 20 to 210 kW/kg for CNT-based supercapacitors [363]. Chen et al. [369] reviewed the recent advancements in high-performance supercapacitors that utilize carbon nanomaterials. They presented effective methods of material engineering toward device performance improvement for applications ranging from consumer electronics to wearable optoelectronics and hybrid electric vehicles. Polymer/CNT composites and CNT/metal oxide (MeOx) hybrid electrodes perform better than pure CNT electrodes. For example, the specific capacitance for the composite electrodes of CNT/polymer is in the range between 160 and 528 F/g, and energy density is from 15.1 to 228 Wh/kg, which is relatively higher compared to the individual bare CNT electrodes [363]. Accordingly, a maximum power density of 4185 kW/h was reached with Ag-decorated PAni/MWCNT electrode due to highly conductive Ag nanoparticles and PAni/MWCNTs, yielding a maximum electrical conductivity of 4.24 S/cm [390]. Unfortunately, the drawback of such composite electrodes is that they face fast capacitance decay owing to the destruction of their structure, which would negatively affect the cycling stability of the supercapacitor [391]. Zhang et al. developed superelastic fiber-shaped supercapacitors (SFSs) using CNT/PAni composite electrodes that

can stretch up to 400%. They reported a high specific capacitance of approximately 79.4 F/g, which remained stable after being stretched to a strain of 300% over 5000 cycles. Furthermore, they achieved a specific capacitance of 100.8 F/g after bending the supercapacitors for 5000 cycles at a current density of 1 A/g (see Figure 5b–d) [392].

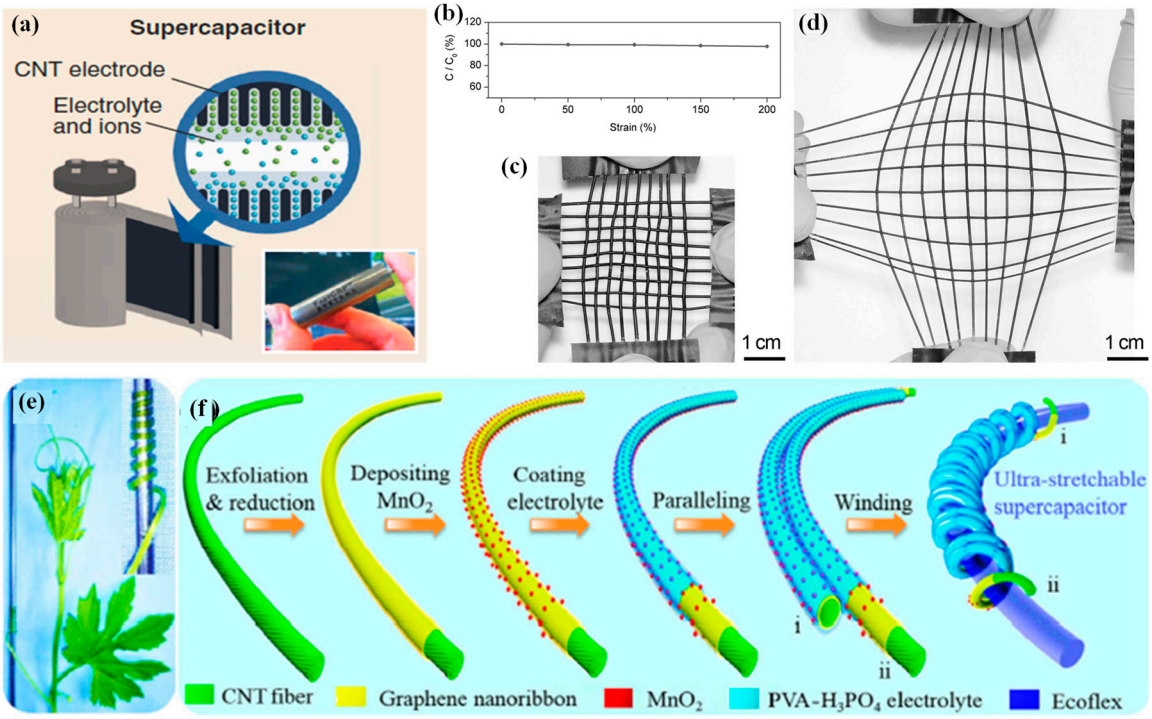

Figure 5. (**a**) CNTs-based supercapacitors. Adopted with permission from [263]. (**b**) The specific capacitance of the supercapacitor textile depends on the strain. C_0 and C correspond to specific capacitances at 0 and the other strains, respectively. (**c**,**d**) Photographs of a flexible and stretchable textile before and after stretching by 100%, respectively. Adopted with permission from [392]. (**e**) Photograph of balsam pear with the stem tendril coiled in a helix around a thin rod; inset is a close-up image showing the helical structure. (**f**) Demonstration of SC fabrication process of ultra-flexible wire-shaped supercapacitor. Adopted with permission from [393].

Recently, Wu et al. successfully developed high-performance supercapacitors using polyaniline vertical-aligned carbon nanotube (PANI/VA-CNT) nanocomposite electrodes. Their study revealed that these electrodes exhibited capacitive performance six times greater than that of disordered carbon nanotubes when using an $HClO_4$ electrolyte, achieving an impressive maximum capacitance of 403.3 F. The specific capacitance reached 314.6 F/g, and the supercapacitors demonstrated good cycling stability, retaining 90.2% of their capacitance after 3000 cycles at a current density of 4 A/g. Additionally, they achieved a high energy density of 98.1 Wh/kg when utilizing an organic electrolyte, such as EMIBF4. The authors explained that the vertically aligned structure provides direct pathways for ion diffusion and enhances electrochemical capacitance, which accounts for the excellent performances [394]. This composite is envisioned to have great potential for portable and wearable electronics.

In this regard, applying transition metal oxides as alternative electrode materials has further improved supercapacitors' specific capacitance and energy density. Among these, the most intensively investigated metal oxides are MnO_2 [393,395,396], RuO_2 [397], Co_3O_4 [398–400], SnO_2 [401–404], NiO [405], ZnO [406], V_2O_5 [407], TiO_2 [408–410], CuO [411,412], Fe_2O_3 [413,414], WO_3 [415–417], and $Ni(OH)_2$ [418–420]. The charge–discharge cycles generate mechanical stresses that influence cycling stability. CNTs have

been incorporated in these metal oxide electrodes to attenuate these effects. MnO_2 is now one of the most utilized materials for supercapacitor electrodes synthesized and characterized to date because of its abundance, low-cost aspect, ease of processing, environmental friendliness, and high theoretical capacity ranging from 1100 to 1300 F/g [421]. In the case of manganese oxide supercapacitors that utilize vertically aligned carbon nanotubes, the specific capacitance was reported to be the highest at 642 F/g for a scan rate of 10 mV/s, accounting for approximately 60% of MnO_2 theoretical capacity [422]. The authors outlined the key factors responsible for such efficiency improvements, which include temperature and deposition time, to control the density, catalyst layer thickness, length, diameter, and structure of the VACNTs.

Several research works have been conducted to design flexible supercapacitors with longer cycle life, high energy density, and fast charge/discharge rates, which are crucial for applications in wearable energy storage devices. For example, Lu et al. recently developed a flexible hybrid wet-spun CNT fiber-based supercapacitor using a conventional wet-spinning process. The specific capacitance of 152 F/g (156 F/cm^3) achieved in this supercapacitor is about 500% higher than that of multi-walled carbon nanotube/MnO_2 yarn-based supercapacitors [393,396,399,414,423]. The supercapacitor exhibits high rate capability, stable performance after 10,000 cycles, and a practical energy density of 14.1 Wh/kg with a power density of 202 W/kg [423]. Another breakthrough was the record-breaking ultra-stretchable wire-shaped supercapacitor realized by Wang et al. [393] by carbon nanotube@graphene@MnO_2 fibers wrapped around a superelastic core fiber withstanding a tensile strain as high as 850%, as demonstrated in Figure 5e,f.

The CGM-SC supercapacitor developed by Wang et al. [393] demonstrated a significant specific capacitance of 14.02 mF/cm^2, an energy density of 3.37 mWh/cm^3, and a power density of 54.0 mW/cm^3. These impressive metrics can be attributed to the outstanding electrical properties of the CNT@graphene fibers and the high specific capacitance of the flower-like MnO_2 structure. The wire-shaped supercapacitor maintained 82% of the electrochemical performance after 1000 stretch–release cycles with strains of 700%, indicating good durability and stability for practical applications in other highly stretchable electronic devices illustrated in Figure 6a–c. This CGM-SC supercapacitor shows suitable specific capacitance with superior stretchability, more than twice that of other wire-shaped supercapacitors developed by other researchers. For example, Zhang et al. reported freestanding, stretchable, and flexible CNTs fiber springs-based supercapacitors [424] with a specific capacitance of about 27.07 mF/cm^2 and a stretchability of 305%. A specific capacitance of about 50.1 mF/cm^2 and a stretchability of 400% was mentioned by Zhang et al. with a PAni/CNT electrode material [392]. A high specific capacitance of 40.9 mF/cm^2 with a lower stretchability of 150% was reported by Choi et al. with CNT/MnO_2/Nylon Fiber Solid-State Supercapacitors [425].

By 2022, the global supercapacitor market is expected to reach USD 2023.33 million, a 21.18% compound annual growth rate (CAGR) from its 2016 valuation of USD 649.25 million [426]. The increasing demand for supercapacitors in renewable energy applications is driving the market. In addition, favorable environmental safety regulations bolster the adoption of supercapacitors, which are considered more eco-friendly than competing technologies. Most supercapacitors currently use liquid organic electrolytes. Solid-state supercapacitors often provide high ionic mobility and rapid charge/discharge performance. However, they may be preferred for safety reasons, as they use polymer membranes or ion-conducting gels instead of liquid electrolytes. Despite this advantage, gels face challenges, such as lower ion mobility and reactivity, compared to devices that use liquid electrolytes [427]. Therefore, more developments are needed before solid-state supercapacitors are commercialized.

The global supercapacitor market, based on applications, is segmented into the following categories:

- Consumer Electronics: Laptops, digital cameras, portable speakers, and mobile computing equipment.
- Industrial Automation: Encompasses applications like memory storage, uninterruptible power supplies (UPSs), and automatic meter readers.
- Power and Energy: Covers used in actuators, wind turbines, and photovoltaic systems.
- Medical: Primarily focused on applications like defibrillators.
- Transport: Includes many vehicles and systems, such as trains, cranes, cars, buses, elevators, aircraft, and hybrid electric vehicles (HEVs).

The key market players in the industry include Advanced Capacitor Technologies Inc., Tokyo, Japan, Axion Power International Inc., New Castle, PA, USA, CAP-XX Ltd., Seven Hills, NSW, Australia, EEStor Corporation, Toronto, ON, Canada, ELTON Inc., Milton, ON, Canada, FastCAP Systems Inc., Woburn, MA, USA, Graphene Energy Inc., Austin, TX, USA, Maxwell Technologies Inc., San Diego, CA, USA, and Nesscap Energy Inc., Brooklyn, NY, USA [428]. Yassine et al. published a list of commercially available supercapacitors (SC) with some of the significant properties—potential (V), capacitance (F), and equivalent series resistance (ESR, mΩ) [429]. Recently, Lamborghini and MIT announced a 3-year collaboration to develop MOFs-enhanced supercapacitors for electric vehicles. They developed electrodes with metal-organic frameworks and some with graphene-like (i.e., 2D) structures that did not contain graphene [430].

4.7.3. Lithium-Ion Batteries

The increasing need for better energy storage in areas such as consumer electronics, hybrid electric vehicles, and remote sensing is driving substantial progress in electrochemical research. Among the different types of batteries available, lithium-ion batteries (LIBs) are separate due to their appealing characteristics, including low cost, safety, minimal side reactions, and superior energy density, voltage, capacity, and tap density. These attributes make LIBs a leading choice for various energy storage requirements [431]. Lithium-ion batteries (LIBs) are composed of a negative electrode (anode), a positive electrode (cathode), a separator, and a conducting electrolyte. These batteries store electrical energy in the two electrodes as lithium-intercalated compounds. The operational principle of LIBs is illustrated in Figure 6d [432], which shows the flow of electrons through the external circuit (dashed lines) and the movement of ions between the electrodes (solid lines) during charging (blue) and discharging (red) operations. Sony, a Japanese corporation, was the first to commercialize LIBs in the 1990s, using $LiCoO_2$ for the cathode and graphite for the anode. The theoretical storage capacity of graphite is 372 mAh/g (LiC_6), where lithium ions intercalate between the graphene layers.

LIBs with carbon-based anodes are widely used in portable computers, mobile telephones, digital cameras, etc. Alternative high-capacity anode materials are now receiving considerable attention. Endo and colleagues [433] were the pioneers in using vapor-grown carbon fibers (VGCFs) instead of graphite in LIBs. This advancement resulted in an increase in both specific and volumetric capacity of the anode, which in turn drove the development of electrodes made from carbon–carbon composites and carbon nanotubes. Frackowiak et al. were the first to report that carbon nanotubes (CNTs) in lithium-ion batteries demonstrated high reversible capacities, ranging from 460 to 1080 mAh/g for single-walled carbon nanotubes (SWCNTs) and multi-walled carbon nanotubes (MWCNTs) [434]. Since then, much research has looked into using carbon nanotubes (CNTs) in lithium-ion batteries because of their better mechanical, electrical, and thermal qualities compared to other carbon materials. Lithium ions (Li^+) populating the internal spaces of carbon nanotubes

(CNTs) are the leading cause of the storage mechanism in LIBs. Nishidate and associates have investigated the diffusion properties of lithium ions entering SWCNTs in several ab initio investigations. Their molecular dynamics simulations measured the effect of flaws on lithium insertion in CNTs [435,436]. Table 1 illustrates the key parameters of CNTs.

Table 1. Key parameters of CNT-based materials in LIBs.

Reference	Electrode Material	Role	Capacity (mAh/g)	Irreversible Capacity (mAh/g)	Electrolyte
[433]	Vapor-grown carbon fibers (VGCF)	Anode	372	280~330	poly(ethylene oxide)
[434]	SWCNTs and MWCNTs	Anode	460–1080	460 to 1080	1 M $LiPF_6$ + EC + DEC
[437]	CNTs	Anode	230	502	1 M $LiPF_6$ + EC + DEC (1:1)
[436]	Open-ended CNTs	Anode	372	25% increase	-
[438]	Chemically/mechanically modified CNTs	Anode	994	720–800	-

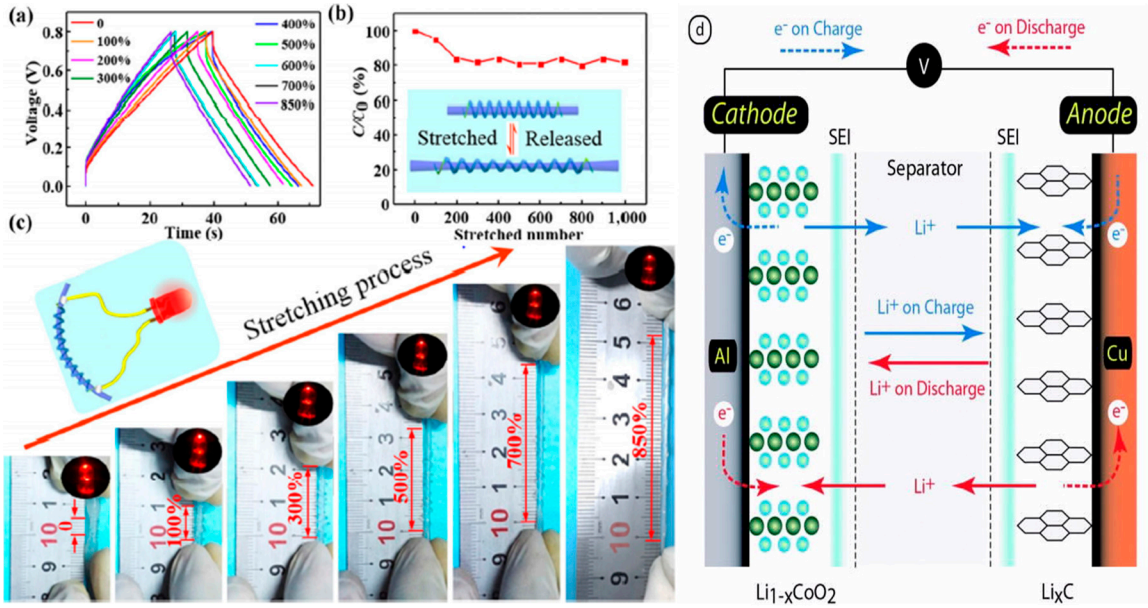

Figure 6. (**a**) Galvanostatic charge/discharge curves of the CGM-SC under strains ranging from 0 to 850%. (**b**) Evolution of the specific capacitance ratio over several stretching–releasing cycles with a 700% strain. The current density for all tests was 0.5 A/cm^3. The inset is a schematic illustration showing the stretching and the release of the CGM-SC. (**c**) Photographs of the CGM-SC with tensile strains of 0, 100%, 300%, 500%, 700%, and 850%, respectively. The insets show the light emission diode powered by the CGM-SC. Adopted with permission from [393]. (**d**) An illustration of a lithium-ion battery's working mechanism. Adopted with permission from [432].

Figure 7a shows the impact of imperfections on the shape of CNTs. Each remaining carbon atom tries to keep its bonds with its neighbor atoms when the carbon atoms are eliminated, creating a hole in the CNT wall. The findings show that CNTs with n = 7 and n = 8 faults and CNTs without flaws have limited lithium diffusion. Lithium ions, however, easily permeate into CNTs with a defect of n = 9. Lithium ions migrate to the interior of these nanotubes and are effectively absorbed there, indicating that lithium ions build up

inside and outside the CNTs. Meunier et al. carried out ab initio studies to elucidate the charge/discharge phenomena in lithium-ion batteries [436]. Researchers found that lithium ions can enter open-ended CNTs, but these nanotubes should be relatively short to facilitate the easy entry and exit of the ions. The length of the nanotubes significantly influences the diffusion coefficient of lithium ions within them, with lower effective diffusion obtained with longer tubes [437]. Modifying the surface (chemically or mechanically) increases the electrochemical storage. This is supported by experimental evidence from Kumar et al. [438]. The theoretical calculations suggest that reversible capacities exceeding the LiC_2 stoichiometry (>1116 mAh/g) are attainable for SWCNTs [435]. Compared to other carbon materials, CNTs have a better electrical percolation network at a lower weight loading. SWCNTs and MWCNTs were investigated as anode materials, conductive additives in both anode and cathode materials as well as binder free-standing electrodes.

CNTs as Anode for LIBs

A high theoretical conductivity of 10^5–10^6 S/m is observed for CNTs and good tensile strength (~60 GPa) [45,439,440]. The simple deposition of SWNCTs and MWCNTs onto a current collector or the direct growth of anode materials for LIBs onto a catalyst-modified current collector is essential. MWCNTs, which consist of multiple layers of graphene sheets, exhibit more complex electronic properties than SWCNTs. Lithium-ion intercalation/deintercalation occurs in the interplanar spacing of graphitic sheets or inside the hollow cores of MWCNTs. The capacity is higher than that obtained with graphite. The capacity of SWCNT-based anodes generally ranges between 400 and 460 mAh/g [434,441]. Shimoda et al. obtained a higher capacity of about 1100 mAh/g by shortening and introducing sidewall defects in the SWCNTs [442]. The n capacities also affect the chirality, and metallic CNTs have higher capacities (~400% higher) than semiconducting ones [443]. The four key factors affecting lithium kinetics in carbon nanotubes are their lengths, chirality, diameter, and structural defects. The irreversible capacity, which relates to solid-electrolyte interphase formation, is significant. It is one of the significant challenges with CNT anodes in lithium-ion batteries. SEI formation contributes to the lithium loss by electrolyte decomposition during the first cycle, which is not recovered in further cycles [434]. Landi et al. showed that by adding propylene carbonate (PC), the reversible capacity of the first cycle is improved and reaches 520 mAh/g [444]. Other studies showed that longer alkyl-chained carbonate co-solvents improve the reversible capacity of SWCNTs [445], reaching a 1000 mAh/g capacity for the first cycle. The same tendency was observed for MWCNTs [446]; an increase in the reversible capacity from 150 to 210 mAh/g and coulombic efficiency exceeding 97% after a few cycles was obtained by changing the co-solvent from dimethyl carbonate to diethyl carbonate. Chemical etching and ball milling are two commonly used methods for modifying the morphologies of carbon nanotubes (CNTs), which directly influence their electrochemical performance. Eom et al. studied the effect of chemical and mechanical modification of the structure of CNTs on lithium insertion [447,448]. The etching time had a significant effect on the reversible capacity of the materials. For purified MWCNTs, the reversible capacity was measured at 351 mAh/g ($Li_{0.9}C_6$). In contrast, the reversible capacity for etched MWCNTs increased to 681 mAh/g ($Li_{1.8}C_6$). Additionally, the irreversible capacity also rose with longer etching times; it increased from 1012 mAh/g ($Li_{2.7}C_6$) for the purified MWCNTs to 1229 mAh/g ($Li_{3.3}C_6$) for the etched MWCNTs. The reversible capacity of ball-milled MWCNTs increased with increasing ball-milling time, namely from 351 mAh/g ($Li_{0.9}C_6$) for purified MWNTs to 641mAh/g ($Li_{1.7}C_6$) for ball-milled MWNTs; Figure 7b,c.

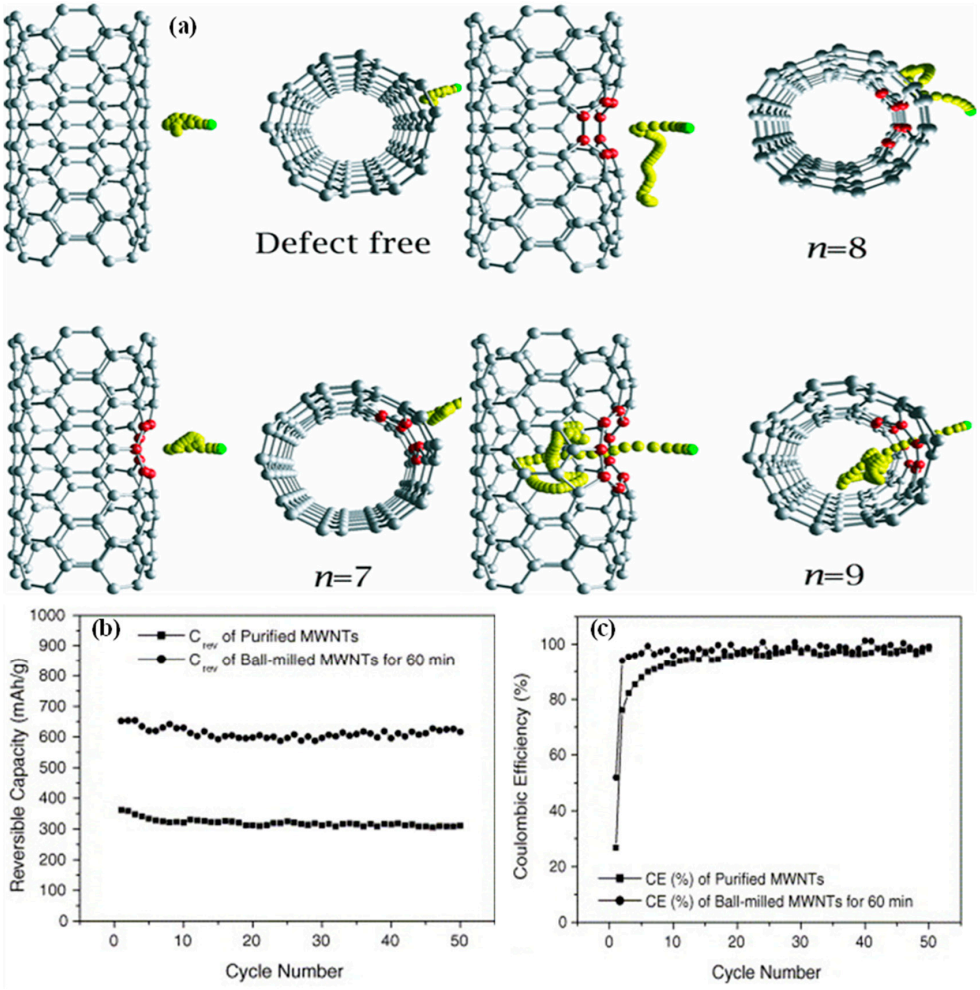

Figure 7. (**a**) Effect of defects on lithium insertion in a (5, 5) SWCNT. Note: For each nanotube structure, both side and top views are provided to illustrate the impact of defects on lithium-ion insertion. Adopted with permission from [435]. (**b**) Purified and 60 min ball-milled MWNT reversible capacity and (**c**) coulombic efficiency as a function of cycle count. Adopted with permission from [448].

From 1012 mAh/g ($Li_{2.7}C_6$) for pure MWNTs to 518 mAh/g ($Li_{1.4}C_6$) for MWNTs ball-milled for 60 min, the irreversible capacity gradually drops with increasing ball-milling duration. Coulombic efficiency rises in tandem with this decrease in irreversible capacity, increasing from 25% for purified MWNTs to 50% for ball-milled MWNTs. In addition, compared to purified MWNTs, ball-milled MWNTs demonstrate better and more consistent capacity retention during charge/discharge cycling. The higher density of surface functional groups created on the CNTs during ball milling is responsible for the increased voltage hysteresis seen in the ball-milled MWNTs [449]. While the high surface area of the etched MWCNTs contributes to a significant irreversible capacity, it also leads to a decrease in coulombic efficiency [447,448]. Lithium diffusion is directly influenced by carbon nanotube (CNT) length. The shorter MWCNTs offer more intercalation sites at the open ends for Li^+ ion storage and shorter reversible pathways for Li^+ ions [450]. Yang et al. [451] compared two types of CNTs as anode materials for LIBs. They looked at the co-pyrolyzed short carbon nanotubes (CNTs-1); the study examined CNTs with varying dimensions. The first type, known as CNTs-1, had an outside diameter ranging from 35 to 65 nm, an interior diameter of 15 to 40 nm, and a length between 150 and 400 nm. The second type, CNTs-2, featured an outside diameter of 15 to 30 nm, an inner diameter of 5 to 10 nm, and lengths of several micrometers. These CNTs-2 were produced using a common chemical vapor deposition (CVD) process. The findings indicated that the reversible capacities of the

CNTs-1 electrodes were nearly twice as high as those of the CNTs-2 electrodes, measuring 266 mAh/g and 170 mAh/g at current densities of 0.2 mA/cm^2 and 0.8 mA/cm^2, respectively. Additionally, the CNTs-1 and CNTs-2 electrodes exhibited differences in voltage hysteresis and lithium-ion storage mechanisms. Researchers discovered that the surface functional groups (some nucleophilic oxygen-containing functional groups such as keto-carbonyl (-C=O), phenolic hydroxyl (-OH), carboxyl (-COOH), epoxy group (-O-)) and electrophilic oxygen-containing functional groups such as carbonyl (-CO=O) and surface resistance of CNTs contributed to the significant voltage hysteresis observed in the CNTs-2 electrode. This led to increased overvoltage and more impediment during lithium extraction from the electrode. The CNTs-1 electrode or shorter CNTs showed more favourable kinetic properties throughout the charge and discharge process, which is promising for Li-ion applications. The AC impedance showed a more significant charge transfer resistance for CNTs-2 (31.2–61.2 Ω) compared to 3–4 Ω for CNTs-1. Other attempts were carried out to improve the reversible capacity of MWCNTs, by surface modification [452,453], by cutting conventional micrometer-long entangled CNTs into shorter ones [454], by modifying the synthesis process [437,455], or by using aligned or CNT arrays [456–458].

Lithium adsorption and diffusion within and on the surface of carbon nanotubes (CNTs) are significantly influenced by their diameter, affecting the lithium-ion capacity. Intercalated Li^+ ions localize close to the sidewalls of the CNTs rather than at the center, according to first-principles calculations by Udomvech et al. [459]. This implies that larger carbon nanotubes (CNTs) with less internal space have a lower capacity than CNTs with smaller diameters, which makes them less appropriate for battery applications. The Li/C ratio and CNT diameter were clearly correlated by Zhao et al. [460]. Figure 8 illustrates the relationship between the lithium-to-carbon nanotube (Li/C) ratio and the diameter of carbon nanotubes (CNTs). This figure demonstrates that as the diameter of the CNTs increases, lithium atoms tend to form a multi-shell structure in equilibrium. Research indicates that lithium has a diffusion barrier of approximately 380 meV in the radial direction while it exhibits high mobility along the tube's axis, with an energy barrier of less than 47 meV. Zhang et al. [461] conducted experiments on MWCNTs of various sizes as anode materials for LIBs. Their findings revealed that MWCNTs with a diameter between 40 and 60 nm achieved the highest specific capacity, reaching 187.4 mAh/g at a charge/discharge rate of 50 mA/g. Furthermore, after 50 cycles, the coulombic efficiency was reported to be 101.9%; see Figure 8b,c. It is commonly acknowledged that heteroatom doping of carbon is a successful method for modifying carbon-based anode materials' physical and chemical characteristics [223,224]. Furthermore, it has been demonstrated that doping CNT-based anodes improves lithium-ion battery (LIB) performance. According to Zhou et al.'s first-principles research on boron- and nitrogen-doped SWCNTs, boron doping stabilizes the absorption of lithium ions on the CNT walls by forming an electron-deficient structure in the nanotubes. Nitrogen doping, on the other hand, produces an electron-rich structure that prevents Li^+ ions from being absorbed [462,463].

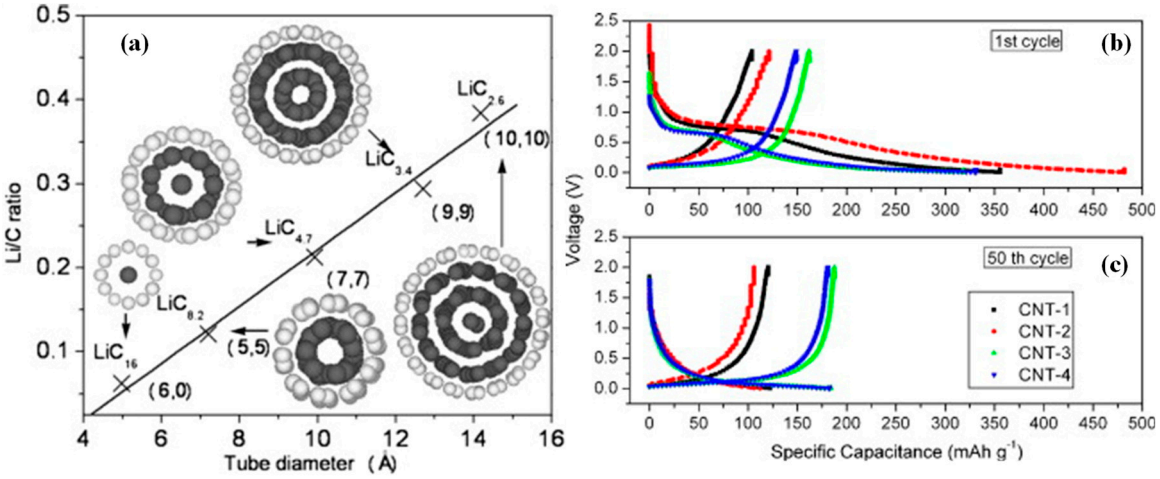

Figure 8. (**a**) The fluctuation of the Li/C ratio with tube diameter is shown. The insets display the equilibrium configurations of SWNTs packed with Li atoms. In the visualization, Li and carbon atoms are represented by white and grey spheres, respectively. Adopted with permission from [460]. (**b**) The 1st and (**c**) the 50th discharge and charge curves for the as-prepared MWCNT electrodes at a current density of 50 mA/g and potential window of 0–2 V. Adopted with permission from [461].

Li et al. studied high-concentration nitrogen-doped carbon nanotube anodes that have enhanced Li^+ storage capabilities for lithium rechargeable batteries. These anodes' electrochemical performance was contrasted with that of pure CNTs. Their findings showed that high-concentration nitrogen-doped carbon nanotubes (HN-CNTs), with up to 16.4%, had a rate capability that was noticeably improved and nearly doubled the reversible capacity of CNTs (494 mAh/g against 260 mAh/g). According to AC impedance studies, HN-CNTs had a lower charge transfer resistance (38 Ω) than CNTs (58 Ω). The increased performance is ascribed to the carbon nanotubes' high nitrogen content, which enhances electrical conductivity and produces more defect sites, providing more active sites for the storage of Li^+ [464].

In CNTs made using the graphite arc process in a non-aqueous solution, the impact of boron doping on electrochemical Li insertion was also examined [465]. Raman spectroscopy verified that the local hexagonal structure in MWCNTs was broken by boron doping [465,466]. Furthermore, doping promoted a preferred zigzag structure by lengthening and 3D organizing the nanotubes. Undoped carbon nanotubes (CNTs) exhibited a reversible capacity of 156 mAh/g in the first cycle. In contrast, boron-doped carbon nanotubes (B-MWNTs) demonstrated a higher capacity of 180 mAh/g, with coulombic efficiencies ranging from 55% to 58%. After completing the second cycle, the coulombic efficiency increased to over 90%. This improvement can be attributed to their higher specific surface area, better 3D ordering, higher defect density, and superior conductivity. B-doped MWNTs demonstrated higher reversible and irreversible capacities than undoped MWNTs [465].

Zhang et al. created porous CNT webs co-doped with high levels of boron (approximately 15.05 at %) and nitrogen (around 6.71 at %). They used polypyrrole (PPy) nanotubes as the precursor and employed boron hydride and ammonia borane (NH_3BH_3) as the sources of boron and nitrogen, respectively [467].

The SEM and TEM micrographs of the PPy and AB@PPy composites as synthesized are shown in Figure 9. The morphology of the AB@PPy composites, characterized by a hollow nanotube structure with a large interior cavity, remained comparable to that of pure PPy. However, AB was deposited on the surface and inner cavity of the PPy nanotubes due to the nanotubes' diameters increasing to 60–70 nm (as opposed to 50–60 nm for

the PPy precursor) and their inner diameter decreasing. Boron–nitrogen-phosphorous carbon nanotubes (BNPCNTs) serve as effective anode materials for lithium-ion batteries due to the synergistic benefits of their porous nanotube structure and the high levels of boron and nitrogen doping. They demonstrate a high reversible capacity of approximately 900 mAh/g at a current density of 200 mA/g, along with excellent rate capability and stable cycling performance [467].

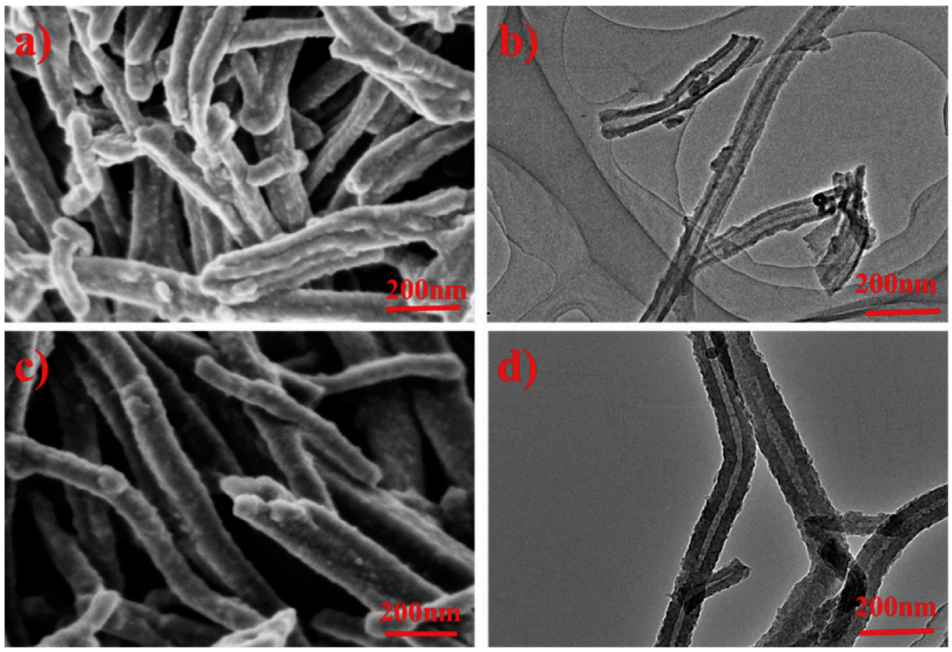

Figure 9. SEM (**a**) and TEM (**b**) micrographs of the as-synthesized PPy; SEM (**c**) and TEM (**d**) image of AB@PPy composites. Adopted with permission from [467].

Yang et al. showed that CNTs pre-doped with copper exhibit a lower specific capacity than the undoped CNTs. The Cu atoms occupy a portion of the pores and surfaces of the CNTs, which reduces the available sites for lithium intercalation [468]. On the other hand, the lithium intercalation of CNTs pre-doped with lithium is higher than the undoped CNTs and the opened CNTs [469]. Despite the large first irreversible capacity (~500 mAh/g), a larger 200 mAh/g capacity was observed with the pre-doped material. The following explanation was provided for this behavior. The leading cause of this behavior is because at high temperatures, $LiNO_3$ that the carbon nanotubes have absorbed breaks down into $LiNO_2$. Before the electrode surface contacts the electrolyte, the lithium nitrite first creates a protective layer on it. By acting as a barrier, this $LiNO_2$ layer reduces the charge used during the electrolyte decomposition by stopping the solvent from breaking down into other by-products [469].

Alumina-coated carbon nanotubes (CNTs) were synthesized on a copper substrate and utilized as anodes in lithium-ion batteries [470]. The anode demonstrated a very high specific capacity of 1100 mAh/g at 2 V after 50 cycles, along with good capacity retention and excellent rate capability. This innovative anode represents a promising electrode material for future lithium-ion batteries, offering a three times higher capacity than the theoretical capacity of graphitic material (372 mAh/g). The aluminum oxide coating enhances the stability of the electrode and improves capacity, while the CNTs provide a core structure that ensures excellent conductivity, structural integrity, and lithium-ion intercalation ability [470].

Despite the high reversible capacity observed in CNTs anodes for lithium-ion batteries, a significant challenge remains: the irreversible capacity. This issue arises from the

formation of the solid electrolyte interface (SEI) on the nanotubes. The irreversible capacity limits the effectiveness of CNTs as a standalone anode material. In the following section, we discuss the application of CNTs as a conductive additive in both anode and cathode electrodes for lithium-ion batteries. Table 2 highlights differences in theoretical capacity, conductivity, structural integrity, irreversible capacity, material modification potential, and lithium-ion diffusion.

Table 2. Comparison of graphite and CNT anodes for LIBs.

Characteristic	Graphite	Carbon Nanotubes (CNTs)	References
Theoretical Capacity	372 mAh/g (LiC_6)	400–460 mAh/g for SWCNTs, up to 1100 mAh/g with modifications	[434,441,442]
Conductivity	Good conductivity but limited by structure	Very high conductivity (10^5–10^6 S/m)	[439,440]
Structural Integrity	Limited flexibility, prone to degradation	High tensile strength (~60 GPa), better structural stability	[439,440]
Irreversible Capacity	Relatively low, minor SEI formation	Higher irreversible capacity, reduced with additives and modifications	[434,444,447]

CNTs as Conductive Additives for LIBs

Composite electrodes were envisioned as an immediate solution to improve the performance of CNT-based electrodes for lithium-ion batteries. Many CNT composites with diverse lithium storage materials were investigated as anodes (e.g., SnO_2 [471,472], TiO_2 [473,474], Si [475,476], Ge [475], Sn [475,477], $CoFe_2O_4$ [478], As [479], P [480,481], Fe_2O_3 [414,415,482–487], MnO [475], MnO_2 [475], Mn_3O_4 [488], Co_3P_4 [489] and $Li_4Ti_5O_{12}$ [490–497]) or cathode materials ($LiFePO_4$ [363,498–505], V_2O_5 [506–509] $LiNi_{0.8}Co_{0.15}Al_{0.05}O_2$ [510], $LiCoO_2$ [511,512], $Li_2Mn_2O_4$ [513–516], Li_2FeSiO_4 [517] and $LiNi_{0.4}Mn_{0.3}Co_{0.3}O_2$ [518]). The CNTs reduce the additive mass by more than an order of magnitude compared to conventional carbon additives and provide a suitable percolation network to achieve acceptable electrical conduction. Group IVA elements (Si, Ge, and Sn) have higher specific capacities (372 mAh/g) than commercial graphite anodes.

With a theoretical specific capacity of about 4200 mAh/g, the lithiated silicon-lithium alloy $Li_{4.4}Si$ makes silicon one of the most promising anode materials for lithium-ion batteries. However, two main obstacles hinder the practical application of pure silicon: (a) its low electrical conductivity and (b) its crystalline alterations during lithiation and delithiation. The electrode experiences severe mechanical strain due to the approximately 300% volume expansion during lithium intercalation, which causes exfoliation and cracking. Furthermore, the mechanical stress breaks the electrical connections between the active materials, leading to anode failure after only a few operating cycles [475]. Several approaches were investigated to overcome these problems. The Si-CNT composite is an effective system for evaluating the attractive properties of CNT and Si. Weng et al. developed three-dimensionally aligned CNT/Si hybrids to create a novel anode material. After 100 cycles, the hybrid anode maintained 93% of its delithiation capacity, achieving 2562 mAh/g at a current density of 1 A/g. After 1000 cycles at 5 A/g, the delithiation capacity remained at 1055 mAh/g [476]. Their research showed that the areal density of the Si-coated CNT sheets and the 3D-aligned CNT/Si hybrid structure significantly impact the electrochemical performance. The impact of areal density on the specific capacity at 5 A/g is seen in Figure 10. Additional layers of both materials might be cross-stacked to raise the areal density from 0.14 to 1.68 mg/cm^2. However, as the areal density rose after the 50th cycle, a sharp decline in capacity was noted for the Si-coated CNT sheets. On the

other hand, the 3D-aligned CNT/Si hybrid demonstrated consistent capacity, making it a viable option for fulfilling the commercial demands of lithium-ion batteries (LIBs).

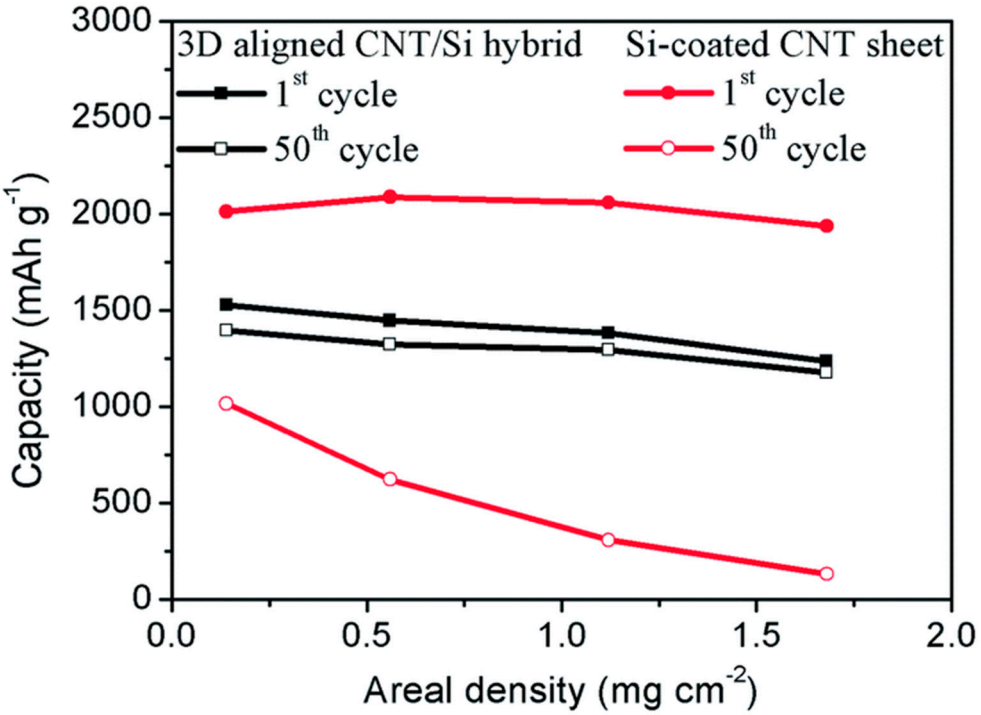

Figure 10. Impact of the areal density on the specific capacity at 5 A/g, Adopted with permission from [476].

Germanium has garnered significant interest due to its theoretical capacity of approximately 1600 mAh/g, along with its fast lithium-ion diffusivity and high electronic conductivity [519]. However, pure germanium (Ge)-based anodes experience significant volume expansion during the alloying reaction with lithium. As a result, electrical connections between the electrode material and the current collector can be disrupted, leading to capacity losses during cycling. To address this issue, Hao et al. developed an anode by electrodepositing Ge onto the surface of CNTs previously deposited on copper current collectors in ionic liquids [520]. The composite demonstrates superior reversible capacity and improved rate performance compared to the Ge nanoparticles. It delivers a reversible capacity of 810 mAh/g after 100 cycles at a rate of 0.2 C, with a coulombic efficiency exceeding 99%. The advantages of this composite include the softening effect of carbon nanotubes (CNTs) during cycling, enhanced charge transfer, and greater energy density [520]. Unfortunately, the production costs of these composites must be reduced before any commercial success as anode materials in LIBs is expected.

Because of its higher theoretical capacity (990 mAh/g) than graphite, tin, which forms lithium alloys, has attracted much study. Theoretically, a single tin atom can combine with 4.4 lithium atoms to create the $Li_{4.4}Sn$ alloy, which has a 993 mAh/g capacity [521]. Tin offers a high volumetric capacity of 2000 mAh/cm^3, but its gravimetric capacity is lower than that of silicon (Si) and germanium (Ge). However, tin's significant volume increase (about 300%) during lithiation is a disadvantage. Rapid tin particle agglomeration results from this expansion, which lowers the lithium storage capacity, breaks electrical contact with the current collector, and eventually impairs cycling efficiency [522]. Recently, Qin et al. produced a Sn-core/CNT-shell nano cable anchored interconnected carbon networks via a simple CVD process using a soluble salt template [477]. The Sn nanorods with a diameter of 50 nm are protected by 3 nm CNTs, as shown in Figure 11. Figure 11a illustrates the

procedure to fabricate the 3DCSn@CNT composites. Figure 11b,c shows the TEM images of the 3DC-SnO_2 composite that consists of numerous nanoparticles embedded in the 3D carbon nanosheets. Figure 11d–h shows the TEM images of the 3DC-Sn@CNT composite, in which the Sn-core/CNT-shell nano cables were successfully grown on the surface of the 3DC. The mesoporous structure observed in Figure 11f was formed during the CVD process and was probably caused by the removal of SnO_2. The 3DC-Sn@CNT composite showed good reversible capacity, 700 mAh/g, after 100 cycles. The 3DC-SnO_2 electrode, in contrast, showed reduced capacity and worse cycle stability. In contrast, the 3DC-Sn@CNT electrode outperformed the 3DC-SnO_2 electrode, achieving impressive average capacities of 550, 400, 300, 240, 180, and 100 mAh/g at current densities of 0.1, 0.2, 0.5, 1, 2, and 5 A/g, respectively. The 3DC-Sn@CNT electrode maintained a 650 mAh/g capacity when the current density was reduced to 0.1 A/g, even after cycling for an additional 130 cycles. This exceptional performance is attributed to the composite's unique architecture, where the core-shell nano cable structure protects the Sn nanorods from breaking apart during cycling. At the same time, the interconnected carbon networks with mesopores allow electrolyte penetration. Rapid electron movement is ensured by the conductive network formed by the entire hierarchical structure. Consequently, the 3DC-Sn@CNT electrode demonstrated exceptional electrochemical stability by delivering a 240 mAh/g capacity at 1 A/g [477].

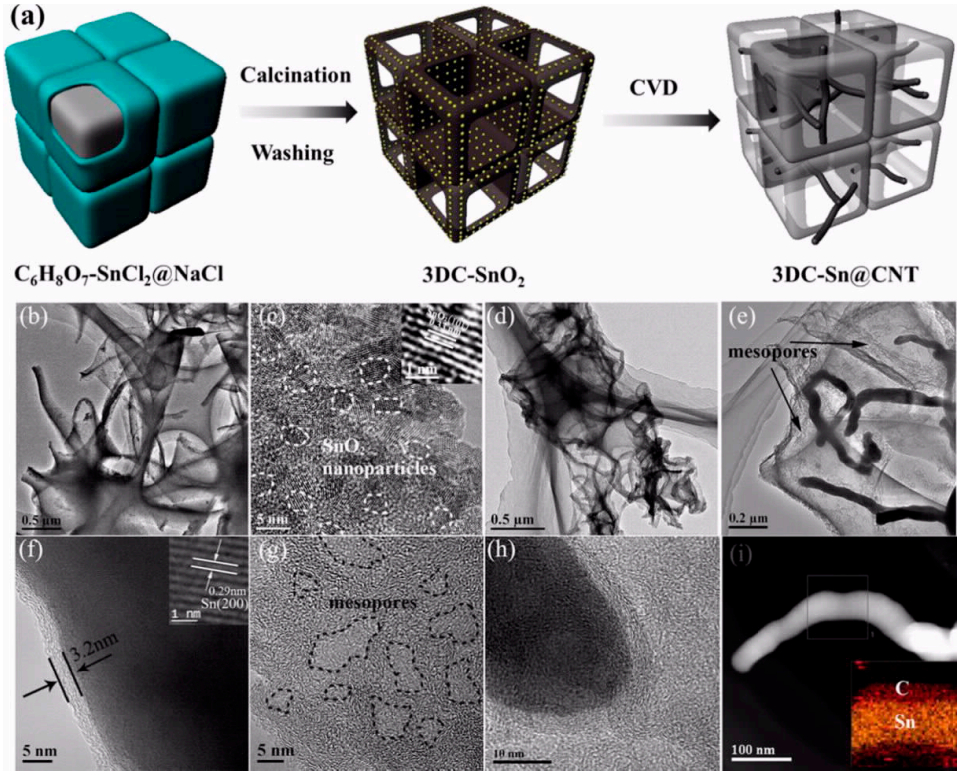

Figure 11. (**a**) The fabrication procedure for the 3DC-Sn@CNT composite. (**b**,**c**) TEM images of the 3DC-SnO_2 composite. (**d**–**h**) TEM images and (**i**) element mapping of the 3DC-Sn@CNT composite. Adopted with permission from [477].

The pnicogens (P, As, Sb, and Bi) have garnered much attention because of their high theoretical capacities based on the formation of Li_3X (X = P, As, Sb, or Bi) [479,523,524]. Arsenic possesses the fourth largest theoretical reversible capacity, 1073 mAh/g of the Li alloying elements (Ge, Si, and P) utilized for Li-ion battery anodes. Also, it has high volumetric capacity, 2057 mAh/cm^3. Unlike Ge, As is inexpensive, with a bulk cost approximately the same as Si [525]. The electrical conductivity of As is 3.3 × 10^6 S/m,

which is 1000 times greater than Si and far more air stable. When combined with multi-walled carbon nanotubes, Hays et al. obtained outstanding performance with Arsenic as a Li alloying anode material [479]. The reversible capacity was 746 mAh/g, and capacity fading was only 17% over 200 cycles, more than two times better than that previously reported (based on the entire electrode formulation mass) [526].

As-nano/MWCNT composite electrode rate performance was assessed between C/10 and 10 C (Figure 12). Under symmetric charge/discharge rates, the cells retained roughly 90% and 60% of their initial capacity at C/5 and C/2, respectively. The discharge (unload) could still be carried out at 2 C with about 85% of the initial discharge capacity when the charge rate was reduced to C/10. This illustrates that modest charge rates can result in excellent output power density. The greater dispersion of arsenic within the conductive matrix is responsible for the increased reversible capacity, less hysteresis, and improved capacity retention. Arsenic's toxicity necessitates an efficient recycling plan because its discharge potential is greater than certain other alloying elements. However, arsenic is desirable for lithium-ion anodes due to its low cost, high capacity, and stable cycling.

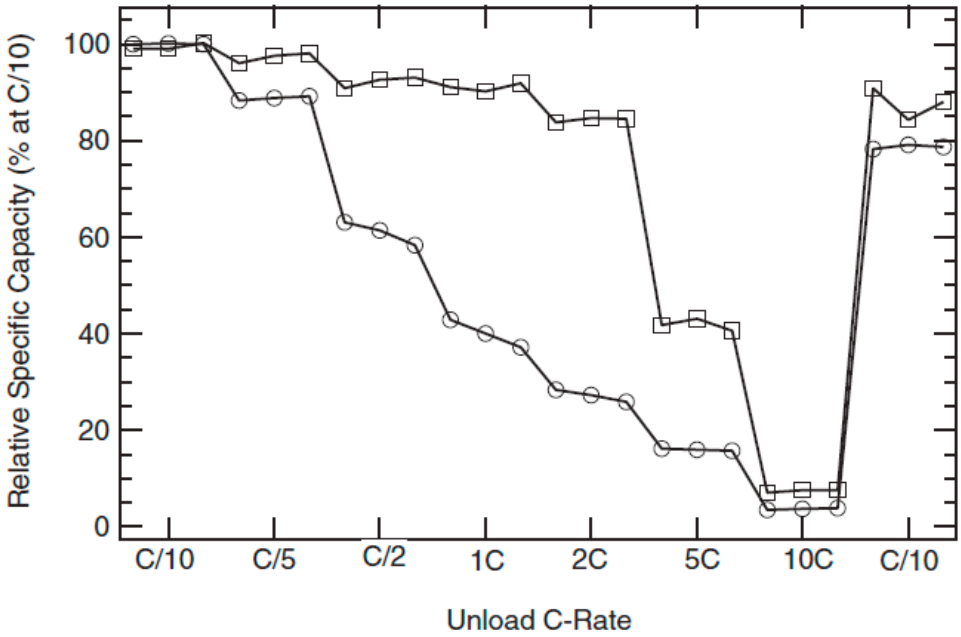

Figure 12. Rate performance of Asnano reduced on MWCNTs (squares, 70:17:13 As MWCNT:PAA *w*:*w*, loaded at C/10, unloaded at the specified rate) and Asnano reduced on MWCNTs (circles, 70:17:13 As MWCNT:PAA *w*:*w*, Symmetric Load/Unload) cycled in 1:1 FEC: DEC *w*:*w* with 1M LiPF6. Lines between data points are to guide the eye. Adopted with permission from [479].

Phosphorous has a remarkable theoretical capacity of 2600 mAh/g, considerably more significant than graphite. Ishii et al. fabricated a phosphorous encapsulated single-walled CNTs as anodes for LIBs [481]. The study demonstrated a high reversible capacity, with a capacity retention of 50% after ten cycles. However, they still suffer from volumetric changes and capacity fading, which indicates that Li^+ insertion and extraction were blocked by the presence of reaction products such as Li_xP [481]. Recently, Tojo et al. investigated a phosphorous-encapsulated/DWCNT composite as an anode for LIBs [480]. The composite material showed an excellent reversible capacity of 700 mAh/g and capacity retention of almost 100% after the 15th cycle, which was attributed to phosphoric oxides in the carbon nanotubes. The phosphorous is trapped in the inner walls of DWCNTs, which helps to mitigate volumetric change during cycling [480].

The use of transition metal oxides in lithium-ion batteries was first reported in 2000 [527]. However, significant obstacles to their use in LIBs include the large hysteresis

in their charge/discharge curves and relatively low electrical conductivity. In contrast, composite electrodes made from transition metal oxides and carbon nanotubes (CNTs) show enhanced electrochemical properties. Li et al. described a general approach to making CNTs-based nanocomposites via self-assembly that showed good potential for large-scale synthesis and exhibited improved electrochemical properties [528].

Room temperature spray deposition was employed to create a nanocomposite composed of vertically aligned CNT arrays decorated with necklace-type $Li_4Ti_5O_{12}$ nanoparticles produced in situ [495]. This composite exhibited outstanding cycling stability, maintaining a capacity retention of 97% after 500 cycles at a rate of 10 C and exceptional rate performance, achieving a specific capacity of 110 mAh/g at 300 C (see Figure 13a–f). The connection between the C-rate, electrode composition, and specific discharge capacity is shown in Figure 13c. These findings demonstrate that the discharge current and electrode composition significantly impact particular capacity. The coin cells demonstrated extraordinarily high capacities, approaching or even surpassing the theoretical capacity of $Li_4Ti_5O_{12}$ (LTO) at very low discharge rates below 2C. However, by increasing the discharge rates, the capacity drops above 30 C (78 wt%, 50 C (70 wt%) and 100 C (60 wt%). For comparison, the 45 wt% composite still maintains a remarkably high capacity of 110 mAh/g up to 300C. The results highlight the importance of LTO particle size, especially at extremely high rates [495].

The combination of short lithium-ion diffusion distances within $Li_4Ti_5O_{12}$ particles, the high electronic conductivity of carbon nanotubes, and a large contact surface area due to open pore geometry is crucial for achieving high-power performance and excellent cycling stability in $L_{i4}Ti_5O_{12}$ anodes. This is particularly effective when these anodes are prepared without the use of additional binders or conductive agents [495]. To create three-dimensional $Li_4Ti_5O_{12}$/carbon nanotubes/graphene composites (LTO-CNT-G), Chen et al. used ball milling and microwave heating [496]. At relatively high current densities, this composite outperformed $Li_4Ti_5O_{12}$/CNTs (LTO-CNT) and $Li_4Ti_5O_{12}$/graphene (LTO-G) composites regarding rate capability and cycling performance. The LTO-CNT-G composite demonstrated outstanding cycle stability and a high initial discharge capacity of 172 mAh/g at 0.2 C and 132 mAh/g at 20 C.

Figure 14A shows the electrochemical impedance spectra of LTO, LTO-CNT, LTO-Graphene, and LTO-CNT-G composite electrodes. The LTO-CNT-G composite electrode exhibits the lowest charge/transfer resistance, which suggests that it facilitates rapid electron transfer from the electrolyte to the LTO-CNT-G active material. This design results in reduced resistance during the intercalation and deintercalation of lithium ions thanks to the three-dimensional networks formed by graphene and carbon nanotubes (CNTs), as shown in Figure 14B [496].

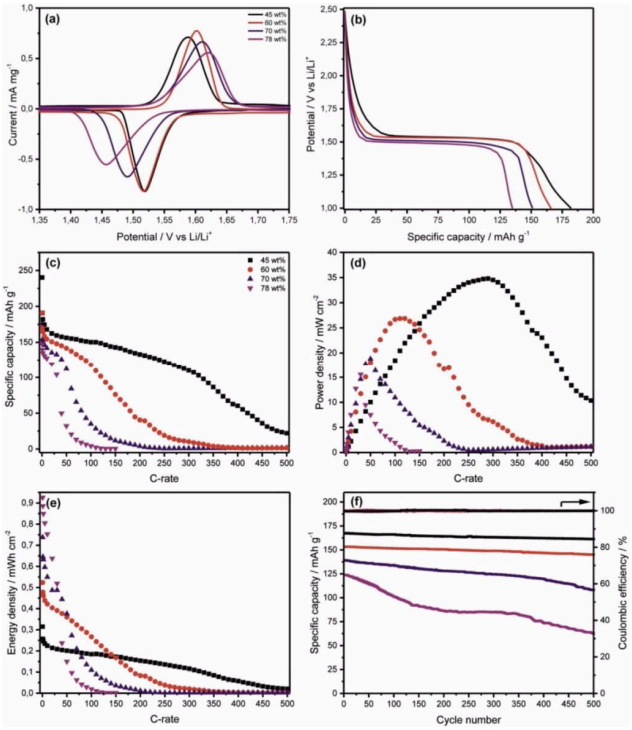

Figure 13. (**a**) Cyclic voltammograms at a sweep rate of 0.1 mV/s, (**b**) voltage profiles at 2C, (**c**) galvanostatic discharging up to 500C, (**d**) areal power density for discharging, (**e**) areal energy density for discharging, (**f**) long-term stability test at 10C. Adopted with permission from [495].

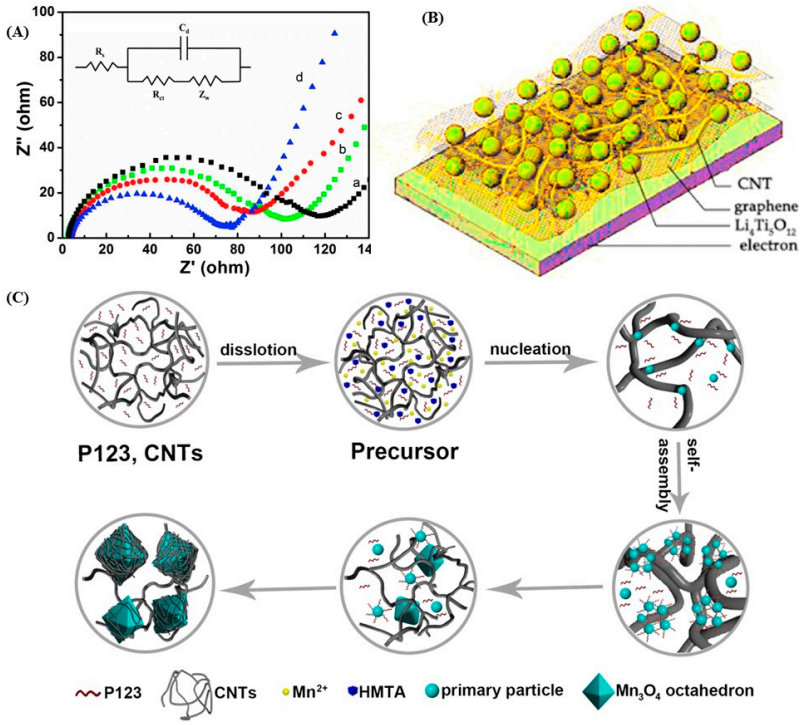

Figure 14. (**A**) EIS spectra of the LTO (a), LTO-CNT (b), LTO-G (c), and LTO-CNT-G (d) electrodes with corresponding equivalent circuit model (inset) [496] (**B**) Schematic diagram of the network structure in the LTO-CNT-G composite. Adopted with permission from [496]. Copyright © 2016 Elsevier. (**C**) Schematic of the forming process of CNT-entangled Mn_3O_4 octahedrons. Adopted with permission from [488].

Nanoscale structure-based anodes are promising candidates for lithium-ion batteries with high power capacity and long cycle life. In their review, Sehrawat et al. summarized the results of numerous research studies using transition metal oxides (TiO_2, Fe_2O_3, etc.) as anodes for LIBs [475]. The ternary CNTs@TiO_2/CoO nanotube composites were reported by Madian et al. as improved anode materials for high-performance LIBs [474]. The synthesis process consists of two main steps. First, well-ordered TiO_2/CoO nanotubes (NTs) are formed anodically from a titanium–cobalt (Ti-Co) alloy. Next, carbon nanotubes (CNTs) are grown horizontally on top of the oxide films using a straightforward spray pyrolysis technique. The CNTs serve as conductive networks, connecting the TiO_2 nanotubes from the opposite side of the current collector. The CNTs@TiO_2/CoO NTs electrode delivered an areal capacity of 455 $\mu Ah/cm^2$ when cycled at 50 $\mu A/cm^2$. Increasing the current from 50 to 500 $\mu A/cm^2$ has only a minor effect on areal capacity, which is still about 400 $\mu Ah/cm^2$. The electrode reversibly retains the same areal capacity, even after 80 charge/discharge cycles, when the current rates gradually decrease, demonstrating the composite electrode's outstanding rate performance. The study demonstrates that CNTs create a highly conductive network, which enhances Li^+-ion diffusivity, facilitating significant lithium insertion into the TiO_2/CoO NT framework, thereby achieving high capacity and excellent reproducibility in rate capability [474].

Fe_2O_3 is a promising transition metal oxide (TMO) considered for anodes in lithium-ion batteries (LIBs). It has a theoretical capacity of approximately 1007 mAh/g, is affordable and environmentally friendly. However, several drawbacks are observed when Fe_2O_3 is used directly as an anode for LIBs [475]. Various approaches were carried out to improve its electrochemical performance. Improvements in preparing CNTs-Fe_2O_3 is a practical approach to tackle these drawbacks. Recently, composites of Fe_2O_3 and COOH-MWCNT were synthesized using a simple hydrothermal method and investigated by Gao et al. [529]. This composite electrode exhibited a remarkable reversible capacity of 711.2 mAh/g at a current density of 500 mA/g after undergoing 400 cycles, in contrast to earlier research where the composites revealed low capacity at elevated current densities [414,415,482–487].

Mn_3O_4 has an initial reversible capacity of 869 mAh/g and 800 mAh/g after over 40 charge/discharge cycles [530]. Cui et al. prepared pompon-like MnO/CNT composite microspheres by pyrolysis of Mn_3O_4 and CNT mixtures [531]. The MnO/CNT composite microsphere anodes exhibited a high specific capacity of 841 mAh/g after 200 cycles at 0.1 A/g. Even at 0.38 A/g, the capacity was still 741 mAh/g after 250 cycles. The CNTs act as a support framework for the dispersion of oxides and electronic channels to strengthen the metal oxide structure and electron transfer. Xia et al. synthesized a nanocomposite of Mn_3O_4 octahedrons entangled in CNTs by a hydrothermal method assisted with a non-ionic surfactant (P123); Figure 14C [488].

High capacity and remarkable cycle life were revealed by the CNT-entangled Mn_3O_4 octahedrons, which showed good capacity of over 800 mAh/g at a 0.2 C rate for 200 cycles and maintained a high capacity of 678.4 mAh/g at a 0.5 C rate even after 400 cycles. By acting as a shape-directing agent, P123 made it easier for MnO_4 octahedrons to form. Meanwhile, CNTs were essential in encouraging the development of homogeneous MnO_4 nuclei, which led to the formation of consistently organized and widely distributed CNT-entangled MnO_4 octahedrons. Furthermore, the CNTs served as elastic buffers, reducing the likelihood that volume variations during cycling would cause MnO_4 octahedrons to break. The material's cyclic stability was much improved by this structural stabilization [488].

Cobalt ferrite ($CoFe_2O_4$, CFO), which is a notable example of a binary transition metal oxide (TMO), has attracted considerable attention for use in lithium-ion batteries (LIBs) because of its high theoretical specific capacity (916 mAh/g), affordability, safety, and non-

toxicity [532]. Nonetheless, CFO encounters difficulties such as low electrical conductivity, significant volume changes, and intense pulverization during charge/discharge cycles, which impair its electrochemical performance [533]. Similar to other TMOs, the incorporation of carbon nanotubes (CNTs) has been shown to effectively enhance the electrochemical characteristics of CFO [534].

In a sustainable manner, alginate was employed as a precursor to create highly porous three-dimensional (3D) aerogels that include cobalt ferrite nanoparticles (CFO NPs) and CNTs. This cost-effective and simple method greatly improved the functionality of CFO as an anode material for lithium-ion batteries (LIBs). Within these hybrid aerogels, CFO NPs linked by CNTs are contained in a carbon aerogel matrix, producing a 3D structure with a large surface area. This configuration accommodates volume expansion and facilitates efficient pathways for ion and electron transport, resulting in enhanced LIB performance. With an optimal CNT content of 20%, the hybrid aerogels demonstrated a reversible capacity of 1033 mAh/g at a current rate of 0.1 A/g, 874 mAh/g after 160 cycles at 1 A/g and 516 mAh/g at 5 A/g. Utilizing raw materials derived from abundant biomass highlights an effective, eco-friendly, and cost-efficient approach for scaling up the production of TMO anodes for high-performance LIBs [478]. The cathode in LIBs, which acts as the source of Li^+ ions, plays a crucial role in influencing battery performance. The addition of CNTs is expected to further propel the advancement of high-performance LIBs. $LiFePO_4$ stands out as a promising cathode material due to its affordability, excellent thermal stability, environmental friendliness, and safety. $LiFePO_4$/CNT hybrid materials significantly improve Li^+ ion diffusion and diminish charge transfer resistance. A composite material C@$LiFePO_4$/CNT (C@LFP/CNT) containing amorphous and graphitized conductive carbons forms a porous structure with favorable kinetics for electron and Li^+ ion transport [535].

Figure 15 shows the electrochemical evaluations reveal that the polarization between the charge and discharge plateaus in C@LFP/CNTs is smaller than in C@LFP, indicating improved kinetics and utilization of LFP. Furthermore, C@LFP/CNT exhibits higher discharge capacities of 126, 115, and 102 mAh/g at 5, 10, and 20 C, respectively, compared to 92, 71, and 50 mAh/g for C@LFP under identical conditions. The C@LFP/CNT electrode delivers a reversible capacity of 113 mAh/g at 10 C over 1000 cycles, retaining 98% of its capacity. Additionally, its volumetric energy density at 10 C reaches 443 Wh/L, approximately 1/3 greater than commercial LFP/C (323 Wh/L). These results emphasize the promise of C@LFP/CNT composites for cutting-edge energy storage uses in electric and hybrid electric vehicles.

Feng et al. studied the effect of CNTs on LFP cathode electrochemical performance [498]. Herein, they used a hydrothermal approach involving ethylene glycol (EG) and prepared a 3D LFP/CNTs cathode in which the network of CNTs effectively coats and connects LFP nanoparticles. A few different weight percentages of CNTs were tested—1 wt%, 4 wt%, 7 wt%, and 10 wt%—and the 4 wt% CNT composites displayed the best discharge specific capacity of 154.6 mAh/g at 0.1 C. This exceeds the capacity noted by Tan et al., who showed a performance of 150 mAh/g at a rate of 0.2 C [501]. The 4 wt% CNT composites maintained the same specific capacity after five cycles across rates of 0.1 C, 0.5 C, 1 C, 5 C, and 10 C.

This material demonstrated excellent stability over 50 cycles, maintaining capacities of 130 mAh/g and 80 mAh/g at 1 C and 10 C, respectively. The improved stability was related to a finer particle size of LFP synthesized via the hydrothermal method with EG. A 3D network structure of CNT improved the conductivity of the material. Such studies show a great opportunity for LFP/CNT composite in Li-ion battery applications [498]. Qiao et al. also prepared the LFP/CNT nanocomposites exhibiting excellent cycling stability [500].

Figure 16 shows the synthesis schemes for (a) PVP-wrapped CNTs and (b) $LiFePO_4$/CNT nanocomposites, illustrating novel methods for fabricating these high-performance materials.

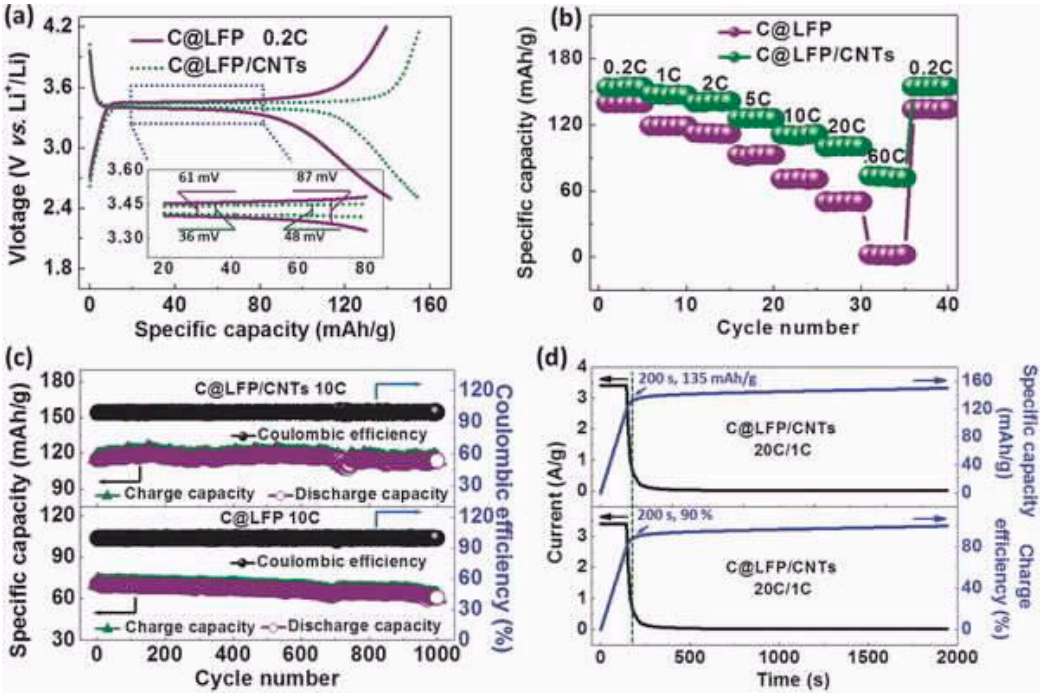

Figure 15. Electrochemical properties: (**a**) charge/discharge profiles at 0.2 C, inset: the magnified selected-region comparing the potential plateaus, (**b**) rate capabilities from 0.2 to 60 C, (**c**) cycling stabilities combined with Coulombic efficiency at 10 C of C@LFP and C@LFP/CNTs, and (**d**) charge current and capacity as well as charge efficiency of C@LFP/CNTs as a function of charge time. Adopted with permission from [535]. Copyright © 2016 WILEY—VCH Verlag GmbH & Co.

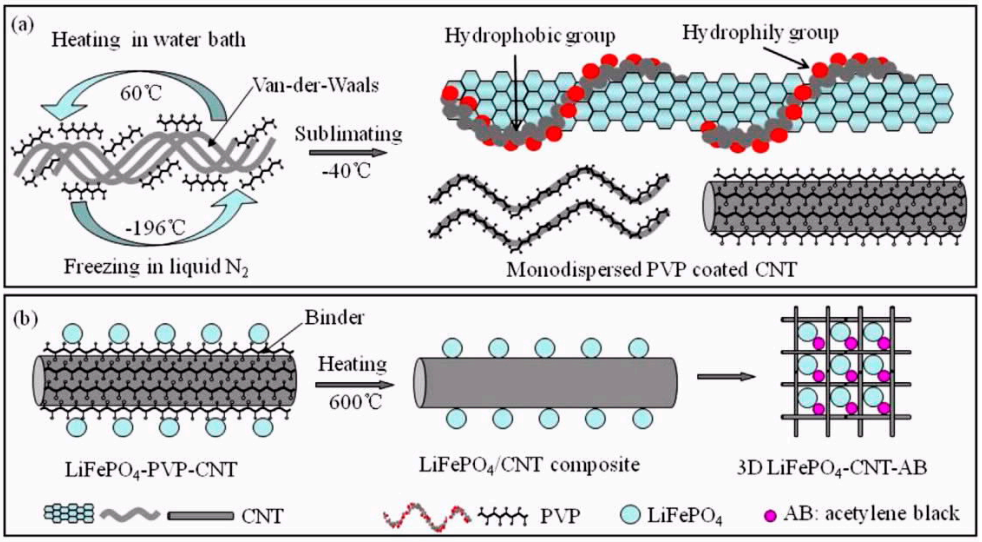

Figure 16. Schematic description of three-dimensional conductive network of monodispersed CNTs. (**a**) PVP-coated CNTs; (**b**) three-dimensional conductive network with CNTs and acetylene black. Adopted with permission from [500]. Copyright © 2016 Elsevier.

This composite electrode demonstrated a high discharge capacity of 123 mAh/g, exceeding the previously reported range of 100–115 mAh/g, and exhibited a low-capacity loss of 1.6%, compared to the previously reported 6–13%. This performance was attained after 1000 cycles at 10 C with 3 wt% CNTs, as shown in Figure 17a–c. After 3400 cycles at

10 C, a capacity of approximately 100 mAh/g was still achieved, indicating a capacity retention of 80%. The major advantage of $LiFePO_4$/CNT nanocomposites is that the capacity loss is four to eight times smaller than that of earlier $LiFePO_4$/CNT and $LiFePO_4$/graphene nanocomposites [500]. The impressive performance and extended cycle life result from the combined effect of the high lithium-ion diffusion rate in $LiFePO_4$ nanoparticles and the highly conductive three-dimensional networks made up of uniform carbon nanotubes that lack broken and tangled structures. These $LiFePO_4$-based electrode materials must be helpful for lithium-ion batteries in electric vehicles such as PHEVs, AEVs, and HEVs [500].

Due to its easy preparation, long cycle life (greater than 500 cycles), and reliable electrochemical cycling performance, LCO has been one of the most prevalent cathodes used in lithium-ion batteries (LIBs) for the past twenty years. In theory, $LiCoO_2$ can achieve a maximum theoretical reversible capacity of 274 mAh/g; however, around 140 mAh/g of reversible capacity is typically obtained since only half of the lithium ions can be reversibly inserted or extracted from cathodes based on $LiCoO_2$. Recently, super-aligned carbon nanotubes, SACNTs, instead of regular CNTs, have gained much attention. This is mainly due to their "superaligned" nature, most significant aspect ratio, clean surface, and strong Van der Waals force between the nanotubes and bundles [536–539]. Luo et al. reported the preparation of binder-free LCO/CNTs composite by USCD [511].

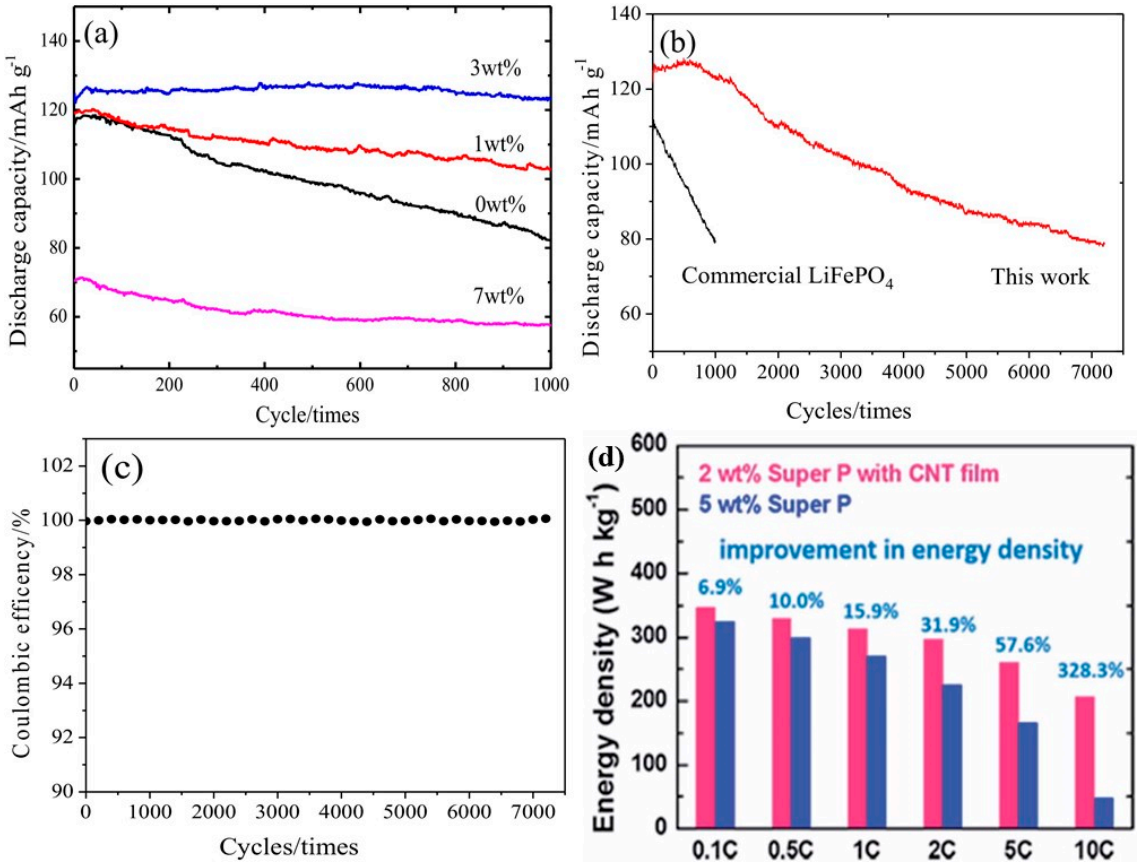

Figure 17. (**a**) Discharge capability vs. charge (1 C)/discharge (10 C) cycle; (**b**) capacity-cycle relation of the $LiFePO_4$/CNTs(3 wt%)/AB(7 wt%) and commercial $LiFePO_4$/AB(10 wt%); (**c**) coulombic efficiency vs. cycle number of the $LiFePO_4$/CNTs(3 wt%)/AB(7 wt%). Adopted with permission from [500]. (**d**) Energy densities (based on the total mass of the electrode material layer and the current collector) of the $LiCoO_2$-2 wt% Super P-SACNT and the sandwich-structured $LiCoO_2$-5 wt% Super P electrodes (of the same thickness). Adopted with permission from [512].

The 3D LCO/SACNT composite cathodes with 3 wt% CNTS exhibited high electrical conductivity, high flexibility, high energy density, and outstanding cycling stability, such as 151.4 mAh/g at 0.1 C with capacity retention of 98.4% after 50 cycles and 137.4 mAh/g at 2 C corresponding to the capacity retention of 90.8%. This cathode has shown the highest rate capability so far for micrometer-sized $LiCoO_2$, owing to the direct conductive bridges that CNTs form with LCO particles, which enabled fast electron transport and optimal utilization of the active material. These composites' high strength and high flexibility are good in withstanding the volume changes in the cathodes with cycling and achieving better cycling stability. No binder is involved, which is astonishing, considering such high energy density for a battery. This binder-free $LiCoO_2$-3 wt% SACNT composite showed a remarkable 20.6% increase in specific mass capacity and a full 64% increase in specific volume capacity over the optimized classical $LiCoO_2$ with 10 wt% Super P and a binder. The processing time in the USCD is very fast, only 10 min for ultra-sonication, and is thus easy to adopt in large-scale production. It was further demonstrated that this process might prepare SACNT composites tailored for other functional materials, extending applications to practically all fields. Yan et al. [512], proposed a straightforward and practical method: using cross-stacked SACNT films as conductive layers to create sandwich-structured $LiCoO_2$ cathodes for lithium-ion batteries (LIBs) with enhanced performance. The three distinct conductive layers of SACNT significantly improved conductivity and in turn the overall performance of the cells.

The sandwich-structured $LiCoO_2$-2 wt% Super P-SACNT cathodes with a compatible thickness for commercial LIBs showed excellent rate capability, such as 109.6 mAh/g at 10 C and a 1668% improvement compared to composites without SACNT films. These are some of the best-reported rate performances for commercial micro-sized $LiCoO_2$ particles with Super P [540–542].

Figure 17d shows the gravimetric energy density of $LiCoO_2$-2 wt% Super P-SACNT electrode vs. $LiCoO_2$-5 wt% Super P electrode. The latter composite contains 5 wt% Super P to render it with similar conductivity as the $LiCoO_2$-2 wt% Super P-SACNT electrode. However, the sandwich-structured electrode outperformed the other electrode at all current densities used in this work. In particular, the $LiCoO_2$-2 wt% Super P-SACNT cathode exhibited a gravimetric energy density of 206.7 Wh/kg at 10 C, which is about 328.3% higher than that of the $LiCoO_2$-5 wt% Super P electrode delivering 48.3 Wh/kg. The $LiCoO_2$-2 wt% Super P-SACNT electrode also exhibited an exceptionally high volumetric energy density of 695.8 Wh/L, which is over 310% higher than that of its counterpart $LiCoO_2$-5 wt% Super P electrode. Such improvements were indispensably linked with the well-engineered sandwich structure of the electrode. This is because each layer of $LiCoO_2$ particles, according to how the electrodes were structured in Figure 18a, was in close contact with the conductive layers of SACNTs. This close interaction between the active material and conductive layers enhances efficient electron transport and lithium-ion diffusion, resulting in the exceptional electrochemical performance of the sandwich-structured cathode.

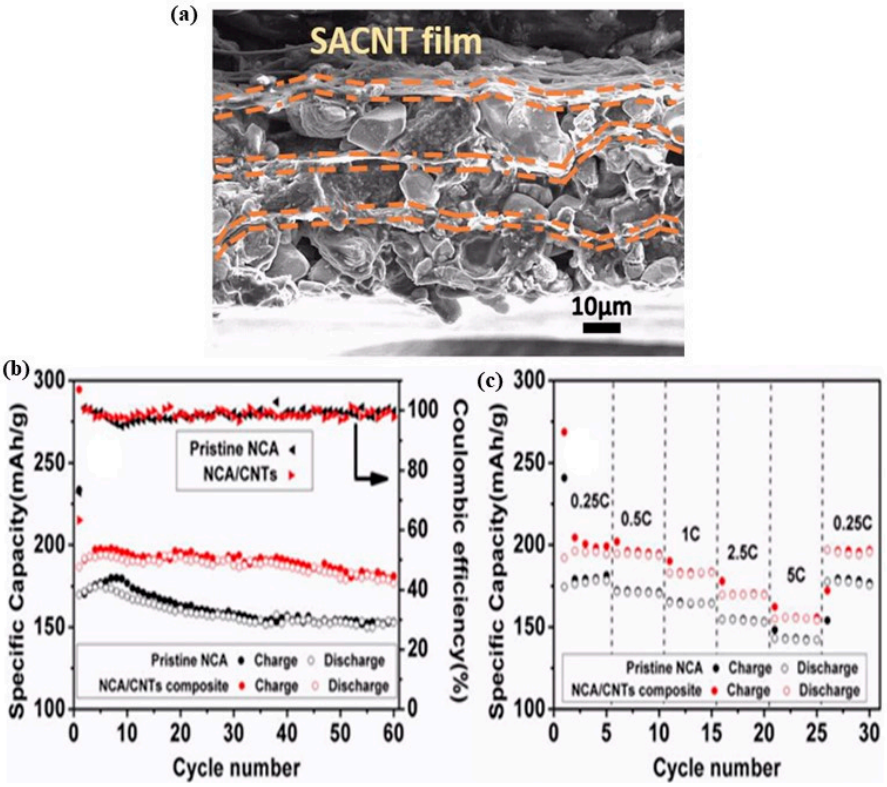

Figure 18. (**a**) Cross-sectional SEM image of the three-layer $LiCoO_2$—Super P—SACNT cathode after 50 cycles. Adopted with permission from [512]. (**b**) Cycling performance at 0.25 C rate. (**c**) Rate performance of pristine NCA and NCA/CNT (10 wt%) composite. Adopted with permission from [510].

These results indicate good electronic transport to almost all the active material in the composite; polarization was also effectively limited while excellent cycle stability and rate capability were achieved for the sandwich-structured $LiCoO_2$ Super P–SACNT electrodes. Besides that, the great performance did not depend on electrode thickness, which means that thickness does not need to be sacrificed for a decent specific capacity. The manufacturing process, the suitable approach for commercialization, affordability, and exceptional electrochemical characteristics of the sandwich-structured electrode indicate that it holds significant promise for large-scale production of high-performance electrodes for LIBs.

Mn is abundant, inexpensive, nontoxic, and safe while operating at higher electrode potential with acceptable theoretic capacity in $LiMn_2O_4$. The rate capability is poor because of low electronic conductivity, which is approximately 10^{-6} S/cm [543]; poor cycling stability caused by manganese dissolution, structural changes due to Jahn–Teller distortion from cubic to tetragonal because of the high spin-state Mn^{3+}, and electrolyte decomposition [544] have remained drawbacks for the large-scale commercial applications of Mn-based electrodes in high-power lithium-ion batteries. In the last years, however, $LiMn_2O_4$/conductive carbon composites have awakened considerable interest since the carbon additive improves electrical conductivity and improves the rate capability and cycling stability. $LiMn_2O_4$-MWCNT composites were prepared by Liu et al. [516], by the sol–gel method.

Furthermore, the nanocomposites demonstrated impressive cycle performance, achieving an exceptional capacity retention of 99% after 20 cycles, while $LiMn_2O_4$ nanoparticles experienced a 9% reduction in initial capacity over the same number of cycles. The charge-transfer resistance of the nanocomposites, as measured by AC impedance, is significantly lower compared to that of spinel $LiMn_2O_4$ [516]. Yan et al. successfully created binder-

free $LiMn_2O_4$–SACNT composite cathodes using USCD, achieving cycling stability with a capacity of 107 mAh/g at a rate of 0.1 C, along with a capacity retention of 90.4% after 90 cycles and a rate performance of 89.6 mAh/g at 2 C. These findings suggest that USCD could be a viable method for fabricating other functional SACNT composites, such as LFP, LCO, LMO, NCA (Nickel Cobalt Aluminum Oxide), and more, thereby expanding the potential uses of SACNT composites. Tang et al. synthesized highly crystalline spinel-type $LiMn_2O_4$/MWCNT composites through an innovative two-step approach, precisely the acetone-accelerated hydrothermal reaction that utilizes MnO_2/MWCNT precursor as the manganese source [515]. The composite of lithium manganate spinel $Li_{0.81}Mn_2O_4$/MWCNT demonstrated a significant specific capacity of 145.4 mAh/g at a C-rate of 0.1, which is nearly equal to the theoretical capacity of $LiMn_2O_4$, recorded at 148 mAh/g.

These electrodes demonstrate remarkable performance at high rates and exhibit good cycling stability. For instance, even with a high charge/discharge current rate of 20 C, the discharge capacity reaches 114.8 mAh/g. After undergoing 1000 cycles at a 1 C rate, the specific capacity decreased from an initial 140.4 mAh/g to 98.7 mAh/g, resulting in a capacity retention of 70.3%. Conjecturally, this long-term cyclability can be achieved when the Li-Mn spinel shows high crystallinity, and besides, the MWCNTs also enhance the conductivity to support both the electrical conduction network and the mechanical framework within the electrode in repeated charge/discharge cycling. $LiNi_{1-x-y}Co_xAlyO_2$ was fabricated by substituting Ni^{3+} with Al^{3+} and Co^{3+} in $LiNiO_2$ [545]. In addition, these cathode materials exhibit better electrochemical properties, thermal stability, and low cost with low toxicity. Among the diverse Ni-based ternary layered metal oxide materials, $LiNi_{0.8}Co_{0.15}Al_{0.05}O_2$ (x = 0.15, y = 0.05) draws most attention in LIBs owing to an optimal balance between capacity and structural stability. However, there are still problems that have not been solved.

1. Residual Ni^{2+} in NCA tends to migrate from the transition metal layers to the Li^+ slabs and form an electrochemically inactive NiO-like phase, which has brought about its degradation during the charge/discharge process;
2. The highly oxidized Ni^{4+} with the electrolyte during cycling involves some side reactions, which account for the degradation of NCA;
3. The pristine material's poor electrical conductivity further deteriorates its electrochemical performance [546,547]. Hence, improving cycling stability and safety are the key concerns for NCA applications.

Yoon et al. first reported the preparation of NCA/graphene composite cathode via ball-milling [548]. Some types of modifiers up to now have been inert materials with good stability; theyhave poor electrical conductivity resulting in an increase in electrode polarization. Zhang et al. for the first time reported that CNTs as surface modifiers for NCA through a simple and mild mechanical grinding method did not destroy the crystal structure and morphology of NCA.

The NCA/CNT-10 wt% composite demonstrates significantly improved electrochemical performance (cycling stability and rate capability) compared to pristine NCA. After 60 cycles at a 0.25 C rate, the reversible specific capacity of the NCA/CNT composite reaches 181 mAh/g, which is 18% greater than that of pristine NCA at 153 mAh/g. The composite exhibits an excellent retention capacity of 99% following 60 cycles. Even at a high current rate of 5 C, the NCA/CNT composite maintains a reversible specific capacity of 160 mAh/g, whereas pristine NCA only achieves 140 mAh/g, as illustrated in Figure 18c. When the current density is reduced to 0.25 C, nearly 100% charge/discharge specific NCA/CNT composite capacity is restored, demonstrating excellent reversibility. Therefore, the CNTs dispersed homogeneously on the surface of NCA particles offer better electrical

conductivity and effectively suppress side reactions with liquid electrolytes. The CNTs enhance the electrochemical performance of NCA cathodes by decreasing the total resistance of the electrode from 145.13 Ω for the pristine NCA to 110.83 Ω for the NCA/CNT composite [510].

Numerous researchers have explored different compounds involved in conversion reactions, including metal nitrides, sulfides, fluorides, and oxides, as part of a novel approach to creating high-capacity electrodes that accommodate more than one lithium ion for every transition metal atom. Vanadium pentoxide (V_2O_5) has been suggested as a potential cathode material, noted for its low cost and abundance, and it demonstrates significantly greater energy density compared to $LiMn_2O_4$, $LiCoO_2$, and $LiFePO_4$ [507,549]. The primary disadvantage is the multiphase transitions during charge and discharge cycles (resulting in multiple voltage plateaus), leading to structural damage in V_2O_5. In the past five years, carbon nanotubes (CNTs) have been effectively utilized as an additive to enhance both the structural stability of V_2O_5 and the electrochemical performance of V_2O_5 cathodes. Zhou et al. developed a composite of vanadium oxide nanosheets and multi-walled carbon nanotubes (MWCNTs) using the sol–gel process followed by hydrothermal treatment. The resulting nanosheet–MWCNT composite demonstrated a clear single-phase transition, producing a high specific capacity and impressive cycling stability due to its sheet-like nanostructure and the uniform distribution of MWCNTs [508]. Cao and Wei developed hybrid films of V_2O_5 and SWCNTs featuring a mesoporous structure using a straightforward floating chemical vapor deposition, followed by the controlled hydrolytic deposition of V_2O_5 nanoparticles [509]. The hybrid films were evaluated as cathodes for LIBs and demonstrated a high-rate capacity of 548 mAh/g at a discharge rate of 1 C (~300 mA/g). A detailed electrochemical analysis concluded that SWNTs improve Li^+-ion diffusivity by two to four orders of magnitude, significantly facilitating lithium-ion transport, and the high electrochemical performance is for these types of cathodes in energy storage devices [509].

Figure 19a shows a schematic representation of the ice-templating "brick-and-mortar" assembly to make ribbon-like V_2O_5 nanoparticles and CNTs into two-dimensional (2D) porous sheet-like V_2O_5-CNT nanocomposites. The sheet-like V_2O_5-CNT nanocomposite possesses unique structural characteristics, including hierarchical porous structure, 2D morphology, large specific surface area, and internal conducting networks, which lead to superior long-term cycle life and significantly enhanced rate capability as a cathode material for LIBs [506].

The 3D composite electrode demonstrated impressive capacities at elevated rates: 240 mAh/g at 5 C, 180 mAh/g at 10 C, and 160 mAh/g at 20 C. After 300 cycles at 5 C, the sheet-like V_2O_5-CNT nanocomposite retained 71% of its initial discharge capacity, exhibiting a minimal capacity loss of only approximately 0.097% per cycle. This represents the lowest capacity fade per cycle reported for V_2O_5 or V_2O_5-based materials [550–559]. The ice-templating approach by Cheng et al. to prepare a sheet-like nanocomposite with an interconnected 2D conducting network provides a new way to rationally design novel cathode materials with a well-defined architecture for next-generation LIBs [506].

Other non-conventional cathodes, such as Li_2FeSiO_4, can achieve a capacity of 331 mAh/g through a potential two-electron transfer reaction [560]; this shows great potential for applications in high-energy batteries. However, its capacity suffers from diminished reaction activity caused by silicates' very low electronic and ionic conductivity, making conductive and flexible carbon materials like CNTs attractive additions [561]. Wang et al. presented a rational engineering strategy for creating a highly active Li_2FeSiO_4 by designing a three-dimensional (3D) porous composite of Li_2FeSiO_4 integrated with CNTs [517].

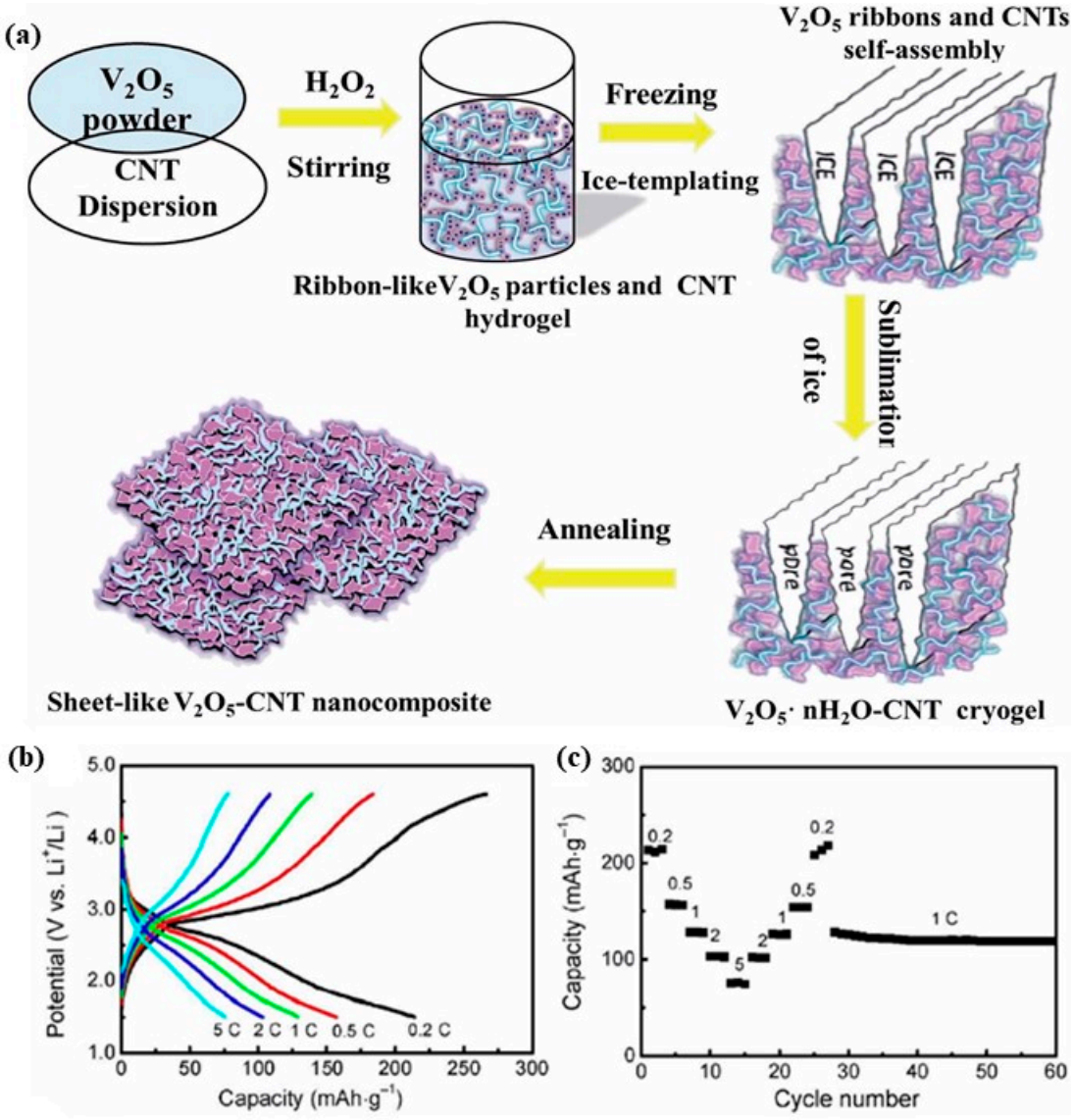

Figure 19. (**a**) A diagram illustrating the creation of a sheet-structured V_2O_5–CNT nanocomposite via ice-templating using a "brick-and-mortar" assembly method. The blue tubes symbolize CNTs while the pink ribbons denote V_2O_5. Adopted with permission from [506]. Rate capability of 3D Li_2FeSiO_4–CNT at various current rates: (**b**) Galvanostatic charge and discharge curves at various rates. (**c**) Rate cycling performance at various rates and a fixed rate of 1 C. Adopted with permission from [517].

The interconnected skeleton composed of CNT facilitates efficient electron transport, while the abundant mesopores allow for unobstructed electrolyte penetration and storage within the 3D Li_2FeSiO_4-CNT structure. This 3D composite achieved a reversible capacity of 214 mAh/g at a rate of 0.2 C and maintained 96% of its capacity after 40 cycles (refer to Figure 19b). Furthermore, it demonstrates significant rate capability when tested at different current rates (Figure 19c). The electrode exhibited capacities of 214, 158, 129, 103, and 79 mAh/g at rates of 0.2, 0.5, 1, 2, and 5 C, respectively, which are considerably higher than those of the Li_2FeSiO_4 electrode without CNT. This impressive rate capability is on par with or exceeds that of many well-constructed Li_2FeSiO_4/C composites [562–564].

The engineering approach helps fabricate other silicate and phosphate electrodes that suffer from poor charge transport, and this approach opens up new opportunities to design electrodes with improved kinetics [565]. Many research efforts are currently focused on identifying electrode couples in batteries that offer high gravimetric and energy densities to

meet the growing demand for energy storage while reducing material costs. Lithium-sulfur and lithium-air batteries are considered promising candidates for the next generation of rechargeable lithium batteries [566,567].

It has garnered significant interest because of its high energy density, affordable raw materials, and eco-friendliness. Despite these qualities, key challenges with the current Li-S battery include limited discharge capacity, inadequate cycle performance, and low coulombic efficiency. The insulating property of sulfur, measured at 5×10^{-30} S/m, along with the migration of polysulfides, contributes to these issues. Li_2S_x; $2 < x < 8$, during the charge/discharge process, causes a capacity fade, which is a serious deterrent to the commercialization of the Li-S battery [568]. Efforts to rectify these challenges include using porous CNTs infused with sulfur to enhance the utilization of sulfur in the pores in the carbon framework and improve cycle life accordingly [569]. This allows for the realization of a lightweight sulfur cathode with excellent electrolyte wetting and decreased polysulfide migration due to a high electrolyte absorbability provided by the CNTs network. Furthermore, the composite hierarchical porous structures were synthesized by synthesizing the CNTs networks with various micro/mesopores/macropores, which might provide better cycling performance. The authors' evaluation of a S-multi-wall carbon nanotube composite cathode, comprising 20 wt % MWCNTs, 20 wt % conductive carbon, 50 wt % sulfur, and 10 wt % poly(vinylidene difluoride), demonstrated a greater discharge capacity and extended cycle life in comparison to a standard sulfur cathode that includes 40 wt % conductive carbon, 50 wt % sulfur, and 10 wt % PVdF. The enhancement in performance is credited to the inclusion of MWCNTs, which offer a high surface area for polysulfide absorption and a three-dimensional conductive network that improves electron transport [570–576]. Kazazi et al. investigated the effect of the preparation method of CNTs on the morphology and electrochemical properties of sulfur/MWCNT composite cathodes [575]. Sulfur–MWCNT composites are prepared by a simple ball-milling method (S/MWCNT-1) and a two-step process involving liquid-phase infiltration followed by melt diffusion (S/MWCNT-2). Compared to the simple ball milling, the latter method offered better distribution of sulfur and favored the penetration of sulfur into the pores and hollow tubes of the MWCNTs, thus showing better electrochemical performance. The infusion of sulfur into MWCNT pores is believed to trap polysulfides and reduce active material loss during cycling, improving cycle performance. For example, at a relatively high current rate of 0.5 C, the initial discharge capacity of composite S/MWCNT-2 reached 866 mAh/g, and the capacity remained as high as 602 mAh/g after 50 cycles, much higher than that of S/MWCNT-1. Moreover, sulfur doping in the pores of MWCNTs reduces the formation of the passive layer (Li_2S_2/Li_2S) on the cathode surface during cycling and hence allows for easier de-intercalation/intercalation of Li^+ ions during the process [575]. On the contrary, most studies propose entrapment of polysulfides since the areal density of the sulfur in the cathode is less than 2 mg/cm^2. Sulfur loading should be further significantly increased (>6 mg/cm^2) to compare it with the electrochemical performance of state-of-the-art Li-ion batteries. This is a research topic currently being pursued. One potential advantage of binder-free cathodes is preventing the rise of so-called "dead weight" (inactive material in electrodes), which has many negative consequences for energy density. Patel et al. also prepared binder-free electrodes that enabled ~3 mg/cm^2 (~40wt.% S) sulfur loading to be increased to ~9 mg/cm^2 (~60wt.% S) in 3D CNTs [577]. The preparation was by a simple thermomechanical pressing of sulfur at ~155 °C onto the 3D free-standing CNTs. In the end, it can reach a maximum areal capacity of ~6 mAh/cm^2 at a sulfur loading of ~9 mg/cm^2 after 100 cycles for the binder-free 3D CNTs/S electrode, which is higher than that of present Li-ion batteries. That the binder-free cathode showed encouraging performance toward Li-S batteries with high loadings deserves further discussion and opens up

new ways to design other binder-free electrodes [577]. Large efforts were concentrated on the problems of polysulfide dissolution and diffusion of dissolved polysulfides. The main part that participates in Li-S batteries and enables the solving of this problem is the separator, which prevents the physical contact of the electrodes and may affect the transport of ions. Compositions, porosities, and wettability are just some of the properties of separators that could impact energy density, cycle life, or even battery safety. Also, conductive coating or layer applied to the separator can be highly beneficial in transporting electrons or ions, improving the electrolyte uptake, and mitigating the shuttle effect of polysulfides. Chung et al. prepared CNT-coated separators through a simple vacuum filtration method, and experiments showed that the modified separator Li-S cells exhibited high discharge capacity, excellent rate performance, and long cycle life. However, low efficiency and safety problems encountered (separator rupture) may be related to the vacuum filtration process. A facile and efficient route to apply the coating of CNTs on a commercial separator is urgently required [578–581]. Lui et al. [572] reported an organically modified carbon nanotube coating layer on the separator to optimize structure and enhance performance for Li-S batteries. (Figure 20). Polysulfides could be accommodated inside the micropores in CNTs formed by grafted long-chain molecules and tube-like CNTs. Hydrophilic groups helped trap polysulfides to suppress the shuttle effect. The coating of organically modified CNTs improved the high-temperature stability of the battery, and the conductive nature of CNTs contributed to a decrease in internal resistance.

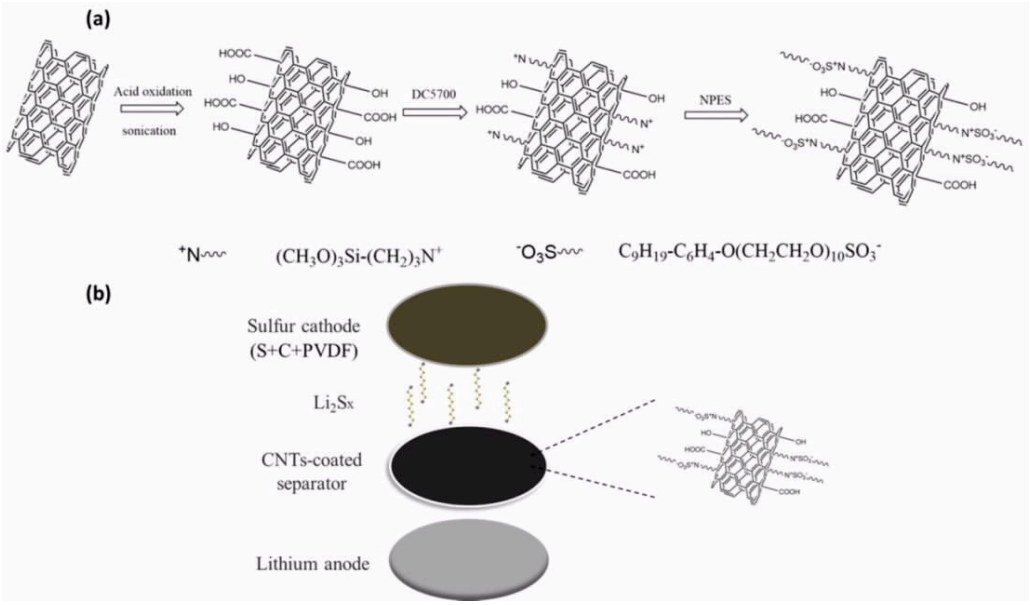

Figure 20. Schematic illustration of (**a**) the organic modification process of carbon nanotubes and (**b**) the cell configuration of lithium-sulfur (Li-S) batteries. Adopted with permission from [572].

According to Figure 21, the cell with the separator coated by CNTs revealed higher performance: the initial discharge capacity was higher by 115%, and the capacity after 100 cycles was higher by 161% in that system. Moreover, concerning the cycling rates from 0.1 C to 2 C, the battery with a CNTs-coated separator still had a capacity of 90.2% of the initial capacity when the current density went back to 0.1 C [572]. In this scenario, if the organically modified CNTs coating can successfully mitigate the shuttle effect during cycling, the CNTs-coated separator may offer a pathway for enhanced lithium-sulfur batteries.

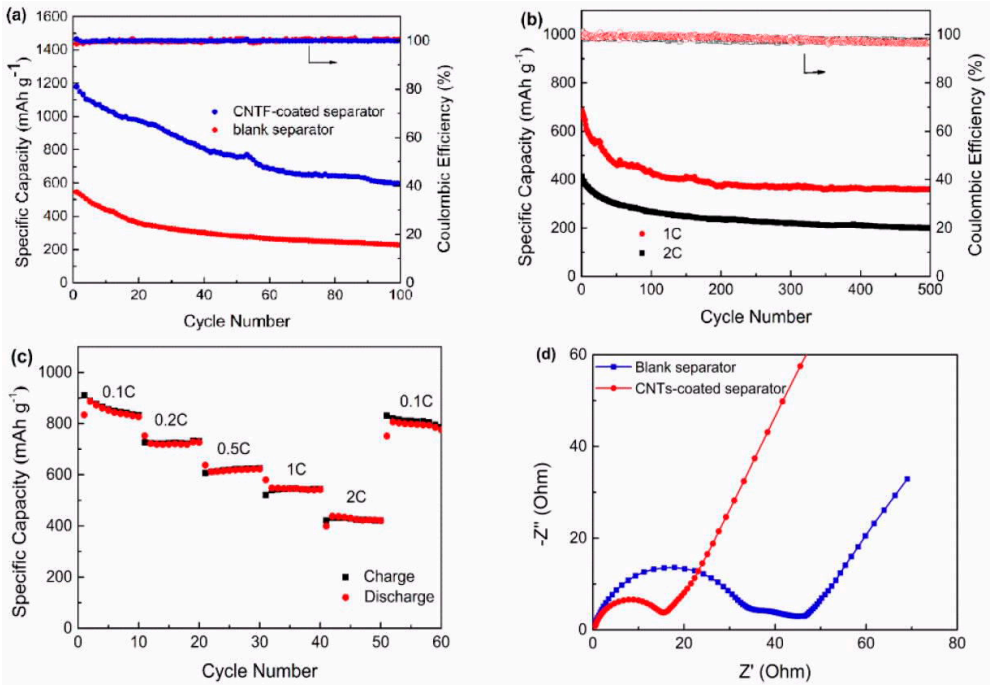

Figure 21. (**a**) Cycling performance of the blank separator and CNTs-coated separator at 0.1 C; (**b**) cycling performance of the CNTs-coated separator at the rates of 1 C and 2 C; (**c**) rate performance of the Li-S batteries with the CNTs-coated separator; (**d**) EIS data of the cells with the blank separator and CNTs-coated separator. Adopted with permission from [572].

Li-O_2 batteries have garnered significant interest for future electrical energy storage because of their impressive theoretical specific energy density of 3505 Wh/kg, surpassing other battery technologies. Nevertheless, the real-world use of Li-O_2 batteries faces substantial challenges due to various technical issues, including low energy efficiency, inadequate rate capability, and restricted cycle life. These issues are, to a great extent, excess buildup of discharge products such as nonconductive Li_2O_2, which is responsible for the poor reversibility and high polarization upon charging [582–585]. An improvement in the catalytic activity of the cathode for the reduction in polarization and enhancement of reversibility will increase coulombic efficiency. Some groups have focused on CNTs as a catalyst for the OER and ORR in the cathodes. The carbonaceous materials showed good catalytic activity toward ORR but poorer catalytic activity toward OER, primarily due to the polarization resulting from the sluggish charge transfer kinetics. Huang et al. [586] investigated a series of noble metal nanoparticles (Pd, Pt, Ru, and Au) encapsulated inside the open end of CNTs by wet impregnation. They reported that encapsulation of nanoparticles significantly enhances the surface electron density of CNTs without creating regional enrichment of electron density on the CNT's surface. Accordingly, ORR takes place all over the surface of CNTs, serving as a catalyst, which ensures homogeneous coverage of Li_2O_2 nanocrystals on the surface of CNTs with strong interaction. Uniform coverage of Li_2O_2 nanocrystals with intense contact to CNTs allows low polarized Li_2O_2 decomposition to 0.3 V during charge [586]. Kwak et al. developed a nanostructured cathode based on molybdenum carbide nanoparticles (Mo_2C) dispersed on carbon nanotubes, which significantly increased the efficiency to 88%, with a cycle life of over 100 cycles. Figure 22a–d illustrates electrochemical tests on pristine-carbon nanotubes, bulk Mo_2C powder, and Mo_2C/CNT composite samples. The Mo_2C/CNT cathode had an energy efficiency of 88%, with Mo_2C powder and pristine-carbon nanotubes having an energy efficiency of 53% and 74%, respectively. For example, the polarization for the Mo_2C/CNT cathode was 0.47 V compared to 2.11 V of Mo_2C powder and 1.10 V of pristine-CNT. The cycle life

of the Mo_2C/CNT cathode was constant up to the 150th cycle at a discharge capacity of 500 mAh/g. Furthermore, at a high current density of 1000 mA/g and with 10 cycles, the polarization of Mo_2C/CNT is still lesser than that of a pristine carbon nanotube electrode operated at a low current of 100 mA/g [587]. The Mo_2C nanoparticle catalysts provide the grounds for forming well-dispersed Li_2O_2 nanolayers with large contact areas on the Mo_2C/carbon nanotubes during the ORR. The Li_2O_2 decomposes at low potentials during the OER by avoiding the energy losses associated with the decomposition of the typical Li_2O_2 discharge products [587].

Recently, efforts were made to replace the metal catalysts with nitrogen-doped carbon nanotubes to improve the ORR in lithium-air batteries [588,589]. González et al. [588] successfully prepared nitrogen-doped multi-walled carbon nanotubes with pyridine as the precursor agent using a two-stage thermal modified chemical vapor deposition method. The XPS results indicated the configuration of N atoms primarily as pyrrolic and pyridinic species in the carbon lattice. As such, the N-CNTs demonstrated good electrocatalytic activity toward the ORR. The lower onset potential and comparable current densities with platinum-based materials suggest that N-CNTs represent a suitable non-precious metal electrocatalyst of cathodes for Li-air batteries.

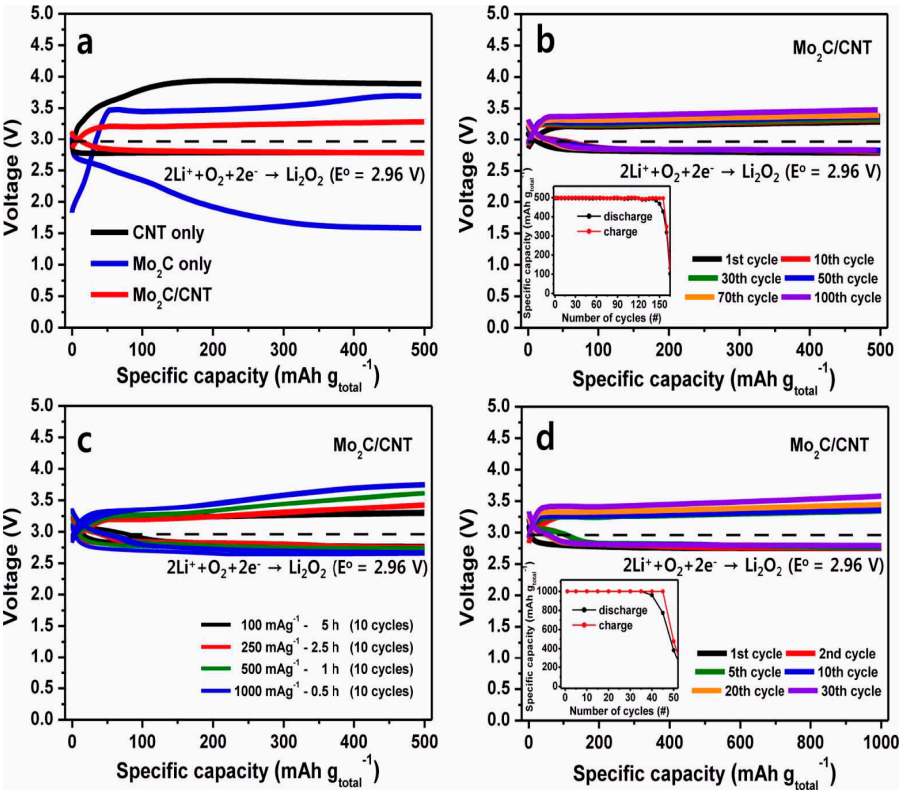

Figure 22. (**a**) Discharge/charge profiles of the Li-O_2 batteries with pristine-CNTs, Mo_2C, and Mo_2C/CNT electrodes at a discharge capacity of 500 mAh/g_{total} and a current density of 100 mAh/g_{total}. (**b**) Cycling performance of the LiO_2 battery with the Mo_2C/carbon nanotube electrode at a discharge capacity of 500 mAh/g_{total} and at a current density of 100 mAh/g_{total}. (**c**) The first 10 cycles of Li-O_2 batteries with the Mo_2C/carbon nanotube electrode at current densities of 100, 200, 500, and 1000 mAh/g_{total} with a discharge capacity of 500 mAh/g_{total}. (**d**) Cycling performance of the Li-O_2 battery with the Mo_2C/carbon nanotube electrode at a discharge capacity of 1000 mAh/g_{total} and at a current density of 200 mAh/g_{total}. Adopted with permission from [587].

All the growth of CNTs on conductive substrates reported are limited to less than 2 mg/cm^2 and no studies were conducted to enhance the mass loads to more than this value. The major challenge in increasing the mass loading of CNTs on metallic substrates is the loss

of the metal catalyst activity due to carbon diffusion into the metallic substrate before CNT growth. Ionescu et al. documented the preparation of carbon nanotubes (CNTs) directly on metallic substrates through a spray-pyrolysis chemical vapor deposition method. In this context, cathodes containing CNTs with mass loads reaching 25.9 mg/cm^2 were explored for lithium-air batteries. Consequently, for a carbon loading of 4.2 mg/cm^2, the highest specific discharge capacity achieved was 3348 mAh/g. These results prove that carbon nanomaterials exhibit exciting electrocatalytic activity toward the cathode reaction and thus create an incentive for the exploration of other carbon materials as cathodic materials towards energy storage devices with improved performances [585]. Carbon powders must be compacted for ease of handling as air electrodes. Still, such rigid solid electrodes are often intolerant of the mechanical stresses caused by the discharge of solid deposits, in particular under deeply discharged conditions.

By sharp contrast, CNTs supply paper-like flexible sheets owing to the tubular constitution and are quickly adopted for air electrodes in lithium-air batteries [590–595]. A fibrous network of CNTs is favorable to keeping the conductive network in the electrode during the deposition/decomposition of the discharged solid. More recently, air electrodes made of SWCNT sheet were investigated by Nomura et al. as a cathode for lithium-air battery applications. The slurry of SWCNTs was filtered under vacuum through a PTFE membrane to obtain a free-standing and binder-free CNT sheet. The deposited discharge product has been identified only as Li_2O_2 deposited on the CNT bundles and grown into an expanded cathode with thicknesses up to a few millimeters in thickness. CNT sheets can be used to attain ultra-high capacity in lithium-air battery cells for achieving a much higher areal cell capacity of up to 30 mAh/cm^2, which is 15 times higher than the capacity of current LIB cells [584]. However, many hurdles are yet to be overcome before commercializing lithium-air batteries. Besides the CNTs cathode materials, further efforts should be paid to developing more advanced electrocatalysts and highly stable electrolytes (such as hybrid electrolyte [596], Aluminum-Substituted Lithium Lanthanum Titanate Solid Electrolyte ($(Li_{0.33}La_{0.56})1.005Ti_{0.99}Al_{0.01}O_3$, A-LLTO) [597], Garnet Solid Electrolyte ($Li_{6.4}La_3Zr_{1.4}Ta_{0.6}O_{12}$, LLZTO) [598] or polymer electrolyte [599], and bifunctional oxygen catalysts for OER and ORR [600–602]. The lithium metal anodes face several limitations also owing to (i) their instability in liquid electrolytes, (ii) reactivity toward O_2, and (iii) safety problems related to Li dendrite formation.

5. Conclusions

Despite the many advantages of CNTs, several challenges remain that need to be addressed for their widespread application and commercialization. These challenges include the following.

1. Control of Defects, Length, and Chirality

The control of defect concentration, length, and chirality separations remains a significant issue in producing monodisperse CNTs with consistent properties. Future research should focus on improving synthesis methods to achieve more uniform CNTs with controlled length and chirality, which is critical for optimizing performance in various applications.

2. Large-Scale Production

Achieving cost-effective, large-scale production of CNTs with high purity, uniformity, and quality remains a key challenge. While methods like arc discharge and laser ablation are expensive, CVD offers higher yields at a lower cost. More research is needed to develop scalable and efficient synthesis techniques that can meet industrial demand without compromising on CNT quality.

3. Electrode Performance in Lithium-Ion Batteries (LIBs)

CNTs have demonstrated potential as additives in composite electrodes for LIBs, but challenges such as high irreversible capacity for bare CNT anodes prevent them from fully replacing graphite anodes. Research should focus on integrating CNTs with other materials, such as silicon and germanium, to enhance storage capacity, stability, and cycle life.

4. Toxicity and Environmental Impact

Concerns over the toxicity of CNTs, which vary depending on their structure, synthesis methods, and concentration, must be addressed. Future research should aim at evaluating the environmental impact and health risks associated with CNT exposure. Moreover, the development of regulations and standards for the safe manufacturing, application, and disposal of CNTs is essential.

Future Research Directions:

1. Improved Synthesis and Purification Methods

Future research should focus on refining the synthesis and purification techniques to produce CNTs that meet the specific requirements for large-scale, cost-effective applications.

2. Understanding Lithium Storage Mechanisms

Further investigation is needed to understand how factors such as nanotube diameter, length, and wall count influence the lithium storage capacity of CNTs. This research could improve capacity retention, stability, and cycling performance for applications in energy storage technologies, particularly LIBs.

3. Collaboration Across Sectors

Enhanced collaboration between industry, academia, and government is crucial to advancing the understanding and application of CNTs. This would accelerate innovation and the development of CNTs in emerging fields like energy storage, microelectronics, and biomedical engineering.

In conclusion, while CNTs have revolutionized various scientific and industrial domains, addressing these challenges through focused research efforts will unlock their full potential and broaden their commercial applications in the future.

Author Contributions: A.K.M.R.R. and A.D. wrote the review manuscript and produced the graphics. M.V.R. and K.Z. designed the structure of the review, collected the papers related to the topic of the review, and completed the language corrections, with all authors contributing equally. All authors have read and agreed to the published version of the manuscript.

Funding: This research funded by Concordia University.

Acknowledgments: The authors would like to thank the Government of Quebec (MEIE) for its financial support.

Conflicts of Interest: The author Ali Darwiche was employed by the company SOLiTHOR and Mogalahalli Venkatashamy Reddy was employed by the company Nouveau Monde Graphite. The remaining authors declare that the research was conducted in the absence of any commercial or financial relationships that could be construed as a potential conflict of interest.

References

1. Harris, P.J.F. *Carbon Nanotube Science—Synthesis, Properties and Applications*; Cambridge University Press: Cambridge, UK, 2009.
2. Oberlin, A.; Endo, M.; Koyama, T. Filamentous growth of carbon through benzene decomposition. *J. Cryst. Growth* **1976**, *32*, 335–349. [CrossRef]
3. Iijima, S. Helical microtubules of graphitic carbon. *Nature* **1991**, *354*, 56. [CrossRef]
4. Terrones, M. Carbon nanotubes: Synthesis and properties, electronic devices and other emerging applications. *Int. Mater. Rev.* **2004**, *49*, 325–377. [CrossRef]

5. Kaushik, B.K.; Majumder, M.K.; Kaushik, B.K.; Majumder, M.K. Carbon nanotube: Properties and applications. In *Carbon Nanotube Based VLSI Interconnects: Analysis and Design*; Springer: Berlin/Heidelberg, Germany, 2015; pp. 17–37.
6. Dai, H. Carbon nanotubes: Opportunities and challenges. *Surf. Sci.* **2002**, *500*, 218–241. [CrossRef]
7. Chico, L.; Crespi, V.H.; Benedict, L.X.; Louie, S.G.; Cohen, M.L. Pure Carbon Nanoscale Devices: Nanotube Heterojunctions. *Phys. Rev. Lett.* **1996**, *76*, 971–974. [CrossRef] [PubMed]
8. Kataura, H.; Kumazawa, Y.; Maniwa, Y.; Umezu, I.; Suzuki, S.; Ohtsuka, Y.; Achiba, Y. Optical properties of single-wall carbon nanotubes. *Synth. Met.* **1999**, *103*, 2555–2558. [CrossRef]
9. Vander Wal, R.L.; Berger, G.M.; Ticich, T.M. Carbon nanotube synthesis in a flame using laser ablation for in situ catalyst generation. *Appl. Phys. A* **2003**, *77*, 885–889. [CrossRef]
10. Hong, G.; Diao, S.; Chang, J.; Antaris, A.L.; Chen, C.; Zhang, B.; Zhao, S.; Atochin, D.N.; Huang, P.L.; Andreasson, K.I.; et al. Through-skull fluorescence imaging of the brain in a new near-infrared window. *Nat. Photonics* **2016**, *8*, 723–730. [CrossRef] [PubMed]
11. Liu, Z.; Robinson, J.T.; Tabakman, S.M.; Yang, K.; Dai, H. Carbon materials for drug delivery & cancer therapy. *Mater. Today* **2011**, *14*, 316–323.
12. Antaris, A.L.; Robinson, J.T.; Yaghi, O.K.; Hong, G.; Diao, S.; Luong, R.; Dai, H. Ultra-Low Doses of Chirality Sorted (6,5) Carbon Nanotubes for Simultaneous Tumor Imaging and Photothermal Therapy. *ACS Nano* **2013**, *7*, 3644–3652. [CrossRef] [PubMed]
13. Liu, X.-M.; Huang, Z.d.; Oh, S.w.; Zhang, B.; Ma, P.-C.; Yuen, M.M.F.; Kim, J.-K. Carbon nanotube (CNT)-based composites as electrode material for rechargeable Li-ion batteries: A review. *Compos. Sci. Technol.* **2012**, *72*, 121–144. [CrossRef]
14. Xiong, Z.; Yun, Y.; Jin, H.-J. Applications of Carbon Nanotubes for Lithium Ion Battery Anodes. *Materials* **2013**, *6*, 1138. [CrossRef] [PubMed]
15. Alejandro, M.-R.; Alejandra, M.-B.; Miguel, A.-C.; Eric, M.R.-M.; Rufino, N.-M.; Rodrigo, V.-C. An Overview of Carbon Nanotubes: Synthesis, Purification and Characterization. *Curr. Org. Chem.* **2013**, *17*, 1858–1866.
16. Eatemadi, A.; Daraee, H.; Karimkhanloo, H.; Kouhi, M.; Zarghami, N.; Akbarzadeh, A.; Abasi, M.; Hanifehpour, Y.; Joo, S.W. Carbon nanotubes: Properties, synthesis, purification, and medical applications. *Nanoscale Res. Lett.* **2014**, *9*, 393. [CrossRef]
17. Wang, C.; Ma, L.; Yang, W. *Advanced Polymer Science and Engineering, Proceedings of the Advanced Polymer Processing International Forum, Qingdao, China, 21–23 October 2010*; Trans Tech Publications Ltd.: Zürich, Switzerland, 2011.
18. Li, J.; Ye, Q.; Cassell, A.; Ng, H.T.; Stevens, R.; Han, J.; Meyyappan, M. Bottom-Up Approach Carbon Nanotub. Interconnects. *Appl. Phys. Lett.* **2003**, *82*, 2491–2493. [CrossRef]
19. Jasti, R.; Bertozzi, C.R. Progress and Challenges for the Bottom-Up Synthesis of Carbon Nanotubes with Discrete Chirality. *Chem. Phys. Lett.* **2010**, *494*, 1–7. [CrossRef]
20. Omachi, H.; Matsuura, S.; Segawa, Y.; Itami, K. A Modular and Size-Selective Synthesis of [n]Cycloparaphenylenes: A Step toward the Selective Synthesis of [n,n] Single-Walled Carbon Nanotubes. *Angew. Chem. Int. Ed.* **2010**, *49*, 10202–10205. [CrossRef]
21. Segawa, Y.; Miyamoto, S.; Omachi, H.; Matsuura, S.; Šenel, P.; Sasamori, T.; Tokitoh, N.; Itami, K. Concise Synthesis and Crystal Structure of [12]Cycloparaphenylene. *Angew. Chem.* **2011**, *123*, 3302–3306. [CrossRef]
22. Omachi, H.; Segawa, Y.; Itami, K. Synthesis and Racemization Process of Chiral Carbon Nanorings: A Step toward the Chemical Synthesis of Chiral Carbon Nanotubes. *Org. Lett.* **2011**, *13*, 2480–2483. [CrossRef] [PubMed]
23. Iwamoto, T.; Watanabe, Y.; Sakamoto, Y.; Suzuki, T.; Yamago, S. Selective and Random Syntheses of [n]Cycloparaphenylenes (n = 8–13) and Size Dependence of Their Electronic Properties. *J. Am. Chem. Soc.* **2011**, *133*, 8354–8361. [CrossRef]
24. Gogotsi, Y.; Libera, J.A.; Yoshimura, M. Hydrothermal synthesis of multiwall carbon nanotubes. *J. Mater. Res.* **2000**, *15*, 2591–2594. [CrossRef]
25. Bai, J.B.; Hamon, A.L.; Marraud, A.; Jouffrey, B.; Zymla, V. Synthesis of SWNTs and MWNTs by a molten salt (NaCl) method. *Chem. Phys. Lett.* **2002**, *365*, 184–188. [CrossRef]
26. Liu, F.; Zhang, X.; Cheng, J.; Tu, J.; Kong, F.; Huang, W.; Chen, C. Preparation of short carbon nanotubes by mechanical ball milling and their hydrogen adsorption behavior. *Carbon* **2003**, *41*, 2527–2532. [CrossRef]
27. Ganesh, E.N. Single Walled and Multi Walled Carbon Nanotube Structure, Synthesis and Applications. *Int. J. Innov. Technol. Explor. Eng.* **2013**, *2*, 311–320.
28. He, Z.B.; Maurice, J.-L.; Lee, C.S.; Gohier, A.; Legagneux, P.; Pribat, D.; Cojocaru, C.S. Etchant-induced shaping of nanoparticle catalysts during chemical vapour growth of carbon nanofibres. *Arab. J. Sci. Eng. Sect. B* **2010**, *35*, 19–28. [CrossRef]
29. Kruusenberg, I.; Alexeyeva, N.; Tammeveski, K.; Kozlova, J.; Matisen, L.; Sammelselg, V.i.; Solla-Gullon, J.; Feliu, J.M. Effect of purification of carbon nanotubes on their electrocatalytic properties for oxygen reduction in acid solution. *Carbon* **2011**, *49*, 4031–4039. [CrossRef]
30. Mubarak, N.M.; Yusof, F.; Alkhatib, M.F. The production of carbon nanotubes using two-stage chemical vapor deposition and their potential use in protein purification. *Chem. Eng. J.* **2011**, *168*, 461–469. [CrossRef]
31. Krätschmer, W.; Lamb, L.D.; Fostiropoulos, K.H.; Huffman, D.R. Solid C60: A new form of carbon. *Nature* **1990**, *347*, 354–358. [CrossRef]

32. Ebbesen, T.W.; Ajayan, P.M. Large-scale synthesis of carbon nanotubes. *Nature* **1992**, *358*, 220. [CrossRef]
33. Ebbesen, T.W.; Hiura, H.; Fujita, J.; Ochiai, Y.; Matsui, S.; Tanigaki, K. Patterns in the bulk growth of carbon nanotubes. *Chem. Phys. Lett.* **1993**, *209*, 83–90. [CrossRef]
34. Seraphin, S.; Zhou, D.; Jiao, J.; Withers, J.C.; Loutfy, R. Effect of processing conditions on the morphology and yield of carbon nanotubes. *Carbon* **1993**, *31*, 685–689. [CrossRef]
35. Yoshinori, A.; Sumio, I. Preparation of Carbon Nanotubes by Arc-Discharge Evaporation. *Jpn. J. Appl. Phys.* **1993**, *32*, L107.
36. Arora, N.; Sharma, N.N. Arc discharge synthesis of carbon nanotubes: Comprehensive review. *Diam. Relat. Mater.* **2014**, *50*, 135–150. [CrossRef]
37. Ando, Y. The Preparation of Carbon Nanotubes. *Fuller. Sci. Technol.* **1994**, *2*, 173–180. [CrossRef]
38. Wang, M.; Zhao, X.; Ohkohchi, M.; Ando, Y. Carbon Nanotubes Grown on the Surface of Cathode Deposit by Arc Discharge. *Fuller. Sci. Technol.* **1996**, *4*, 1027–1039. [CrossRef]
39. Zhao, X.; Ohkohchi, M.; Wang, M.; Iijima, S.; Ichihashi, T.; Ando, Y. Preparation of high-grade carbon nanotubes by hydrogen arc discharge. *Carbon* **1997**, *35*, 775–781. [CrossRef]
40. Zhao, X.; Ohkohchi, M.; Shimoyama, H.; Ando, Y. Morphology of carbon allotropes prepared by hydrogen arc discharge. *J. Cryst. Growth* **1999**, *198–199*, 934–938. [CrossRef]
41. Jiang, Y.; Wang, H.; Shang, X.F.; Li, Z.H.; Wang, M. Influence of NH_3 atmosphere on the growth and structures of carbon nanotubes synthesized by the arc-discharge method. *Inorg. Mater.* **2009**, *45*, 1237. [CrossRef]
42. Shimotani, K.; Anazawa, K.; Watanabe, H.; Shimizu, M. New synthesis of multi-walled carbon nanotubes using an arc discharge technique under organic molecular atmospheres. *Appl. Phys. A* **2001**, *73*, 451–454. [CrossRef]
43. Parkansky, N.; Boxman, R.L.; Alterkop, B.; Zontag, I.; Lereah, Y.; Barkay, Z. Single-pulse arc production of carbon nanotubes in ambient air. *J. Phys. D Appl. Phys.* **2004**, *37*, 2715. [CrossRef]
44. Tsai, Y.Y.; Su, J.S.; Su, C.Y.; He, W.H. Production of carbon nanotubes by single-pulse discharge in air. *J. Mater. Process. Technol.* **2009**, *209*, 4413–4416. [CrossRef]
45. Kumar, S.; Rani, R.; Dilbaghi, N.; Tankeshwar, K.; Kim, K.H. Carbon nanotubes: A novel material for multifaceted applications in human healthcare. *Chem. Soc. Rev.* **2017**, *46*, 158–196. [CrossRef] [PubMed]
46. Jung, S.H.; Kim, M.R.; Jeong, S.H.; Kim, S.U.; Lee, O.J.; Lee, K.H.; Suh, J.H.; Park, C.K. High-yield synthesis of multi-walled carbon nanotubes by arc discharge in liquid nitrogen. *Appl. Phys. A* **2003**, *76*, 285–286. [CrossRef]
47. Montoro, L.A.; Lofrano, R.C.Z.; Rosolen, J.M. Synthesis of single-walled and multi-walled carbon nanotubes by arc-water method. *Carbon* **2005**, *43*, 200–203. [CrossRef]
48. Guo, J.; Wang, X.; Yao, Y.; Yang, X.; Liu, X.; Xu, B. Structure of nanocarbons prepared by arc discharge in water. *Mater. Chem. Phys.* **2007**, *105*, 175–178. [CrossRef]
49. Xing, G.; Jia, S.-L.; Shi, Z.-Q. The production of carbon nano-materials by arc discharge under water or liquid nitrogen. *New Carbon Mater.* **2007**, *22*, 337–341. [CrossRef]
50. Ben Belgacem, A.; Hinkov, I.; Yahia, S.B.; Brinza, O.; Farhat, S. Arc discharge boron nitrogen doping of carbon nanotubes. *Mater. Today Commun.* **2016**, *8*, 183–195. [CrossRef]
51. Hutchison, J.L.; Kiselev, N.A.; Krinichnaya, E.P.; Krestinin, A.V.; Loutfy, R.O.; Morawsky, A.P.; Muradyan, V.E.; Obraztsova, E.D.; Sloan, J.; Terekhov, S.V.; et al. Double-walled carbon nanotubes fabricated by a hydrogen arc discharge method. *Carbon* **2001**, *39*, 761–770. [CrossRef]
52. Sugai, T.; Yoshida, H.; Shimada, T.; Okazaki, T.; Shinohara, H.; Bandow, S. New Synthesis of High-Quality Double-Walled Carbon Nanotubes by High-Temperature Pulsed Arc Discharge. *Nano Lett.* **2003**, *3*, 769–773. [CrossRef]
53. Qiu, J.; Wang, Z.; Zhao, Z.; Wang, T. Synthesis of double-walled carbon nanotubes from coal in hydrogen-free atmosphere. *Fuel* **2007**, *86*, 282–286. [CrossRef]
54. Liu, Q.; Ren, W.; Li, F.; Cong, H.; Cheng, H.M. Synthesis and High Thermal Stability of Double-Walled Carbon Nanotubes Using Nickel Formate Dihydrate as Catalyst Precursor. *J. Phys. Chem. C* **2007**, *111*, 5006–5013. [CrossRef]
55. Li, L.; Li, F.; Liu, C.; Cheng, H.M. Synthesis and characterization of double-walled carbon nanotubes from multi-walled carbon nanotubes by hydrogen-arc discharge. *Carbon* **2005**, *43*, 623–629. [CrossRef]
56. Bethune, D.S.; Kiang, C.H.; De Vries, M.S.; Gorman, G.; Savoy, R.; Vazquez, J.; Beyers, R. Cobalt-catalysed growth of carbon nanotubes with single-atomic-layer walls. *Nature* **1993**, *363*, 605–607. [CrossRef]
57. Subramoney, S.; Ruoff, R.S.; Lorents, D.C.; Malhotra, R. Radial single-layer nanotubes. *Nature* **1993**, *366*, 637. [CrossRef]
58. Lambert, J.M.; Ajayan, P.M.; Bernier, P.; Planeix, J.M.; Brotons, V.; Coq, B.; Castaing, J. Improving conditions towards isolating single-shell carbon nanotubes. *Chem. Phys. Lett.* **1994**, *226*, 364–371. [CrossRef]
59. Journet, C.; Maser, W.K.; Bernier, P.; Loiseau, A.; de la Chapelle, M.L.; Lefrant, S.; Deniard, P.; Lee, R.; Fischer, J.E. Large-scale production of single-walled carbon nanotubes by the electric-arc technique. *Nature* **1997**, *388*, 756. [CrossRef]
60. Saito, Y.; Tani, Y.; Miyagawa, N.; Mitsushima, K.; Kasuya, A.; Nishina, Y. High yield of single-wall carbon nanotubes by arc discharge using Rh-Pt mixed catalysts. *Chem. Phys. Lett.* **1998**, *294*, 593–598. [CrossRef]

61. Huang, H.; Kajiura, H.; Tsutsui, S.; Hirano, Y.; Miyakoshi, M.; Yamada, A.; Ata, M. Large-scale rooted growth of aligned super bundles of single-walled carbon nanotubes using a directed arc plasma method. *Chem. Phys. Lett.* **2001**, *343*, 7–14. [CrossRef]
62. Askeland, D.R.; Phul, P.P. *The Science and Engineering of Materials*; Springer: Dordrecht, The Netherlands, 2003.
63. Saito, R.; Dresselhaus, G.; Dresselhaus, M. *Physical Properties of Carbon Nanotubes*, 4th ed.; World Scientific: Hackensack, NJ, USA, 1998.
64. Chen, B.; Inoue, S.; Ando, Y. Raman spectroscopic and thermogravimetric studies of high-crystallinity SWNTs synthesized by FH-arc discharge method. *Diam. Relat. Mater.* **2009**, *18*, 975–978. [CrossRef]
65. Chen, B.; Zhao, X.; Inoue, S.; Ando, Y. Fabrication and dispersion evaluation of single-wall carbon nanotubes produced by FH-arc discharge method. *J. Nanosci. Nanotechnol.* **2010**, *10*, 3973–3977. [CrossRef]
66. Wang, H.; Li, Z.; Inoue, S.; Ando, Y. Influence of Mo on the Growth of Single-Walled Carbon Nanotubes in Arc Discharge. *J. Nanosci. Nanotechnol.* **2010**, *10*, 3988–3993. [CrossRef] [PubMed]
67. Li, Z.; Liu, P.; Zhao, B.; Wang, H.; Zhang, Y. Improving the synthesis of single-walled carbon nanotubes by pulsed arc discharge in air by preheating the catalysts. *Carbon* **2008**, *46*, 1819–1822. [CrossRef]
68. Maria, K.H.; Mieno, T. Synthesis of single-walled carbon nanotubes by low-frequency bipolar pulsed arc discharge method. *Vacuum* **2015**, *113*, 11–18. [CrossRef]
69. Kroto, H.W.; Heath, J.R.; O'Brien, S.C.; Curl, R.F.; Smalley, R.E. C60: Buckminsterfullerene. *Nature* **1985**, *318*, 162. [CrossRef]
70. Guo, T.; Nikolaev, P.; Thess, A.; Colbert, D.T.; Smalley, R.E. Catalytic growth of single-walled manotubes by laser vaporization. *Chem. Phys. Lett.* **1995**, *243*, 49–54. [CrossRef]
71. Abbasi, E.; Aval, S.F.; Akbarzadeh, A.; Milani, M.; Nasrabadi, H.T.; Joo, S.W.; Hanifehpour, Y.; Nejati-Koshki, K.; Pashaei-Asl, R. Dendrimers: Synthesis, applications, and properties. *Nanoscale Res. Lett.* **2014**, *9*, 247. [CrossRef]
72. Kusaba, M.; Tsunawaki, Y. Production of single-wall carbon nanotubes by a XeCl excimer laser ablation. *Thin Solid Film.* **2006**, *506–507*, 255–258. [CrossRef]
73. Lebel, L.L.; Aissa, B.; Khakani, M.A.E.; Therriault, D. Preparation and mechanical characterization of laser ablated single-walled carbon-nanotubes/polyurethane nanocomposite microbeams. *Compos. Sci. Technol.* **2010**, *70*, 518–524. [CrossRef]
74. Gore, J.P.; Sane, A.; Yellampalli, S. Flame Synthesis of Carbon Nanotubes. In *Carbon Nanotubes—Synthesis, Characterization, Applications*; InTech: Rijeka, Croatia, 2011; Chapter 7.
75. Thess, A.; Lee, R.; Nikolaev, P.; Dai, H.; Petit, P.; Robert, J.; Xu, C.; Lee, Y.H.; Kim, S.G.; Rinzler, A.G.; et al. Crystalline Ropes of Metallic Carbon Nanotubes. *Science* **1996**, *273*, 483–487. [CrossRef]
76. Prasek, J.; Drbohlavova, J.; Chomoucka, J.; Hubalek, J.; Jasek, O.; Adam, V.; Kizek, R. Methods for carbon nanotubes synthesis-review. *J. Mater. Chem.* **2011**, *21*, 15872–15884. [CrossRef]
77. José-Yacamán, M.; Miki-Yoshida, M.; Rendón, L.; Santiesteban, J.G. Catalytic growth of carbon microtubules with fullerene structure. *Appl. Phys. Lett.* **1993**, *62*, 202–204. [CrossRef]
78. Arepalli, S. Laser Ablation Process for Single-Walled Carbon Nanotube Production. *J. Nanosci. Nanotechnol.* **2004**, *4*, 317–325. [CrossRef] [PubMed]
79. Bonaccorso, F.; Bongiorno, C.; Fazio, B.; Gucciardi, P.G.; Marago, O.M.; Morone, A.; Spinella, C. Pulsed laser deposition of multiwalled carbon nanotubes thin films. *Appl. Surf. Sci.* **2007**, *254*, 1260–1263. [CrossRef]
80. Bolshakov, A.P.; Uglov, S.A.; Saveliev, A.V.; Konov, V.I.; Gorbunov, A.A.; Pompe, W.; Graff, A. A novel CW laser-powder method of carbon single-wall nanotubes production. *Diam. Relat. Mater.* **2002**, *11*, 927–930. [CrossRef]
81. Marchiori, R.; Braga, W.F.; Mantelli, M.B.H.; Lago, A. Analytical solution to predict laser ablation rate in a graphitic target. *J. Mater. Sci.* **2010**, *45*, 1495–1502. [CrossRef]
82. Stramel, A.A.; Gupta, M.C.; Lee, H.R.; Yu, J.; Edwards, W.C. Pulsed laser deposition of carbon nanotube and polystyrene–carbon nanotube composite thin films. *Opt. Lasers Eng.* **2010**, *48*, 1291–1295. [CrossRef]
83. Karimi, M.; Solati, N.; Amiri, M.; Mirshekari, H.; Mohamed, E.; Taheri, M.; Hashemkhani, M.; Saeidi, A.; Estiar, M.A.; Kiani, P.; et al. Carbon nanotubes part I: Preparation of a novel and versatile drug-delivery vehicle. *Expert Opin. Drug Deliv.* **2015**, *12*, 1071–1087. [CrossRef]
84. Mizuno, K.; Ishii, J.; Kishida, H.; Hayamizu, Y.; Yasuda, S.; Futaba, D.N.; Yumura, M.; Hata, K. A black body absorber from vertically aligned single-walled carbon nanotubes. *Proc. Natl. Acad. Sci. USA* **2009**, *106*, 6044–6047. [CrossRef]
85. See, C.H.; Harris, A.T. A Review of Carbon Nanotube Synthesis via Fluidized-Bed Chemical Vapor Deposition. *Ind. Eng. Chem. Res.* **2007**, *46*, 997–1012. [CrossRef]
86. Kumar, M.; Ando, Y. Chemical Vapor Deposition of Carbon Nanotubes: A Review on Growth Mechanism and Mass Production. *J. Nanosci. Nanotechnol.* **2010**, *10*, 3739–3758. [CrossRef]
87. Hata, K.; Futaba, D.N.; Mizuno, K.; Namai, T.; Yumura, M.; Iijima, S. Water-Assisted Highly Efficient Synthesis of Impurity-Free Single-Walled Carbon Nanotubes. *Science* **2004**, *306*, 1362–1364. [CrossRef] [PubMed]
88. Yardimci, A.I.; Yilmaz, S.; Selamet, Y. The effects of catalyst pretreatment, growth atmosphere and temperature on carbon nanotube synthesis using Co-Mo/MgO catalyst. *Diam. Relat. Mater.* **2015**, *60*, 81–86. [CrossRef]

89. Iijima, S.; Ajayan, P.M.; Ichihashi, T. Growth model for carbon nanotubes. *Phys. Rev. Lett.* **1992**, *69*, 3100–3103. [CrossRef] [PubMed]
90. Smajda, R.; Andresen, J.C.; Duchamp, M.; Meunier, R.; Casimirius, S.; Hernádi, K.; Forró, L.; Magrez, A. Synthesis and mechanical properties of carbon nanotubes produced by the water assisted CVD process. *Phys. Status Solidi B* **2009**, *246*, 2457–2460. [CrossRef]
91. He, Z.B.; Maurice, J.-L.; Lee, C.S.; Cojocaru, C.S.; Pribat, D. Nickel catalyst faceting in plasma-enhanced direct current chemical vapor deposition of carbon nanofibers. *Arab. J. Sci. Eng.* **2010**, *35*, 19.
92. Ajayan, P.M.; Charlier, J.C.; Rinzler, A.G. Carbon nanotubes: From macromolecules to nanotechnology. *Proc. Natl. Acad. Sci. USA* **1999**, *96*, 14199–14200. [CrossRef] [PubMed]
93. Dervishi, E.; Li, Z.; Xu, Y.; Saini, V.; Biris, A.R.; Lupu, D.; Biris, A.S. Carbon Nanotubes: Synthesis, Properties, and Applications. *Part. Sci. Technol.* **2009**, *27*, 107–125. [CrossRef]
94. Zhang, Q.; Huang, J.-Q.; Zhao, M.-Q.; Qian, W.-Z.; Wei, F. Carbon Nanotube Mass Production: Principles and Processes. *ChemSusChem* **2011**, *4*, 864–889. [CrossRef] [PubMed]
95. Fathy, N.A. Carbon nanotubes synthesis using carbonization of pretreated rice straw through chemical vapor deposition of camphor. *RSC Adv.* **2017**, *7*, 28535–28541. [CrossRef]
96. Bernd, M.G.S.; Bragança, S.R.; Heck, N.; Filho, L.C.P.d.S. Synthesis of carbon nanostructures by the pyrolysis of wood sawdust in a tubular reactor. *J. Mater. Res. Technol.* **2017**, *6*, 171–177. [CrossRef]
97. Araga, R.; Sharma, C.S. One step direct synthesis of multiwalled carbon nanotubes from coconut shell derived charcoal. *Mater. Lett.* **2017**, *188*, 205–207. [CrossRef]
98. Dresselhaus, M.S.; Dresselhaus, G.; Jorio, A.; Souza Filho, A.G.; Pimenta, M.A.; Saito, R. Single Nanotube Raman Spectroscopy. *Acc. Chem. Res.* **2002**, *35*, 1070–1078. [CrossRef]
99. Lobiak, E.V.; Shlyakhova, E.V.; Bulusheva, L.G.; Plyusnin, P.E.; Shubin, Y.V.; Okotrub, A.V. Ni-Mo and Co-Mo alloy nanoparticles for catalytic chemical vapor deposition synthesis of carbon nanotubes. *J. Alloys Compd.* **2015**, *621*, 351–356. [CrossRef]
100. Landi, B.J.; Raffaelle, R.P.; Castro, S.L.; Bailey, S.G. Single-wall carbon nanotube–polymer solar cells. *Prog. Photovolt. Res. Appl.* **2005**, *13*, 165–172. [CrossRef]
101. Mohammed, I.h.A.; Bankole, M.T.; Abdulkareem, A.S.; Ochigbo, S.S.; Afolabi, A.S.; Abubakre, O.K. Full factorial design approach to carbon nanotubes synthesis by CVD method in argon environment. *S. Afr. J. Chem. Eng.* **2017**, *24*, 17–42. [CrossRef]
102. Michiko, K.; Masumi, R.; Toshiyuki, S. Epitaxial carbon nanotube film self-organized by sublimation decomposition of silicon carbide. *Appl. Phys. Lett.* **1997**, *71*, 2620–2622.
103. Takagi, D.; Hibino, H.; Suzuki, S.; Kobayashi, Y.; Homma, Y. Carbon Nanotube Growth from Semiconductor Nanoparticles. *Nano Lett.* **2007**, *7*, 2272–2275. [CrossRef]
104. Schneider, J.J.; Maksimova, N.I.; Engstler, J.; Joshi, R.; Schierholz, R.; Feile, R. Catalyst free growth of a carbon nanotube-alumina composite structure. *Inorganica Chim. Acta* **2008**, *361*, 1770–1778. [CrossRef]
105. Bae, E.J.; Choi, W.B.; Jeong, K.S.; Chu, J.U.; Park, G.S.; Song, S.; Yoo, I.K. Selective Growth of Carbon Nanotubes on Pre-patterned Porous Anodic Aluminum Oxide. *ADMA Adv. Mater.* **2002**, *14*, 277–279. [CrossRef]
106. Baker, R.T.K.; Chludzinski, J.J. Filamentous carbon growth on nickel-iron surfaces: The effect of various oxide additives. *J. Catal.* **1980**, *64*, 464–478. [CrossRef]
107. Tempel, H.; Joshi, R.; Schneider, J.J. Ink jet printing of ferritin as method for selective catalyst patterning and growth of multiwalled carbon nanotubes. *Mater. Chem. Phys.* **2010**, *121*, 178–183. [CrossRef]
108. Baird, T.; Fryer, J.R.; Grant, B. Carbon formation on iron and nickel foils by hydrocarbon pyrolysis—Reactions at 700 °C. *Carbon* **1974**, *12*, 591–602. [CrossRef]
109. Gary, G.T. Carbon fibers produced by pyrolysis of natural gas in stainless steel tubes. *Appl. Phys. Lett.* **1983**, *42*, 666–668.
110. Shiv Charan, P.S.; Shanmugam, S.; Kamaraj, V. Carbon Nanotubes—Synthesis and Application. *Trans. Indian Ceram. Soc.* **2009**, *68*, 163–172. [CrossRef]
111. Zhang, D.; Shi, L.; Fang, J.; Dai, K.; Li, X. Preparation and desalination performance of multiwall carbon nanotubes. *Mater. Chem. Phys.* **2006**, *97*, 415–419. [CrossRef]
112. Jiang, Q.; Song, L.J.; Yang, H.; He, Z.W.; Zhao, Y. Preparation and characterization on the carbon nanotube chemically modified electrode grown in situ. *Electrochem. Commun.* **2008**, *10*, 424–427. [CrossRef]
113. Edgar, K.; Spencer, J.L. Aerosol-based synthesis of carbon nanotubes. *Curr. Appl. Phys.* **2004**, *4*, 121–124. [CrossRef]
114. Chen, M.; Chen, C.-M.; Chen, C.-F. Growth of carbon nanotubes by microwave plasma chemical vapor deposition using CH_4 and CO_2 gas mixture. *Thin Solid Film.* **2002**, *420*, 230–234. [CrossRef]
115. Yan, Y.; Miao, J.; Yang, Z.; Xiao, F.-X.; Yang, H.B.; Liu, B.; Yang, Y. Carbon nanotube catalysts: Recent advances in synthesis, characterization and applications. *Chem. Soc. Rev.* **2015**, *44*, 3295–3346. [CrossRef] [PubMed]
116. Liu, Y.C.; Sun, B.M.; Ding, Z.Y. Effect of helium on synthesis of carbon nanotubes from the V-type pyrolysis flame. *Adv. Mater. Res.* **2011**, *221*, 540–544. [CrossRef]

117. Liu, Y.C.; Sun, B.M.; Ding, Z.Y. Effect of hydrogen on V-type pyrolysis flame synthesis of carbon nanotubes. *Adv. Mater. Res.* **2011**, *221*, 545–549. [CrossRef]
118. Liu, Y.C.; Sun, B.M.; Ding, Z.Y. Influence analysis of sampling time for synthesis of carbon nanotubes in the V-type pyrolysis flame. *Adv. Mater. Res.* **2011**, *221*, 235–239. [CrossRef]
119. Jun, L.; Qi, Y.; Alan, C.; Hou Tee, N.; Ramsey, S.; Jie, H.; Meyyappan, M. Bottom-up approach for carbon nanotube interconnects. *Appl. Phys. Lett.* **2003**, *82*, 2491–2493.
120. Liu, B.; Wu, F.; Gui, H.; Zheng, M.; Zhou, C. Chirality-Controlled Synthesis and Applications of Single-Wall Carbon Nanotubes. *ACS Nano* **2017**, *11*, 31–53. [CrossRef] [PubMed]
121. Hsu, W.K.; Hare, J.P.; Terrones, M. Condensed-phase nanotubes. *Nature* **1995**, *377*, 687–689. [CrossRef]
122. Hsu, W.K.; Terrones, M.; Hare, J.P.; Terrones, H.; Kroto, H.W.; Walton, D.R.M. Electrolytic formation of carbon nanostructures. *Chem. Phys. Lett.* **1996**, *262*, 161–166. [CrossRef]
123. Hsu, W.K.; Li, J.; Terrones, H.; Terrones, M.; Grobert, N.; Zhu, Y.Q.; Trasobares, S.; Hare, J.P.; Pickett, C.J.; Kroto, H.W.; et al. Electrochemical production of low-melting metal nanowires. *Chem. Phys. Lett.* **1999**, *301*, 159–166. [CrossRef]
124. Laplaze, D.; Bernier, P.; Maser, W.K.; Flamant, G.; Guillard, T.; Loiseau, A. Carbon nanotubes: The solar approach. *Carbon* **1998**, *36*, 685–688. [CrossRef]
125. Guillard, T.; Flamant, G.; Robert, J.F.; Rivoire, B.; Olalde, G.; Laplaze, D.; Alvarez, L. A large scale fullerenes synthesis solar reactor modelling and first experimental results. *Le J. Phys. IV* **1999**, *9*, Pr3-59–Pr53–64. [CrossRef]
126. Alvarez, L.; Guillard, T.; Olalde, G.; Rivoire, B.; Robert, J.F.; Bernier, P.; Flamant, G.; Laplaze, D. Large scale solar production of fullerenes and carbon nanotubes. *Synth. Met.* **1999**, *103*, 2476–2477. [CrossRef]
127. Alvarez, L.; Guillard, T.; Sauvajol, J.L.; Flamant, G.; Laplaze, D. Solar production of single-wall carbon nanotubes: Growth mechanisms studied by electron microscopy and Raman spectroscopy. *Appl. Phys. A* **2000**, *70*, 169–173. [CrossRef]
128. Guillard, T.; Flamant, G.; Robert, J.F.; Rivoire, B.; Giral, J.; Laplaze, D.; Alvarez, L. Scale up of a Solar Reactor for Fullerene and Nanotube Synthesis. *J. Sol. Energy Eng. Trans. ASME* **2002**, *124*, 22–27. [CrossRef]
129. Meier, A.; Kirillov, V.A.; Kuvshinov, G.G.; Mogilnykh, Y.I.; Weidenkaff, A.; Steinfeld, A. Production of catalytic filamentous carbon by solar thermal decomposition of hydrocarbons. *Le J. Phys. IV* **1999**, *9*, Pr3-393–Pr393–398. [CrossRef]
130. Hiremath, N.; Mays, J.; Bhat, G. Recent Developments in Carbon Fibers and Carbon Nanotube-Based Fibers: A Review. *Polym. Rev.* **2017**, *57*, 339–368. [CrossRef]
131. Meng, J.; Niu, C.; Xu, L.; Li, J.; Liu, X.; Wang, X.; Wu, Y.; Xu, X.; Chen, W.; Li, Q.; et al. General Oriented Formation of Carbon Nanotubes from Metal-Organic Frameworks. *J. Am. Chem. Soc.* **2017**, *139*, 8212–8221. [CrossRef]
132. Patole, S.P.; Alegaonkar, P.S.; Lee, H.C.; Yoo, J.B. Optimization of water assisted chemical vapor deposition parameters for super growth of carbon nanotubes. *Carbon* **2008**, *46*, 1987–1993. [CrossRef]
133. Ebbesen, T.W.; Ajayan, P.M.; Hiura, H.; Tanigaki, K. Purification of nanotubes. *Nature* **1994**, *367*, 519. [CrossRef]
134. Grobert, N. Carbon nanotubes—Becoming clean. *Mater. Today* **2007**, *10*, 28–35. [CrossRef]
135. Hauke, F.; Hirsch, A. Covalent Functionalization of Carbon Nanotubes. In *Carbon Nanotubes and Related Structures*; Wiley-VCH Verlag GmbH & Co. KGaA: Weinheim, Germany, 2010; pp. 135–198.
136. Hu, H.; Zhao, B.; Itkis, M.E.; Haddon, R.C. Nitric Acid Purification of Single-Walled Carbon Nanotubes. *J. Phys. Chem. B* **2003**, *107*, 13838–13842. [CrossRef]
137. Xu, Y.-Q.; Peng, H.; Hauge, R.H.; Smalley, R.E. Controlled Multistep Purification of Single-Walled Carbon Nanotubes. *Nano Lett.* **2005**, *5*, 163–168. [CrossRef] [PubMed]
138. Wang; Shan, H.; Hauge, R.H.; Pasquali, M.; Smalley, R.E. A Highly Selective, One-Pot Purification Method for Single-Walled Carbon Nanotubes. *J. Phys. Chem. B* **2007**, *111*, 1249–1252. [CrossRef] [PubMed]
139. Han, S.-W.; Oh, S.-J.; Tan, L.-S.; Baek, J.-B. One-pot purification and functionalization of single-walled carbon nanotubes in less-corrosive poly(phosphoric acid). *Carbon* **2008**, *46*, 1841–1849. [CrossRef]
140. Tobias, G.; Shao, L.; Salzmann, C.G.; Huh, Y.; Green, M.L.H. Purification and Opening of Carbon Nanotubes Using Steam. *J. Phys. Chem. B* **2006**, *110*, 22318–22322. [CrossRef] [PubMed]
141. Datsyuk, V.; Kalyva, M.; Papagelis, K.; Parthenios, J.; Tasis, D.; Siokou, A.; Kallitsis, I.; Galiotis, C. Chemical oxidation of multiwalled carbon nanotubes. *Carbon* **2008**, *46*, 833–840. [CrossRef]
142. Park, T.-J.; Banerjee, S.; Hemraj-Benny, T.; Wong, S.S. Purification strategies and purity visualization techniques for single-walled carbon nanotubes. *J. Mater. Chem.* **2006**, *16*, 141–154. [CrossRef]
143. Harutyunyan, A.R.; Pradhan, B.K.; Chang, J.; Chen, G.; Eklund, P.C. Purification of Single-Wall Carbon Nanotubes by Selective Microwave Heating of Catalyst Particles. *J. Phys. Chem. B* **2002**, *106*, 8671–8675. [CrossRef]
144. Martinez, M.T.; Callejas, M.A.; Benito, A.M.; Maser, W.K.; Cochet, M.; Andres, J.M.; Schreiber, J.; Chauvet, O.; Fierro, J.L.G. Microwave single walled carbon nanotubes purification. *Chem. Commun.* **2002**, *9*, 1000–1001. [CrossRef]
145. Shelimov, K.B.; Esenaliev, R.O.; Rinzler, A.G.; Huffman, C.B.; Smalley, R.E. Purification of single-wall carbon nanotubes by ultrasonically assisted filtration. *Chem. Phys. Lett.* **1998**, *282*, 429–434. [CrossRef]

146. Bandow, S.; Rao, A.M.; Williams, K.A.; Thess, A.; Smalley, R.E.; Eklund, P.C. Purification of Single-Wall Carbon Nanotubes by Microfiltration. *J. Phys. Chem. B* **1997**, *101*, 8839–8842. [CrossRef]
147. Brown, B.; Parker, C.B.; Stoner, B.R.; Glass, J.T. Growth of vertically aligned bamboo-like carbon nanotubes from ammonia/methane precursors using a platinum catalyst. *Carbon* **2011**, *49*, 266–274. [CrossRef]
148. Xu, Y.; Dervishi, E.; Biris, A.R.; Biris, A.S. Chirality-enriched semiconducting carbon nanotubes synthesized on high surface area MgO-supported catalyst. *Mater. Lett.* **2011**, *65*, 1878–1881. [CrossRef]
149. Huang, X.; McLean, R.S.; Zheng, M. High-Resolution Length Sorting and Purification of DNA-Wrapped Carbon Nanotubes by Size-Exclusion Chromatography. *Anal. Chem.* **2005**, *77*, 6225–6228. [CrossRef] [PubMed]
150. Ghosh, S.; Bachilo, S.M.; Weisman, R.B. Advanced sorting of single-walled carbon nanotubes by nonlinear density-gradient ultracentrifugation. *Nat. Nanotechnol.* **2017**, *5*, 443. [CrossRef]
151. Ago, H.; Kugler, T.; Cacialli, F.; Salaneck, W.R.; Shaffer, M.S.P.; Windle, A.H.; Friend, R.H. Work Functions and Surface Functional Groups of Multiwall Carbon Nanotubes. *J. Phys. Chem. B* **1999**, *103*, 8116–8121. [CrossRef]
152. Felten, A.; Bittencourt, C.; Pireaux, J.J. Gold clusters on oxygen plasma functionalized carbon nanotubes: XPS and TEM studies. *Nanotechnology* **2006**, *17*, 1954. [CrossRef]
153. Alexandre, F.; Jacques, G.; Jean-Jacques, P.; Robert, L.J.; Caroline, M.W.; Duoduo, L.; Gustaaf Van, T.; Carla, B. Effect of oxygen rf-plasma on electronic properties of CNTs. *J. Phys. D Appl. Phys.* **2007**, *40*, 7379.
154. Rueckes, T.; Kim, K.; Joselevich, E.; Tseng, G.Y.; Cheung, C.-L.; Lieber, C.M. Carbon Nanotube-Based Nonvolatile Random Access Memory for Molecular Computing. *Science* **2000**, *289*, 94–97. [CrossRef]
155. Ryabenko, A.G.; Dorofeeva, T.V.; Zvereva, G.I. UV-VIS-NIR spectroscopy study of sensitivity of single-wall carbon nanotubes to chemical processing and Van-der-Waals SWNT/SWNT interaction. Verification of the SWNT content measurements by absorption spectroscopy. *Carbon* **2004**, *42*, 1523–1535. [CrossRef]
156. Jiang, H.; Nasibulin, A.G.; Brown, D.P.; Kauppinen, E.I. Unambiguous atomic structural determination of single-walled carbon nanotubes by electron diffraction. *Carbon* **2007**, *45*, 662–667. [CrossRef]
157. Zhao, B.; Hu, H.; Niyogi, S.; Itkis, M.E.; Hamon, M.A.; Bhowmik, P.; Meier, M.S.; Haddon, R.C. Chromatographic Purification and Properties of Soluble Single-Walled Carbon Nanotubes. *J. Am. Chem. Soc.* **2001**, *123*, 11673–11677. [CrossRef]
158. Sherehiy, A.; Dumpala, S.; Safir, A.; Mudd, D.; Arnold, I.; Cohn, R.W.; Sunkara, M.K.; Sumanasekera, G.U. Thermionic emission properties and the work function determination of arrays of conical carbon nanotubes. *Diam. Relat. Mater.* **2013**, *34*, 1–8. [CrossRef]
159. Yehia, H.N.; Draper, R.K.; Mikoryak, C.; Walker, E.K.; Bajaj, P.; Musselman, I.H.; Daigrepont, M.C.; Dieckmann, G.R.; Pantano, P. Single-walled carbon nanotube interactions with HeLa cells. *J. Nanobiotechnol.* **2007**, *5*, 8. [CrossRef]
160. Ren, Z.F.; Huang, Z.P.; Xu, J.W.; Wang, J.H.; Bush, P.; Siegal, M.P.; Provencio, P.N. Synthesis of Large Arrays of Well-Aligned Carbon Nanotubes on Glass. *Science* **1998**, *282*, 1105–1107. [CrossRef]
161. Yu, R.; Chen, L.; Liu, Q.; Lin, J.; Tan, K.-L.; Ng, S.C.; Chan, H.S.O.; Xu, G.-Q.; Hor, T.S.A. Platinum Deposition on Carbon Nanotubes via Chemical Modification. *Chem. Mater.* **1998**, *10*, 718–722. [CrossRef]
162. Das, R. Carbon Nanotube Purification. In *Nanohybrid Catalyst Based on Carbon Nanotube: A Step-By-Step Guideline from Preparation to Demonstration*; Springer International Publishing: Cham, Switzerland, 2017; pp. 53–73.
163. Jishi, R.A.; Dresselhaus, M.S.; Dresselhaus, G. Electron-phonon coupling and the electrical conductivity of fullerene nanotubules. *Phys. Rev. B* **1993**, *48*, 11385–11389. [CrossRef] [PubMed]
164. Wilder, J.W.G.; Venema, L.C.; Rinzler, A.G.; Smalley, R.E.; Dekker, C. Electronic structure of atomically resolved carbon nanotubes. *Nature* **1998**, *391*, 59. [CrossRef]
165. Hassanien, A.; Tokumoto, M.; Kumazawa, Y.; Kataura, H.; Maniwa, Y.; Suzuki, S.; Achiba, Y. Atomic structure and electronic properties of single-wall carbon nanotubes probed by scanning tunneling microscope at room temperature. *Appl. Phys. Lett.* **1998**, *73*, 3839–3841. [CrossRef]
166. Hassanien, A.; Tokumoto, M.; Umek, P.; Mihailovic, D.; Mrzel, A. Fermi electron wave packet interference images on carbon nanotubes at room temperature. *Appl. Phys. Lett.* **2001**, *78*, 808–810. [CrossRef]
167. Singh, P.; Da Ros, T.; Kostarelos, K.; Prato, M.; Bianco, A. Carbon-Based Nanomaterial Applications in Biomedicine. In *Carbon Nanotubes and Related Structures*; Wiley-VCH Verlag GmbH & Co. KGaA: Weinheim, Germany, 2010; pp. 199–232.
168. Xue, Y.; Li, Q.; Chen, T. Chapter 11—Carbon Nanotubes for Biomedical Applications A2—Peng, Huisheng. In *Industrial Applications of Carbon Nanotubes*; Elsevier: Boston, MA, USA, 2017; pp. 323–346.
169. Yang, W.; Ratinac, K.R.; Ringer, S.P.; Thordarson, P.; Gooding, J.J.; Braet, F. Carbon Nanomaterials in Biosensors: Should You Use Nanotubes or Graphene? *Angew. Chem. Int. Ed.* **2010**, *49*, 2114–2138. [CrossRef] [PubMed]
170. Sudibya, H.G.; Ma, J.; Dong, X.; Ng, S.; Li, L.-J.; Liu, X.-W.; Chen, P. Interfacing Glycosylated Carbon-Nanotube-Network Devices with Living Cells to Detect Dynamic Secretion of Biomolecules. *Angew. Chem. Int. Ed.* **2009**, *48*, 2723–2726. [CrossRef]

171. Hu, F.X.; Kang, Y.J.; Du, F.; Zhu, L.; Xue, Y.H.; Chen, T.; Dai, L.M.; Li, C.M. Living Cells Directly Growing on a DNA/$Mn_3(PO_4)2$-Immobilized and Vertically Aligned CNT Array as a Free-Standing Hybrid Film for Highly Sensitive In Situ Detection of Released Superoxide Anions. *Adv. Funct. Mater.* **2015**, *25*, 5924–5932. [CrossRef]
172. Iverson, N.M.; Barone, P.W.; Shandell, M.; Trudel, L.J.; Sen, S.; Sen, F.; Ivanov, V.; Atolia, E.; Farias, E.; McNicholas, T.P.; et al. In vivo biosensing via tissue-localizable near-infrared-fluorescent single-walled carbon nanotubes. *Nat. Nanotechnol.* **2013**, *8*, 873. [CrossRef]
173. Jin, H.; Heller, D.A.; Kalbacova, M.; Kim, J.-H.; Zhang, J.; Boghossian, A.A.; Maheshri, N.; Strano, M.S. Detection of single-molecule H_2O_2 signalling from epidermal growth factor receptor using fluorescent single-walled carbon nanotubes. *Nat. Nanotechnol.* **2010**, *5*, 302. [CrossRef]
174. Xiang, L.; Yu, P.; Hao, J.; Zhang, M.; Zhu, L.; Dai, L.; Mao, L. Vertically Aligned Carbon Nanotube-Sheathed Carbon Fibers as Pristine Microelectrodes for Selective Monitoring of Ascorbate in Vivo. *Anal. Chem.* **2014**, *86*, 3909–3914. [CrossRef] [PubMed]
175. Snow, E.S.; Perkins, F.K.; Houser, E.J.; Badescu, S.C.; Reinecke, T.L. Chemical Detection with a Single-Walled Carbon Nanotube Capacitor. *Science* **2005**, *307*, 1942–1945. [CrossRef]
176. Esser, B.; Schnorr, J.M.; Swager, T.M. Selective Detection of Ethylene Gas Using Carbon Nanotube-based Devices: Utility in Determination of Fruit Ripeness. *Angew. Chem. Int. Ed.* **2012**, *51*, 5752–5756. [CrossRef] [PubMed]
177. Shi, H.; Xia, T.; Nel, A.E.; Yeh, J.I. Part II: Coordinated biosensors—Development of enhanced nanobiosensors for biological and medical applications. *Nanomedicine* **2007**, *2*, 599–614. [CrossRef]
178. Dastagir, T.; Forzani, E.S.; Zhang, R.; Amlani, I.; Nagahara, L.A.; Tsui, R.; Tao, N. Electrical detection of hepatitis C virus RNA on single wall carbon nanotube-field effect transistors. *Analyst* **2007**, *132*, 738–740. [CrossRef]
179. Wang, J.; Musameh, M. Carbon Nanotube/Teflon Composite Electrochemical Sensors and Biosensors. *Anal. Chem.* **2003**, *75*, 2075–2079. [CrossRef]
180. Rivas, G.A.; Rodroguez, M.C.; Rubianes, M.D.; Gutierrez, F.A.; Eguilaz, M.; Dalmasso, P.R.; Primo, E.N.; Tettamanti, C.; Ramirez, M.L.; Montemerlo, A.; et al. Carbon nanotubes-based electrochemical (bio)sensors for biomarkers. *Appl. Mater. Today* **2017**, *9*, 566–588. [CrossRef]
181. Li, Y.-W.; Chen, Y.; Ma, Y.-H.; Shi, J.-G.; Wang, Y.-X.; Qi, C.-H.; Li, Q.-S. Recent Advances in the Dehydrogenase Biosensors Based on Carbon Nanotube Modified Electrodes. *Chin. J. Anal. Chem.* **2014**, *42*, 759–765. [CrossRef]
182. Azadbakht, A.; Roushani, M.; Abbasi, A.R.; Menati, S.; Derikvand, Z. A label-free aptasensor based on polyethyleneimine wrapped carbon nanotubes in situ formed gold nanoparticles as signal probe for highly sensitive detection of dopamine. *Mater. Sci. Eng. C* **2016**, *68*, 585–593. [CrossRef] [PubMed]
183. Yang, C.; Trikantzopoulos, E.; Jacobs, C.B.; Venton, B.J. Evaluation of carbon nanotube fiber microelectrodes for neurotransmitter detection: Correlation of electrochemical performance and surface properties. *Anal. Chim. Acta* **2017**, *965*, 1–8. [CrossRef]
184. Mann, F.; Herrmann, N.; Meyer, D.; Kruss, S. Tuning Selectivity of Fluorescent Carbon Nanotube-Based Neurotransmitter Sensors. *Sensors* **2017**, *17*, 1521. [CrossRef] [PubMed]
185. Batra, B.; Pundir, C.S. An amperometric glutamate biosensor based on immobilization of glutamate oxidase onto carboxylated multiwalled carbon nanotubes/gold nanoparticles/chitosan composite film modified Au electrode. *Biosens. Bioelectron.* **2013**, *47*, 496–501. [CrossRef] [PubMed]
186. Gutierrez, F.A.; Rubianes, M.D.; Rivas, G.A. Electrochemical sensor for amino acids and glucose based on glassy carbon electrodes modified with multi-walled carbon nanotubes and copper microparticles dispersed in polyethylenimine. *J. Electroanal. Chem.* **2016**, *765*, 16–21. [CrossRef]
187. Wang, Y.; Li, J. A carbon nanotubes assisted strategy for insulin detection and insulin proteolysis assay. *Anal. Chim. Acta* **2009**, *650*, 49–53. [CrossRef] [PubMed]
188. Choi, Y.-E.; Kwak, J.-W.; Park, J.W. Nanotechnology for Early Cancer Detection. *Sensors* **2009**, *10*, 428. [CrossRef]
189. Kierny, M.R.; Cunningham, T.D.; Kay, B.K. Detection of biomarkers using recombinant antibodies coupled to nanostructured platforms. *Nano Rev.* **2012**, *3*, 17240. [CrossRef] [PubMed]
190. Juzgado, A.; Solda, A.; Ostric, A.; Criado, A.; Valenti, G.; Rapino, S.; Conti, G.; Fracasso, G.; Paolucci, F.; Prato, M. Highly sensitive electrochemiluminescence detection of a prostate cancer biomarker. *J. Mater. Chem. B* **2017**, *5*, 6681–6687. [CrossRef] [PubMed]
191. Wang, B.; Akiba, U.; Anzai, J.-I. Recent Progress in Nanomaterial-Based Electrochemical Biosensors for Cancer Biomarkers: A Review. *Molecules* **2017**, *22*, 1048. [CrossRef]
192. Mandal, D.; Nunna, B.B.; Zhuang, S.; Rakshit, S.; Lee, E.S. Carbon nanotubes based biosensor for detection of cancer antigens (CA-125) under shear flow condition. *Nano-Struct. Nano-Objects* **2017**, *15*, 180–185. [CrossRef]
193. Feng, T.; Wang, Y.; Qiao, X. Recent Advances of Carbon Nanotubes-based Electrochemical Immunosensors for the Detection of Protein Cancer Biomarkers. *Electroanalysis* **2016**, *29*, 662–675. [CrossRef]
194. Zhou, N.; Yang, T.; Jiang, C.; Du, M.; Jiao, K. Highly sensitive electrochemical impedance spectroscopic detection of DNA hybridization based on Aunano-CNT/PANnano films. *Talanta* **2009**, *77*, 1021–1026. [CrossRef] [PubMed]

195. Li, J.; Lee, E.-C. Functionalized multi-wall carbon nanotubes as an efficient additive for electrochemical DNA sensor. *Sens. Actuators B Chem.* **2017**, *239*, 652–659. [CrossRef]
196. Saeedfar, K.; Heng, L.Y.; Chiang, C.P. A DNA biosensor based on gold nanoparticle decorated on carboxylated multi-walled carbon nanotubes for gender determination of Arowana fish. *Bioelectrochemistry* **2017**, *118*, 106–113. [CrossRef] [PubMed]
197. Lin, Y.; Lu, F.; Tu, Y.; Ren, Z. Glucose Biosensors Based on Carbon Nanotube Nanoelectrode Ensembles. *Nano Lett.* **2004**, *4*, 191–195. [CrossRef]
198. Wang, J. Carbon-Nanotube Based Electrochemical Biosensors: A Review. *Electroanalysis* **2005**, *17*, 7–14. [CrossRef]
199. Sinha, N.; Ma, J.; Yeow, J.T.W. Carbon Nanotube-Based Sensors. *J. Nanosci. Nanotechnol.* **2006**, *6*, 573–590. [CrossRef]
200. Puett, C.; Inscoe, C.; Hartman, A.; Calliste, J.; Franceschi, D.K.; Lu, J.; Zhou, O.; Lee, Y.Z. An update on carbon nanotube-enabled X-ray sources for biomedical imaging. *Wiley Interdiscip. Rev. Nanomed. Nanobiotechnol.* **2017**, *10*, e1475. [CrossRef] [PubMed]
201. Kruss, S.; Salem, D.P.; VukoviÄ‡, L.; Lima, B.; Vander Ende, E.; Boyden, E.S.; Strano, M.S. High-resolution imaging of cellular dopamine efflux using a fluorescent nanosensor array. *Proc. Natl. Acad. Sci. USA* **2017**, *114*, 1789–1794. [CrossRef] [PubMed]
202. Wilson, N.R.; Macpherson, J.V. Carbon nanotube tips for atomic force microscopy. *Nat. Nanotechnol.* **2009**, *4*, 483. [CrossRef] [PubMed]
203. Keller, D.J.; Chih-Chung, C. Imaging steep, high structures by scanning force microscopy with electron beam deposited tips. *Surf. Sci.* **1992**, *268*, 333–339. [CrossRef]
204. Ramsey, M.D.S.; Neil, A.F.; Bettye, L.S.; Daniel, E.M.; Galen, D.S.; Paul, K.H. Carbon nanotubes as probes for atomic force microscopy. *Nanotechnology* **2000**, *11*, 1.
205. Wong, S.S.; Woolley, A.T.; Joselevich, E.; Cheung, C.L.; Lieber, C.M. Covalently-Functionalized Single-Walled Carbon Nanotube Probe Tips for Chemical Force Microscopy. *J. Am. Chem. Soc.* **1998**, *120*, 8557–8558. [CrossRef]
206. Goldstein, D.; Nassar, T.; Lambert, G.; Kadouche, J.; Benita, S. The design and evaluation of a novel targeted drug delivery system using cationic emulsion-antibody conjugates. *J. Control. Release* **2005**, *108*, 418–432. [CrossRef]
207. Tsai, H.-C.; Lin, J.-Y.; Maryani, F.; Huang, C.-C.; Imae, T. Drug-loading capacity and nuclear targeting of multiwalled carbon nanotubes grafted with anionic amphiphilic copolymers. *Int. J. Nanomed.* **2013**, *8*, 4427–4440. [CrossRef]
208. Liu, P. Modification Strategies for Carbon Nanotubes as a Drug Delivery System. *Ind. Eng. Chem. Res.* **2013**, *52*, 13517–13527. [CrossRef]
209. Lu, Q.; Moore, J.M.; Huang, G.; Mount, A.S.; Rao, A.M.; Larcom, L.L.; Ke, P.C. RNA Polymer Translocation with Single-Walled Carbon Nanotubes. *Nano Lett.* **2004**, *4*, 2473–2477. [CrossRef]
210. Martin, C.R.; Kohli, P. The emerging field of nanotube biotechnology. *Nat. Rev. Drug Discov.* **2003**, *2*, 29. [CrossRef] [PubMed]
211. Jorgensen, W.L. The Many Roles of Computation in Drug Discovery. *Science* **2004**, *303*, 1813–1818. [CrossRef]
212. Hilder, T.A.; Hill, J.M. Carbon nanotubes as drug delivery nanocapsules. *Curr. Appl. Phys.* **2008**, *8*, 258–261. [CrossRef]
213. Serpell, C.J.; Kostarelos, K.; Davis, B.G. Can Carbon Nanotubes Deliver on Their Promise in Biology? Harnessing Unique Properties for Unparalleled Applications. *ACS Cent. Sci.* **2016**, *2*, 190–200. [CrossRef] [PubMed]
214. Bian, Z.; Wang, R.J.; Wang, W.H.; Zhang, T.; Inoue, A. Carbon-Nanotube-Reinforced Zr-Based Bulk Metallic Glass Composites and Their Properties. *Adv. Funct. Mater.* **2004**, *14*, 55–63. [CrossRef]
215. Wang, Y.; Da, S.; Kim, M.J.; Kelly, K.F.; Guo, W.; Kittrell, C.; Hauge, R.H.; Smalley, R.E. Ultrathin "Bed-of-Nails" Membranes of Single-Wall Carbon Nanotubes. *J. Am. Chem. Soc.* **2004**, *126*, 9502–9503. [CrossRef] [PubMed]
216. Namgung, S.; Baik, K.Y.; Park, J.; Hong, S. Controlling the Growth and Differentiation of Human Mesenchymal Stem Cells by the Arrangement of Individual Carbon Nanotubes. *ACS Nano* **2011**, *5*, 7383–7390. [CrossRef] [PubMed]
217. Pok, S.; Vitale, F.; Eichmann, S.L.; Benavides, O.M.; Pasquali, M.; Jacot, J.G. Biocompatible Carbon Nanotube-Chitosan Scaffold Matching the Electrical Conductivity of the Heart. *ACS Nano* **2014**, *8*, 9822–9832. [CrossRef] [PubMed]
218. Aoki, N.; Yokoyama, A.; Nodasaka, Y.; Akasaka, T.; Uo, M.; Sato, Y.; Tohji, K.; Watari, F. Cell Culture on a Carbon Nanotube Scaffold. *J. Biomed. Nanotechnol.* **2005**, *1*, 402–405. [CrossRef]
219. Abarrategi, A.; Gutiérrez, M.C.; Moreno-Vicente, C.; Hortigüela, M.J.; Ramos, V.; López-Lacomba, J.L.; Ferrer, M.L.; del Monte, F. Multiwall carbon nanotube scaffolds for tissue engineering purposes. *Biomaterials* **2008**, *29*, 94–102. [CrossRef]
220. Meng, J.; Kong, H.; Han, Z.; Wang, C.; Zhu, G.; Xie, S.; Xu, H. Enhancement of nanofibrous scaffold of multiwalled carbon nanotubes/polyurethane composite to the fibroblasts growth and biosynthesis. *J. Biomed. Mater. Res. Part A* **2009**, *88*, 105–116. [CrossRef]
221. Chao, T.-I.; Xiang, S.; Chen, C.-S.; Chin, W.-C.; Nelson, A.J.; Wang, C.; Lu, J. Carbon nanotubes promote neuron differentiation from human embryonic stem cells. *Biochem. Biophys. Res. Commun.* **2009**, *384*, 426–430. [CrossRef] [PubMed]
222. Hirata, E.; Uo, M.; Takita, H.; Akasaka, T.; Watari, F.; Yokoyama, A. Development of a 3D collagen scaffold coated with multiwalled carbon nanotubes. *J. Biomed. Mater. Res. Part B Appl. Biomater.* **2009**, *90*, 629–634. [CrossRef] [PubMed]
223. Joshi, A.; Punyani, S.; Bale, S.S.; Yang, H.; Borca-Tasciuc, T.; Kane, R.S. Nanotube-assisted protein deactivation. *Nat. Nanotechnol.* **2007**, *3*, 41. [CrossRef]

224. Du, Z.; Yu, Y.-L.; Chen, X.-W.; Wang, J.-H. The Isolation of Basic Proteins by Solid-Phase Extraction with Multiwalled Carbon Nanotubes. *Chem.—A Eur. J.* **2007**, *13*, 9679–9685. [CrossRef]
225. Kang, S.; Pinault, M.; Pfefferle, L.D.; Elimelech, M. Single-Walled Carbon Nanotubes Exhibit Strong Antimicrobial Activity. *Langmuir* **2007**, *23*, 8670–8673. [CrossRef] [PubMed]
226. Aslan, S.; Maatta, J.; Haznedaroglu, B.Z.; Goodman, J.P.M.; Pfefferle, L.D.; Elimelech, M.; Pauthe, E.; Sammalkorpi, M.; Van Tassel, P.R. Carbon nanotube bundling: Influence on layer-by-layer assembly and antimicrobial activity. *Soft Matter* **2012**, *9*, 2136–2144. [CrossRef]
227. Liu, S.; Wei, L.; Hao, L.; Fang, N.; Chang, M.W.; Xu, R.; Yang, Y.; Chen, Y. Sharper and Faster "Nano Darts" Kill More Bacteria: A Study of Antibacterial Activity of Individually Dispersed Pristine Single-Walled Carbon Nanotube. *ACS Nano* **2009**, *3*, 3891–3902. [CrossRef] [PubMed]
228. Liu, Z.; Fan, A.C.; Rakhra, K.; Sherlock, S.; Goodwin, A.; Chen, X.; Yang, Q.; Felsher, D.W.; Dai, H. Supramolecular Stacking of Doxorubicin on Carbon Nanotubes for In Vivo Cancer Therapy. *Angew. Chem. Int. Ed.* **2009**, *48*, 7668–7672. [CrossRef] [PubMed]
229. Wu, H.; Shi, H.; Zhang, H.; Wang, X.; Yang, Y.; Yu, C.; Hao, C.; Du, J.; Hu, H.; Yang, S. Prostate stem cell antigen antibody-conjugated multiwalled carbon nanotubes for targeted ultrasound imaging and drug delivery. *Biomaterials* **2014**, *35*, 5369–5380. [CrossRef]
230. Kang, B.; Yu, D.; Dai, Y.; Chang, S.; Chen, D.; Ding, Y. Cancer-Cell Targeting and Photoacoustic Therapy Using Carbon Nanotubes as "Bomb" Agents. *Small* **2009**, *5*, 1292–1301. [CrossRef] [PubMed]
231. Zhou, F.; Wu, S.; Yuan, Y.; Chen, W.R.; Xing, D. Mitochondria-Targeting Photoacoustic Therapy Using Single-Walled Carbon Nanotubes. *Small* **2012**, *8*, 1543–1550. [CrossRef] [PubMed]
232. Liang, C.; Diao, S.; Wang, C.; Gong, H.; Liu, T.; Hong, G.; Shi, X.; Dai, H.; Liu, Z. Tumor Metastasis Inhibition by Imaging-Guided Photothermal Therapy with Single-Walled Carbon Nanotubes. *Adv. Mater.* **2014**, *26*, 5646–5652. [CrossRef]
233. Wang, L.; Shi, J.; Liu, R.; Liu, Y.; Zhang, J.; Yu, X.; Gao, J.; Zhang, C.; Zhang, Z. Photodynamic effect of functionalized single-walled carbon nanotubes: A potential sensitizer for photodynamic therapy. *Nanoscale* **2014**, *6*, 4642–4651. [CrossRef] [PubMed]
234. Shi, J.; Ma, R.; Wang, L.; Zhang, J.; Liu, R.; Li, L.; Liu, Y.; Hou, L.; Yu, X.; Gao, J.; et al. The application of hyaluronic acid-derivatized carbon nanotubes in hematoporphyrin monomethyl ether-based photodynamic therapy for in vivo and in vitro cancer treatment. *Int. J. Nanomed.* **2013**, *8*, 2361–2373. [CrossRef] [PubMed]
235. Jia, G.; Wang, H.; Yan, L.; Wang, X.; Pei, R.; Yan, T.; Zhao, Y.; Guo, X. Cytotoxicity of Carbon Nanomaterials: Single-Wall Nanotube, Multi-Wall Nanotube, and Fullerene. *Environ. Sci. Technol.* **2005**, *39*, 1378–1383. [CrossRef] [PubMed]
236. Nel, A.; Xia, T.; Madler, L.; Li, N. Toxic Potential of Materials at the Nanolevel. *Science* **2006**, *311*, 622–627. [CrossRef] [PubMed]
237. Magrez, A.; Kasas, S.; Salicio, V.; Pasquier, N.; Seo, J.W.; Celio, M.; Catsicas, S.; Schwaller, B.; Forró, L. Cellular Toxicity of Carbon-Based Nanomaterials. *Nano Lett.* **2006**, *6*, 1121–1125. [CrossRef] [PubMed]
238. Kobayashi, N.; Izumi, H.; Morimoto, Y. Review of toxicity studies of carbon nanotubes. *J. Occup. Health* **2017**, *59*, 394–407. [CrossRef]
239. Kolosnjaj-Tabi, J.; Szwarc, H.; Moussa, F. Carbon nanotubes: Culprit or witness of air pollution? *Nano Today* **2017**, *15*, 11–14. [CrossRef]
240. Chen, M.; Qin, X.; Zeng, G. Biodegradation of Carbon Nanotubes, Graphene, and Their Derivatives. *Trends Biotechnol.* **2017**, *35*, 836–846. [CrossRef] [PubMed]
241. Zhang, L.; Petersen, E.J.; Habteselassie, M.Y.; Mao, L.; Huang, Q. Degradation of multiwall carbon nanotubes by bacteria. *Environ. Pollut.* **2013**, *181*, 335–339. [CrossRef] [PubMed]
242. Chen, M.; Qin, X.; Li, J.; Zeng, G. Probing molecular basis of single-walled carbon nanotube degradation and nondegradation by enzymes based on manganese peroxidase and lignin peroxidase. *RSC Adv.* **2016**, *6*, 3592–3599. [CrossRef]
243. Kharraz, J.E.; El-Sadek, A.; Ghaffour, N.; Mino, E. Water scarcity and drought in WANA countries. *Procedia Eng.* **2012**, *33*, 14–29. [CrossRef]
244. Lee, B.; Baek, Y.; Lee, M.; Jeong, D.H.; Lee, H.H.; Yoon, J.; Kim, Y.H. A carbon nanotube wall membrane for water treatment. *Nat. Commun.* **2015**, *6*, 7109. [CrossRef]
245. Khan, W.; Sharma, R.; Saini, P.; Berber, M.R.; Hafez, I.H. Carbon Nanotube-Based Polymer Composites: Synthesis, Properties and Applications. In *Carbon Nanotubes—Current Progress of their Polymer Composites*; InTech: Rijeka, Croatia, 2016; Chapter 1.
246. Ma, L.; Dong, X.; Chen, M.; Zhu, L.; Wang, C.; Yang, F.; Dong, Y. Fabrication and Water Treatment Application of Carbon Nanotubes (CNTs)-Based Composite Membranes: A Review. *Membranes* **2017**, *7*, 16. [CrossRef]
247. Das, R. Carbon Nanotube in Water Treatment. In *Nanohybrid Catalyst Based on Carbon Nanotube: A Step-by-Step Guideline from Preparation to Demonstration*; Springer International Publishing: Cham, Switzerland, 2017; pp. 23–54.
248. Deng, Q.; Lu, C.; Ou, C.; Liu, W. Effects of early life exposure to outdoor air pollution and indoor renovation on childhood asthma in China. *Build. Environ.* **2015**, *93 Pt 1*, 84–91. [CrossRef]
249. Forouzanfar, M.H.; Alexander, L.; Anderson, H.R.; Bachman, V.F.; Biryukov, S.; Brauer, M.; Burnett, R.; Casey, D.; Coates, M.M.; Cohen, A.; et al. Global, regional, and national comparative risk assessment of 79 behavioural, environmental and occupational,

and metabolic risks or clusters of risks in 188 countries, 1990–2013: A systematic analysis for the Global Burden of Disease Study 2013. *Lancet* **2015**, *386*, 2287–2323. [CrossRef] [PubMed]
250. Crutzen, P.J. Photochemical reactions initiated by and influencing ozone in unpolluted tropospheric air. *Tellus* **1974**, *26*, 47–57. [CrossRef]
251. Huang, R.J.; Zhang, Y.; Bozzetti, C.; Ho, K.F.; Cao, J.J.; Han, Y.; Daellenbach, K.R.; Slowik, J.G.; Platt, S.M.; Canonaco, F.; et al. High secondary aerosol contribution to particulate pollution during haze events in China. *Nature* **2015**, *514*, 218–222. [CrossRef] [PubMed]
252. Siegel, J.A. Primary and secondary consequences of indoor air cleaners. *Indoor Air* **2016**, *26*, 88–96. [CrossRef]
253. Viswanathan, G.; Kane, D.B.; Lipowicz, P.J. High Efficiency Fine Particulate Filtration Using Carbon Nanotube Coatings. *Adv. Mater.* **2004**, *16*, 2045–2049. [CrossRef]
254. Nasibulin, A.G.; Kaskela, A.; Mustonen, K.; Anisimov, A.S.; Ruiz, V.; Kivisto, S.; Rackauskas, S.; Timmermans, M.Y.; Pudas, M.; Aitchison, B.; et al. Multifunctional Free-Standing Single-Walled Carbon Nanotube Films. *ACS Nano* **2011**, *5*, 3214–3221. [CrossRef] [PubMed]
255. Yildiz, O.; Bradford, P.D. Aligned carbon nanotube sheet high efficiency particulate air filters. *Carbon* **2013**, *64*, 295–304. [CrossRef]
256. Wang, C.; Li, P.; Zong, Y.; Zhang, Y.; Li, S.; Wei, F. A high efficiency particulate air filter based on agglomerated carbon nanotube fluidized bed. *Carbon* **2014**, *79*, 424–431. [CrossRef]
257. Yang, S.; Nie, J.; Wei, F.; Yang, X. Removal of Ozone by Carbon Nanotubes/Quartz Fiber Film. *Environ. Sci. Technol.* **2016**, *50*, 9592–9598. [CrossRef]
258. Park, K.-T.; Hwang, J. Filtration and inactivation of aerosolized bacteriophage MS2 by a CNT air filter fabricated using electro-aerodynamic deposition. *Carbon* **2014**, *75*, 401–410. [CrossRef]
259. Li, P.; Zong, Y.; Zhang, Y.; Yang, M.; Zhang, R.; Li, S.; Wei, F. In situ fabrication of depth-type hierarchical CNT/quartz fiber filters for high efficiency filtration of sub-micron aerosols and high water repellency. *Nanoscale* **2013**, *5*, 3367–3372. [CrossRef]
260. Karwa, A.N.; Tatarchuk, B.J. Aerosol filtration enhancement using carbon nanostructures synthesized within a sintered nickel microfibrous matrix. *Sep. Purif. Technol.* **2012**, *87*, 84–94. [CrossRef]
261. Jiang, K.; Li, Q.; Chen, T. Chapter 4—Carbon Nanotubes for Displaying A2—Peng, Huisheng. In *Industrial Applications of Carbon Nanotubes*; Elsevier: Boston, MA, USA, 2017; pp. 101–127.
262. Huang, S.; Zhao, C.; Pan, W.; Cui, Y.; Wu, H. Direct Writing of Half-Meter Long CNT Based Fiber for Flexible Electronics. *Nano Lett.* **2015**, *15*, 1609–1614. [CrossRef] [PubMed]
263. De Volder, M.F.L.; Tawfick, S.H.; Baughman, R.H.; Hart, A.J. Carbon Nanotubes: Present and Future Commercial Applications. *Science* **2013**, *339*, 535–539. [CrossRef]
264. Yahachi, S.; Sashiro, U.; Koji, H. Cathode Ray Tube Lighting Elements with Carbon Nanotube Field Emitters. *Jpn. J. Appl. Phys.* **1998**, *37*, L346.
265. Yang, W.; Lin, X.; Feng, Z.; Liang, L.; Jie, T.; Peng, L.; Shoushan, F. Cold linear cathodes with carbon nanotube emitters and their application in luminescent tubes. *Nanotechnology* **2007**, *18*, 325702.
266. Wu, Z.; Chen, Z.; Du, X.; Logan, J.M.; Sippel, J.; Nikolou, M.; Kamaras, K.; Reynolds, J.R.; Tanner, D.B.; Hebard, A.F.; et al. Transparent, Conductive Carbon Nanotube Films. *Science* **2004**, *305*, 1273–1276. [CrossRef] [PubMed]
267. De, S.; Coleman, J.N. The effects of percolation in nanostructured transparent conductors. *MRS Bull.* **2011**, *36*, 774–781. [CrossRef]
268. Tans, S.J.; Verschueren, A.R.M.; Dekker, C. Room-temperature transistor based on a single carbon nanotube. *Nature* **1998**, *393*, 49. [CrossRef]
269. Yu-Mo, C.; Florent, L.; Ishiang, S.; Ricardo, I. A solution processed top emission OLED with transparent carbon nanotube electrodes. *Nanotechnology* **2010**, *21*, 134020.
270. Zhang, J.; Fu, Y.; Wang, C.; Chen, P.-C.; Liu, Z.; Wei, W.; Wu, C.; Thompson, M.E.; Zhou, C. Separated Carbon Nanotube Macroelectronics for Active Matrix Organic Light-Emitting Diode Displays. *Nano Lett.* **2011**, *11*, 4852–4858. [CrossRef] [PubMed]
271. Wang, H.; Wei, P.; Li, Y.; Han, J.; Lee, H.R.; Naab, B.D.; Liu, N.; Wang, C.; Adijanto, E.; Tee, B.C.-K.; et al. Tuning the threshold voltage of carbon nanotube transistors by n-type molecular doping for robust and flexible complementary circuits. *Proc. Natl. Acad. Sci. USA* **2014**, *111*, 4776–4781. [CrossRef]
272. Liu, P.; Liu, L.; Wei, Y.; Liu, K.; Chen, Z.; Jiang, K.; Li, Q.; Fan, S. Fast High-Temperature Response of Carbon Nanotube Film and Its Application as an Incandescent Display. *Adv. Mater.* **2009**, *21*, 3563–3566. [CrossRef]
273. Wei, Y.; Liu, P.; Jiang, K.; Fan, S. A Display Module Implemented by the Fast High-Temperatue Response of Carbon Nanotube Thin Yarns. *Nano Lett.* **2012**, *12*, 2548–2553. [CrossRef]
274. Liu, P.; Liu, L.; Jiang, K.; Fan, S. Carbon-Nanotube-Film Microheater on a Polyethylene Terephthalate Substrate and Its Application in Thermochromic Displays. *Small* **2011**, *7*, 732–736. [CrossRef] [PubMed]
275. Liu, P.; Zhou, D.; Wei, Y.; Jiang, K.; Wang, J.; Zhang, L.; Li, Q.; Fan, S. Load Characteristics of a Suspended Carbon Nanotube Film Heater and the Fabrication of a Fast-Response Thermochromic Display Prototype. *ACS Nano* **2015**, *9*, 3753–3759. [CrossRef]

276. Baughman, R.H.; Zakhidov, A.A.; de Heer, W.A. Carbon Nanotubes--The Route Toward Applications. *Science* **2002**, *297*, 787–792. [CrossRef]
277. Sugie, H.; Tanemura, M.; Filip, V.; Iwata, K.; Takahashi, K.; Okuyama, F. Carbon nanotubes as electron source in an x-ray tube. *Appl. Phys. Lett.* **2001**, *78*, 2578–2580. [CrossRef]
278. Matthew, T.C.; Parmee, R.J.; William, I.M. Nanomaterial-based x-ray sources. *Nanotechnology* **2016**, *27*, 082501.
279. Lee, S.H.; Han, J.S.; Yun, K.N.; Jeon, J.; Lee, C.J.; Song, Y.H. CNT point emitter for x-ray source applications. In Proceedings of the 30th International Vacuum Nanoelectronics Conference (IVNC 2017), Regensburg, Germany, 10–14 July 2017; pp. 308–309.
280. Pyatkov, F.; Futterling, V.; Khasminskaya, S.; Flavel, B.S.; Hennrich, F.; Kappes, M.M.; Krupke, R.; Pernice, W.H.P. Cavity-enhanced light emission from electrically driven carbon nanotubes. *Nat. Photonics* **2016**, *10*, 420. [CrossRef]
281. Shan, X.; Bade, S.G.R.; Geske, T.; Davis, M.; Smith, R.; Yu, Z. Organometal halide perovskite light-emitting diodes with laminated carbon nanotube electrodes. In *Organic Light Emitting Materials and Devices XXI*; SPIE: Bellingham, WA, USA, 2017; Volume 10362, pp. 12–17.
282. Zhang, X.; Cui, H.; Gui, Y.; Tang, J. Mechanism and Application of Carbon Nanotube Sensors in SF(6) Decomposed Production Detection: A Review. *Nanoscale Res. Lett.* **2017**, *12*, 177. [CrossRef]
283. Kong, J.; Franklin, N.R.; Zhou, C.; Chapline, M.G.; Peng, S.; Cho, K.; Dai, H. Nanotube Molecular Wires as Chemical Sensors. *Science* **2000**, *287*, 622–625. [CrossRef] [PubMed]
284. Wang, Y.; Duncan, T.V. Nanoscale sensors for assuring the safety of food products. *Curr. Opin. Biotechnol.* **2017**, *44*, 74–86. [CrossRef]
285. Rana, M.M.; Ibrahim, D.S.; Mohd Asyraf, M.R.; Jarin, S.; Tomal, A. A review on recent advances of CNTs as gas sensors. *Sens. Rev.* **2016**, *37*, 127–136. [CrossRef]
286. Fam, D.W.H.; Palaniappan, A.; Tok, A.I.Y.; Liedberg, B.; Moochhala, S.M. A review on technological aspects influencing commercialization of carbon nanotube sensors. *Sens. Actuators B Chem.* **2011**, *157*, 1–7. [CrossRef]
287. Zaporotskova, I.V.; Boroznina, N.P.; Parkhomenko, Y.N.; Kozhitov, L.V. Carbon nanotubes: Sensor properties. A review. *Mod. Electron. Mater.* **2016**, *2*, 95–105. [CrossRef]
288. Dhall, S.; Jaggi, N.; Nathawat, R. Functionalized multiwalled carbon nanotubes based hydrogen gas sensor. *Sens. Actuators A Phys.* **2013**, *201*, 321–327. [CrossRef]
289. Dhall, S.; Jaggi, N. Hydrogen Gas Sensing Characteristics of Multiwalled Carbon Nanotubes Based Hybrid Composites. *J. Electron. Mater.* **2016**, *45*, 695–702. [CrossRef]
290. Shivani, D.; Kapil, S.; Neena, J. A hydrogen gas sensor using a Pt-sputtered MWCNTs/ZnO nanostructure. *Meas. Sci. Technol.* **2014**, *25*, 085103.
291. Zhang, W.-D.; Zhang, W.-H. Carbon Nanotubes as Active Components for Gas Sensors. *J. Sens.* **2009**, *2009*, 16. [CrossRef]
292. de Jonge, N.; Lamy, Y.; Schoots, K.; Oosterkamp, T.H. High brightness electron beam from a multi-walled carbon nanotube. *Nature* **2002**, *420*, 393. [CrossRef] [PubMed]
293. Yeow, J.T.W.; She, J.P.M. Carbon nanotube-enhanced capillary condensation for a capacitive humidity sensor. *Nanotechnology* **2006**, *17*, 5441. [CrossRef]
294. Chopra, S.; Pham, A.; Gaillard, J.; Parker, A.; Rao, A.M. Carbon-nanotube-based resonant-circuit sensor for ammonia. *Appl. Phys. Lett.* **2002**, *80*, 4632–4634. [CrossRef]
295. Chopra, S.; McGuire, K.; Gothard, N.; Rao, A.M.; Pham, A. Selective gas detection using a carbon nanotube sensor. *Appl. Phys. Lett.* **2003**, *83*, 2280–2282. [CrossRef]
296. Eleftheriadou, M.; Pyrgiotakis, G.; Demokritou, P. Nanotechnology to the rescue: Using nano-enabled approaches in microbiological food safety and quality. *Curr. Opin. Biotechnol.* **2017**, *44*, 87–93. [CrossRef]
297. Yu, M.-F.; Lourie, O.; Dyer, M.J.; Moloni, K.; Kelly, T.F.; Ruoff, R.S. Strength and Breaking Mechanism of Multiwalled Carbon Nanotubes Under Tensile Load. *Science* **2000**, *287*, 637–640. [CrossRef]
298. Mukerji, J. Ceramic matrix composites. *Def. Sci. J.* **1993**, *43*, 385–395. [CrossRef]
299. Zapata-Solvas, E.; Gómez-García, D.; Domínguez-Rodríguez, A. Towards physical properties tailoring of carbon nanotubes-reinforced ceramic matrix composites. *J. Eur. Ceram. Soc.* **2012**, *32*, 3001–3020. [CrossRef]
300. Cho, J.; Boccaccini, A.R.; Shaffer, M.S.P. Ceramic matrix composites containing carbon nanotubes. *J. Mater. Sci.* **2009**, *44*, 1934–1951. [CrossRef]
301. Ma, R.Z.; Wu, J.; Wei, B.Q.; Liang, J.; Wu, D.H. Processing and properties of carbon nanotubes–nano-SiC ceramic. *J. Mater. Sci.* **1998**, *33*, 5243–5246. [CrossRef]
302. Lau, K.-T.; Hui, D. Effectiveness of using carbon nanotubes as nano-reinforcements for advanced composite structures. *Carbon* **2002**, *40*, 1605–1606. [CrossRef]
303. Bernholc, J.; Brenner, D.; Nardelli, M.B.; Meunier, V.; Roland, C. Mechanical and Electrical Properties of Nanotubes. *Annu. Rev. Mater. Res.* **2002**, *32*, 347–375. [CrossRef]

304. Kasperski, A.; Weibel, A.; Estournès, C.; Laurent, C.; Peigney, A. Multi-walled carbon nanotube–Al_2O_3 composites: Covalent or non-covalent functionalization for mechanical reinforcement. *Scr. Mater.* **2014**, *75*, 46–49. [CrossRef]
305. Yamamoto, G.; Hashida, T.; Hu, N. Carbon Nanotube Reinforced Alumina Composite Materials. In *Composites and Their Properties*; InTech: Rijeka, Croatia, 2012; Chapter 21.
306. Yang, K.; Cheng, L.; An, L.; Shao, G. Ceramic nanocomposites reinforced with a high volume fraction of carbon nanotubes. *J. Wuhan Univ. Technol.-Mater. Sci. Ed.* **2017**, *32*, 47–50. [CrossRef]
307. Thostenson, E.T.; Ren, Z.; Chou, T.-W. Advances in the science and technology of carbon nanotubes and their composites: A review. *Compos. Sci. Technol.* **2001**, *61*, 1899–1912. [CrossRef]
308. Liu, Y.; Kumar, S. Polymer/Carbon Nanotube Nano Composite Fibers—A Review. *ACS Appl. Mater. Interfaces* **2014**, *6*, 6069–6087. [CrossRef] [PubMed]
309. El Moumen, A.; Tarfaoui, M.; Lafdi, K. Mechanical characterization of carbon nanotubes based polymer composites using indentation tests. *Compos. Part B Eng.* **2017**, *114*, 1–7. [CrossRef]
310. Saini, P.; Arora, M.; Gomes, A.D.S. Microwave Absorption and EMI Shielding Behavior of Nanocomposites Based on Intrinsically Conducting Polymers, Graphene and Carbon Nanotubes. In *New Polymers for Special Applications*; InTech: Rijeka, Croatia, 2012; Chapter 3.
311. Thostenson, E.T.; Li, C.; Chou, T.-W. Nanocomposites in context. *Compos. Sci. Technol.* **2005**, *65*, 491–516. [CrossRef]
312. Ma, P.-C.; Siddiqui, N.A.; Marom, G.; Kim, J.-K. Dispersion and functionalization of carbon nanotubes for polymer-based nanocomposites: A review. *Compos. Part A Appl. Sci. Manuf.* **2010**, *41*, 1345–1367. [CrossRef]
313. Moniruzzaman, M.; Winey, K.I. Polymer Nanocomposites Containing Carbon Nanotubes. *Macromolecules* **2006**, *39*, 5194–5205. [CrossRef]
314. Saini, P.; Choudhary, V. Enhanced electromagnetic interference shielding effectiveness of polyaniline functionalized carbon nanotubes filled polystyrene composites. *J. Nanoparticle Res.* **2013**, *15*, 1415. [CrossRef]
315. Jeon, I.-Y.; Chang, D.W.; Kumar, N.A.; Baek, J.-B.; Yellampalli, S. Functionalization of Carbon Nanotubes. In *Carbon Nanotubes—Polymer Nanocomposites*; InTech: Rijeka, Croatia, 2011; Chapter 5.
316. Liu, P. Polypyrrole/Inorganic Nanocomposites for Supercapacitors. In *Fundamentals of Conjugated Polymer Blends, Copolymers and Composites*; John Wiley & Sons, Inc.: Hoboken, NJ, USA, 2015; pp. 419–447.
317. Arici, E.; Karazhanov, S. Carbon nanotubes for organic/inorganic hybrid solar cells. *Mater. Sci. Semicond. Process.* **2016**, *41*, 137–149. [CrossRef]
318. Kar, P.; Choudhury, A.; Verma, S.K. Conjugated Polymer Nanocomposites-Based Chemical Sensors. In *Fundamentals of Conjugated Polymer Blends, Copolymers and Composites*; John Wiley & Sons, Inc.: Hoboken, NJ, USA, 2015; pp. 619–686.
319. Andrews, R.; Weisenberger, M.C. Carbon nanotube polymer composites. *Curr. Opin. Solid State Mater. Sci.* **2004**, *8*, 31–37. [CrossRef]
320. Spitalsky, Z.; Tasis, D.; Papagelis, K.; Galiotis, C. Carbon nanotube-polymer composites: Chemistry, processing, mechanical and electrical properties. *Prog. Polym. Sci.* **2010**, *35*, 357–401. [CrossRef]
321. Ajayan, P.M.; Stephan, O.; Colliex, C.; Trauth, D. Aligned Carbon Nanotube Arrays Formed by Cutting a Polymer Resin–Nanotube Composite. *Science* **1994**, *265*, 1212–1214. [CrossRef] [PubMed]
322. Wagner, H.D.; Lourie, O.; Feldman, Y.; Tenne, R. Stress-induced fragmentation of multiwall carbon nanotubes in a polymer matrix. *Appl. Phys. Lett.* **1998**, *72*, 188–190. [CrossRef]
323. Ruan, S.L.; Gao, P.; Yang, X.G.; Yu, T.X. Toughening high performance ultrahigh molecular weight polyethylene using multiwalled carbon nanotubes. *Polymer* **2003**, *44*, 5643–5654. [CrossRef]
324. Ren, Y.; Li, F.; Cheng, H.-M.; Liao, K. Tension-tension fatigue behavior of unidirectional single-walled carbon nanotube reinforced epoxy composite. *Carbon* **2003**, *41*, 2177–2179. [CrossRef]
325. Erik, T.T.; Tsu-Wei, C. Aligned multi-walled carbon nanotube-reinforced composites: Processing and mechanical characterization. *J. Phys. D Appl. Phys.* **2002**, *35*, L77.
326. Wu, M.L.; Chen, Y.; Zhang, L.; Zhan, H.; Qiang, L.; Wang, J.N. High-Performance Carbon Nanotube/Polymer Composite Fiber from Layer-by-Layer Deposition. *ACS Appl. Mater. Interfaces* **2016**, *8*, 8137–8144. [CrossRef]
327. Fenta, E.W.; Mebratie, B.A. Advancements in carbon nanotube-polymer composites: Enhancing properties and applications through advanced manufacturing techniques. *Heliyon* **2024**, *10*, 36490. [CrossRef]
328. Chakraborty, B.; Modak, P.; Banerjee, S. Hydrogen Storage in Yttrium-Decorated Single Walled Carbon Nanotube. *J. Phys. Chem. C* **2012**, *116*, 22502–22508. [CrossRef]
329. Suarez, J.; Huarte-Larrañaga, F. Hydrogen confined in single-wall carbon nanotubes: Anisotropy effects on ro-vibrational quantum levels. *J. Chem. Phys.* **2012**, *137*, 064320. [CrossRef] [PubMed]
330. Dillon, A.C.; Jones, K.M.; Bekkedahl, T.A.; Kiang, C.H.; Bethune, D.S.; Heben, M.J. Storage of hydrogen in single-walled carbon nanotubes. *Nature* **1997**, *386*, 377. [CrossRef]

331. Hirscher, M.; Becher, M.; Haluska, M.; Dettlaff-Weglikowska, U.; Quintel, A.; Duesberg, G.S.; Choi, Y.-M.; Downes, P.; Hulman, M.; Roth, S.; et al. Hydrogen storage in sonicated carbon materials. *Appl. Phys. A* **2001**, *72*, 129–132. [CrossRef]
332. Liu, C.; Fan, Y.Y.; Liu, M.; Cong, H.T.; Cheng, H.M.; Dresselhaus, M.S. Hydrogen Storage in Single-Walled Carbon Nanotubes at Room Temperature. *Science* **1999**, *286*, 1127–1129. [CrossRef] [PubMed]
333. Hwang, J.; Gommans, H.H.; Ugawa, A.; Tashiro, H.; Haggenmueller, R.; Winey, K.I.; Fischer, J.E.; Tanner, D.B.; Rinzler, A.G. Polarized spectroscopy of aligned single-wall carbon nanotubes. *Phys. Rev. B* **2000**, *62*, R13310–R13313. [CrossRef]
334. Lee, S.M.; An, K.H.; Lee, Y.H.; Seifert, G.; Frauenheim, T. A Hydrogen Storage Mechanism in Single-Walled Carbon Nanotubes. *J. Am. Chem. Soc.* **2001**, *123*, 5059–5063. [CrossRef]
335. Ye, Y.; Ahn, C.C.; Witham, C.; Fultz, B.; Liu, J.; Rinzler, A.G.; Colbert, D.; Smith, K.A.; Smalley, R.E. Hydrogen adsorption and cohesive energy of single-walled carbon nanotubes. *Appl. Phys. Lett.* **1999**, *74*, 2307–2309. [CrossRef]
336. Nishimiya, N.; Ishigaki, K.; Takikawa, H.; Ikeda, M.; Hibi, Y.; Sakakibara, T.; Matsumoto, A.; Tsutsumi, K. Hydrogen sorption by single-walled carbon nanotubes prepared by a torch arc method. *J. Alloys Compd.* **2002**, *339*, 275–282. [CrossRef]
337. Ritschel, M.; Uhlemann, M.; Gutfleisch, O.; Leonhardt, A.; Graff, A.; TÃ¤schner, C.; Fink, J. Hydrogen storage in different carbon nanostructures. *Appl. Phys. Lett.* **2002**, *80*, 2985–2987. [CrossRef]
338. Ghosh, S.; Padmanabhan, V.C.E.R.R. Hydrogen storage capacity of bundles of single-walled carbon nanotubes with defects. *Int. J. Energy Res.* **2017**, *41*, 1108–1117. [CrossRef]
339. Zhao, T.; Ji, X.; Jin, W.; Yang, W.; Li, T. Hydrogen storage capacity of single-walled carbon nanotube prepared by a modified arc discharge. *Fuller. Nanotub. Carbon Nanostruct.* **2017**, *25*, 355–358. [CrossRef]
340. Zhou, S.; Liu, X.; Yang, K.; Zou, H. Study of H_2 physical adsorption in single-walled carbon nanotube array. *AIP Adv.* **2013**, *3*, 082119. [CrossRef]
341. Rashidi, A.M.; Nouralishahi, A.; Khodadadi, A.A.; Mortazavi, Y.; Karimi, A.; Kashefi, K. Modification of single wall carbon nanotubes (SWNT) for hydrogen storage. *Int. J. Hydrogen Energy* **2010**, *35*, 9489–9495. [CrossRef]
342. Wang, L.; Yang, R.T. New sorbents for hydrogen storage by hydrogen spillover—A review. *Energy Environ. Sci.* **2008**, *1*, 268–279. [CrossRef]
343. Zhang, G.; Qi, P.; Wang, X.; Lu, Y.; Mann, D.; Li, X.; Dai, H. Hydrogenation and Hydrocarbonation and Etching of Single-Walled Carbon Nanotubes. *J. Am. Chem. Soc.* **2006**, *128*, 6026–6027. [CrossRef]
344. Vasu, V.; Silambarasan, D. Carbon Nanotubes as Future Energy Storage System. *Mech. Mater. Sci. Eng. J.* **2017**, *9*.
345. Wu, X.B.; Chen, P.; Lin, J.; Tan, K.L. Hydrogen uptake by carbon nanotubes. *Int. J. Hydrogen Energy* **2000**, *25*, 261–265. [CrossRef]
346. Tibbetts, G.G.; Meisner, G.P.; Olk, C.H. Hydrogen storage capacity of carbon nanotubes, filaments, and vapor-grown fibers. *Carbon* **2001**, *39*, 2291–2301. [CrossRef]
347. Badzian, A.; Badzian, T.; Breval, E.; Piotrowski, A. Nanostructured, nitrogen-doped carbon materials for hydrogen storage. *Thin Solid Film.* **2001**, *398–399*, 170–174. [CrossRef]
348. Chen, Y.; Shaw, D.T.; Bai, X.D.; Wang, E.G.; Lund, C.; Lu, W.M.; Chung, D.D.L. Hydrogen storage in aligned carbon nanotubes. *Appl. Phys. Lett.* **2001**, *78*, 2128–2130. [CrossRef]
349. Elyassi, M.; Rashidi, A.; Hantehzadeh, M.R.; Elahi, S.M. Hydrogen Storage Behaviors by Adsorption on Multi-Walled Carbon Nanotubes. *J. Inorg. Organomet. Polym. Mater.* **2017**, *27*, 285–295. [CrossRef]
350. Mehrabi, M.; Parvin, P.; Reyhani, A.; Mortazavi, S.Z. Hydrogen storage in multi-walled carbon nanotubes decorated with palladium nanoparticles using laser ablation/chemical reduction methods. *Mater. Res. Express* **2017**, *4*, 095030. [CrossRef]
351. Kim, H.-S.; Lee, H.; Han, K.-S.; Kim, J.-H.; Song, M.-S.; Park, M.-S.; Lee, J.-Y.; Kang, J.-K. Hydrogen Storage in Ni Nanoparticle-Dispersed Multiwalled Carbon Nanotubes. *J. Phys. Chem. B* **2005**, *109*, 8983–8986. [CrossRef] [PubMed]
352. Reyhani, A.; Mortazavi, S.Z.; Mirershadi, S.; Moshfegh, A.Z.; Parvin, P.; Golikand, A.N. Hydrogen Storage in Decorated Multiwalled Carbon Nanotubes by Ca, Co, Fe, Ni, and Pd Nanoparticles under Ambient Conditions. *J. Phys. Chem. C* **2011**, *115*, 6994–7001. [CrossRef]
353. Wang, Y.; Li, A.; Wang, K.; Guan, C.; Deng, W.; Li, C.; Wang, X. Reversible hydrogen storage of multi-wall carbon nanotubes doped with atomically dispersed lithium. *J. Mater. Chem.* **2010**, *20*, 6490–6494. [CrossRef]
354. Ning, G.Q.; Wei, F.; Luo, G.H.; Wang, Q.X.; Wu, Y.L.; Yu, H. Hydrogen storage in multi-wall carbon nanotubes using samples up to 85 g. *Appl. Phys. A* **2004**, *78*, 955–959. [CrossRef]
355. Mosquera, E.; Diaz-Droguett, D.E.; Carvajal, N.; Roble, M.; Morel, M.; Espinoza, R. Characterization and hydrogen storage in multi-walled carbon nanotubes grown by aerosol-assisted CVD method. *Diam. Relat. Mater.* **2014**, *43*, 66–71. [CrossRef]
356. Lee, S.-Y.; Park, S.-J. Influence of the pore size in multi-walled carbon nanotubes on the hydrogen storage behaviors. *J. Solid State Chem.* **2012**, *194*, 307–312. [CrossRef]
357. Liu, W.; Zhao, Y.H.; Li, Y.; Jiang, Q.; Lavernia, E.J. Enhanced Hydrogen Storage on Li-Dispersed Carbon Nanotubes. *J. Phys. Chem. C* **2009**, *113*, 2028–2033. [CrossRef]
358. Chen, C.-H.; Huang, C.-C. Hydrogen storage by KOH-modified multi-walled carbon nanotubes. *Int. J. Hydrogen Energy* **2007**, *32*, 237–246. [CrossRef]

359. Reyhani, A.; Mortazavi, S.Z.; Mirershadi, S.; Golikand, A.N.; Moshfegh, A.Z. H_2 adsorption mechanism in Mg modified multi-walled carbon nanotubes for hydrogen storage. *Int. J. Hydrogen Energy* **2012**, *37*, 1919–1926. [CrossRef]
360. Zheng, J.; Duan, X.; Lin, H.; Gu, Z.; Fang, H.; Li, J.; Yuan, Y. Silver nanoparticles confined in carbon nanotubes: On the understanding of the confinement effect and promotional catalysis for the selective hydrogenation of dimethyl oxalate. *Nanoscale* **2016**, *8*, 5959–5967. [CrossRef] [PubMed]
361. Terrones, M.; Kamalakaran, R.; Seeger, T.; Rühle, M. Novel nanoscale gas containers: Encapsulation of N2 in CNx nanotubes. *Chem. Commun.* **2000**, *23*, 2335–2336. [CrossRef]
362. Popp, D.C. The effect of new technology on energy consumption. *Resour. Energy Econ.* **2001**, *23*, 215–239. [CrossRef]
363. Kumar, S.; Nehra, M.; Kedia, D.; Dilbaghi, N.; Tankeshwar, K.; Kim, K.-H. Carbon nanotubes: A potential material for energy conversion and storage. *Prog. Energy Combust. Sci.* **2018**, *64*, 219–253. [CrossRef]
364. Keru, G.; Ndungu, P.G.; Nyamori, V.O. A review on carbon nanotube/polymer composites for organic solar cells. *Int. J. Energy Res.* **2014**, *38*, 1635–1653. [CrossRef]
365. Yan, J.; Saunders, B.R. Third-generation solar cells: A review and comparison of polymer:fullerene, hybrid polymer and perovskite solar cells. *RSC Adv.* **2014**, *4*, 43286–43314. [CrossRef]
366. Cataldo, S.; Salice, P.; Menna, E.; Pignataro, B. Carbon nanotubes and organic solar cells. *Energy Environ. Sci.* **2012**, *5*, 5919–5940. [CrossRef]
367. Pan, H.; Li, J.; Feng, Y. Carbon Nanotubes for Supercapacitor. *Nanoscale Res. Lett.* **2009**, *5*, 654–668. [CrossRef] [PubMed]
368. Abdalla, S.; Al-Marzouki, F.; Al-Ghamdi, A.A.; Abdel-Daiem, A. Different Technical Applications of Carbon Nanotubes. *Nanoscale Res. Lett.* **2015**, *10*, 358. [CrossRef] [PubMed]
369. Chen, T.; Dai, L. Carbon nanomaterials for high-performance supercapacitors. *Mater. Today* **2013**, *16*, 272–280. [CrossRef]
370. Lu, W.; Dai, L.; Marulanda, J.M. Carbon Nanotube Supercapacitors. In *Carbon Nanotubes*; InTech: Rijeka, Croatia, 2010; Chapter 29.
371. O'Regan, B.; Grätzel, M. A low-cost, high-efficiency solar cell based on dye-sensitized colloidal TiO_2 films. *Nature* **1991**, *353*, 737. [CrossRef]
372. Ma, L.; Niu, H. Application of Carbon Nanotubes in Dye-Sensitized Solar Cells. In *Handbook of Polymer Nanocomposites. Processing, Performance and Application: Volume B: Carbon Nanotube Based Polymer Composites*; Kar, K.K., Pandey, J.K., Rana, S., Eds.; Springer: Berlin/Heidelberg, Germany, 2015; pp. 391–413.
373. Mugadza, K.; Nyamori, V.O.; Mola, G.T.; Simoyi, R.H.; Ndungu, P.G. Low temperature synthesis of multiwalled carbon nanotubes and incorporation into an organic solar cell. *J. Exp. Nanosci.* **2017**, *12*, 363–383. [CrossRef]
374. Keru, G.; Ndungu, P.G.; Mola, G.T.; Nogueira, A.F.; Nyamori, V.O. Organic solar cells with boron- or nitrogen-doped carbon nanotubes in the P3HT: PCBM photoactive layer. *J. Nanomater.* **2016**, *2016*, 35. [CrossRef]
375. Habisreutinger, S.N.; Nicholas, R.J.; Snaith, H.J. Carbon Nanotubes in Perovskite Solar Cells. *Adv. Energy Mater.* **2016**, *7*, 1601839. [CrossRef]
376. Kyaw, A.K.; Tantang, H.; Wu, T.; Ke, L.; Wei, J.; Demir, H.V.; Zhang, Q.; Sun, X.W. Dye-sensitized solar cell with a pair of carbon-based electrodes. *J. Phys. D Appl. Phys.* **2012**, *45*, 165103. [CrossRef]
377. Sharma, S.; Bulkesh, S.; Ghoshal, S.K.; Mohan, D. Dye sensitized solar cells: From genesis to recent drifts. *Renew. Sustain. Energy Rev.* **2017**, *70*, 529–537. [CrossRef]
378. Gao, F.; Wang, Y.; Shi, D.; Zhang, J.; Wang, M.; Jing, X.; Humphry-Baker, R.; Wang, P.; Zakeeruddin, S.M.; Gratzel, M. Enhance the Optical Absorptivity of Nanocrystalline TiO_2 Film with High Molar Extinction Coefficient Ruthenium Sensitizers for High Performance Dye-Sensitized Solar Cells. *J. Am. Chem. Soc.* **2008**, *130*, 10720–10728. [CrossRef] [PubMed]
379. Tang, Q.; Zhang, H.; Meng, Y.; He, B.; Yu, L. Dissolution Engineering of Platinum Alloy Counter Electrodes in Dye-Sensitized Solar Cells. *Angew. Chem. Int. Ed.* **2015**, *54*, 11448–11452. [CrossRef] [PubMed]
380. Al-Marzouki, F.M.; Abdalla, S.; Al-Ameer, S. Dye Sensitized Solar Cells with Low Cost Carbon Nanotubes Electrodes. *Adv. Mater. Sci. Eng.* **2016**, *2016*, 13. [CrossRef]
381. Prasetio, A.; Subagio, A.; Purwanto, A.; Widiyandari, H. Dye-sensitized solar cell based carbon nanotube as counter electrode. *AIP Conf. Proc.* **2016**, *1710*, 030054.
382. Leu, Y.-A.; Yeh, M.-H.; Lin, L.-Y.; Li, T.-J.; Chang, L.-Y.; Shen, S.-Y.; Li, Y.-S.; Chen, G.-L.; Chiang, W.-H.; Lin, J.-J.; et al. Thermally Stable Boron-Doped Multiwalled Carbon Nanotubes as a Pt-free Counter Electrode for Dye-Sensitized Solar Cells. *ACS Sustain. Chem. Eng.* **2017**, *5*, 537–546. [CrossRef]
383. Batmunkh, M.; Biggs, M.J.; Shapter, J.G. Carbon Nanotubes for Dye-Sensitized Solar Cells. *Small* **2015**, *11*, 2963–2989. [CrossRef] [PubMed]
384. Frackowiak, E. Carbon materials for supercapacitor application. *Phys. Chem. Chem. Phys.* **2007**, *9*, 1774–1785. [CrossRef] [PubMed]
385. Purkait, T.; Singh, G.; Singh, M.; Kumar, D.; Dey, R.S. Large area few-layer graphene with scalable preparation from waste biomass for high-performance supercapacitor. *Sci. Rep.* **2017**, *7*, 15239. [CrossRef]

386. Beidaghi, M.; Gogotsi, Y. Capacitive energy storage in micro-scale devices: Recent advances in design and fabrication of micro-supercapacitors. *Energy Environ. Sci.* **2014**, *7*, 867–884. [CrossRef]
387. Niu, C.; Sichel, E.K.; Hoch, R.; Moy, D.; Tennent, H. High power electrochemical capacitors based on carbon nanotube electrodes. *Appl. Phys. Lett.* **1997**, *70*, 1480–1482. [CrossRef]
388. Choi, C.; Lee, J.A.; Choi, A.Y.; Kim, Y.T.; Lepró, X.; Lima, M.D.; Baughman, R.H.; Kim, S.J. Flexible Supercapacitor Made of Carbon Nanotube Yarn with Internal Pores. *Adv. Mater.* **2014**, *26*, 2059–2065. [CrossRef]
389. Zhi, M.; Xiang, C.; Li, J.; Li, M.; Wu, N. Nanostructured carbon-metal oxide composite electrodes for supercapacitors: A review. *Nanoscale* **2012**, *5*, 72–88. [CrossRef]
390. Dhibar, S.; Das, C.K. Silver Nanoparticles Decorated Polyaniline/Multiwalled Carbon Nanotubes Nanocomposite for High-Performance Supercapacitor Electrode. *Ind. Eng. Chem. Res.* **2014**, *53*, 3495–3508. [CrossRef]
391. Sun, L.; Wang, X.; Zhang, K.; Zou, J.; Yan, Z.; Hu, X.; Zhang, Q. Bi-functional electrode for UV detector and supercapacitor. *Nano Energy* **2015**, *15*, 445–452. [CrossRef]
392. Zhang, Z.; Deng, J.; Li, X.; Yang, Z.; He, S.; Chen, X.; Guan, G.; Ren, J.; Peng, H. Superelastic Supercapacitors with High Performances during Stretching. *Adv. Mater.* **2015**, *27*, 356–362. [CrossRef]
393. Wang, H.; Wang, C.; Jian, M.; Wang, Q.; Xia, K.; Yin, Z.; Zhang, M.; Liang, X.; Zhang, Y. Superelastic wire-shaped supercapacitor sustaining 850% tensile strain based on carbon nanotube@graphene fiber. *Nano Res.* **2017**, *11*, 2347–2356. [CrossRef]
394. Wu, G.; Tan, P.; Wang, D.; Li, Z.; Peng, L.; Hu, Y.; Wang, C.; Zhu, W.; Chen, S.; Chen, W. High-performance Supercapacitors Based on Electrochemical-induced Vertical-aligned Carbon Nanotubes and Polyaniline Nanocomposite Electrodes. *Sci. Rep.* **2017**, *7*, 43676. [CrossRef]
395. Choi, C.; Kim, K.M.; Kim, K.J.; Lepró, X.; Spinks, G.M.; Baughman, R.H.; Kim, S.J. Improvement of system capacitance via weavable superelastic biscrolled yarn supercapacitors. *Nat. Commun.* **2016**, *7*, 13811. [CrossRef]
396. Wu, P.; Cheng, S.; Yang, L.; Lin, Z.; Gui, X.; Ou, X.; Zhou, J.; Yao, M.; Wang, M.; Zhu, Y.; et al. Synthesis and Characterization of Self-Standing and Highly Flexible δ-MnO_2@CNTs/CNTs Composite Films for Direct Use of Supercapacitor Electrodes. *ACS Appl. Mater. Interfaces* **2016**, *8*, 23721–23728. [CrossRef]
397. Zhou, J.G.; Fang, H.T.; Hu, Y.F.; Sham, T.K.; Wu, C.X.; Liu, M.; Li, F. Immobilization of RuO_2 on Carbon Nanotube: An X-ray Absorption Near-Edge Structure Study. *J. Phys. Chem. C* **2009**, *113*, 10747–10750. [CrossRef]
398. Tao, L.; Shengjun, L.; Bowen, Z.; Bei, W.; Dayong, N.; Zeng, C.; Ying, Y.; Ning, W.; Weifeng, Z. Supercapacitor electrode with a homogeneously Co(3)O(4)-coated multiwalled carbon nanotube for a high capacitance. *Nanoscale Res. Lett.* **2015**, *10*, 208. [CrossRef]
399. Zhou, X.; Wang, A.; Pan, Y.; Yu, C.; Zou, Y.; Zhou, Y.; Chen, Q.; Wu, S. Facile synthesis of a Co_3O_4@carbon nanotubes/polyindole composite and its application in all-solid-state flexible supercapacitors. *J. Mater. Chem. A* **2015**, *3*, 13011–13015. [CrossRef]
400. Wang, X.; Li, M.; Chang, Z.; Yang, Y.; Wu, Y.; Liu, X. Co_3O_4@MWCNT Nanocable as Cathode with Superior Electrochemical Performance for Supercapacitors. *ACS Appl. Mater. Interfaces* **2015**, *7*, 2280–2285. [CrossRef] [PubMed]
401. Lim, S.P.; Huang, N.M.; Lim, H.N. Solvothermal synthesis of SnO_2/graphene nanocomposites for supercapacitor application. *Ceram. Int.* **2013**, *39*, 6647–6655. [CrossRef]
402. Xu, C.H.; Chiu, Y.F.; Yeh, P.W.; Chen, J.Z. SnO_2/CNT nanocomposite supercapacitors fabricated using scanning atmospheric-pressure plasma jets. *Mater. Res. Express* **2016**, *3*, 085002. [CrossRef]
403. Vinoth, V.; Wu, J.J.; Asiri, A.M.; Lana-Villarreal, T.; Bonete, P.; Anandan, S. SnO_2-decorated multiwalled carbon nanotubes and Vulcan carbon through a sonochemical approach for supercapacitor applications. *Ultrason. Sonochem.* **2016**, *29*, 205–212. [CrossRef]
404. Liao, C.-Y.; Kuok, F.-H.; Chen, C.-W.; Hsu, C.-C.; Chen, J.-Z. Flexible quasi-solid-state SnO_2/CNT supercapacitor processed by a dc-pulse nitrogen atmospheric-pressure plasma jet. *J. Energy Storage* **2017**, *11*, 237–241. [CrossRef]
405. Wang, D.-W.; Li, F.; Cheng, H.-M. Hierarchical porous nickel oxide and carbon as electrode materials for asymmetric supercapacitor. *J. Power Sources* **2008**, *185*, 1563–1568. [CrossRef]
406. Saranya, M.; Ramachandran, R.; Wang, F. Graphene-zinc oxide (G-ZnO) nanocomposite for electrochemical supercapacitor applications. *J. Sci. Adv. Mater. Devices* **2016**, *1*, 454–460. [CrossRef]
407. Lao, Z.J.; Konstantinov, K.; Tournaire, Y.; Ng, S.H.; Wang, G.X.; Liu, H.K. Synthesis of vanadium pentoxide powders with enhanced surface-area for electrochemical capacitors. *J. Power Sources* **2006**, *162*, 1451–1454. [CrossRef]
408. Wu, H.; Li, D.; Zhu, X.; Yang, C.; Liu, D.; Chen, X.; Song, Y.; Lu, L. High-performance and renewable supercapacitors based on TiO_2 nanotube array electrodes treated by an electrochemical doping approach. *Electrochim. Acta* **2014**, *116*, 129–136. [CrossRef]
409. Lamberti, A.; Pirri, C.F. TiO_2 nanotube array as biocompatible electrode in view of implantable supercapacitors. *J. Energy Storage* **2016**, *8*, 193–197. [CrossRef]
410. Zhou, M.; Glushenkov, A.M.; Kartachova, O.; Li, Y.; Chen, Y. Titanium Dioxide Nanotube Films for Electrochemical Supercapacitors: Biocompatibility and Operation in an Electrolyte Based on a Physiological Fluid. *J. Electrochem. Soc.* **2015**, *162*, A5065–A5069. [CrossRef]

411. Bhise, S.C.; Awale, D.V.; Vadiyar, M.M.; Patil, S.K.; Kokare, B.N.; Kolekar, S.S. Facile synthesis of CuO nanosheets as electrode for supercapacitor with long cyclic stability in novel methyl imidazole-based ionic liquid electrolyte. *J. Solid State Electrochem.* **2017**, *21*, 2585–2591. [CrossRef]
412. Moosavifard, S.E.; El-Kady, M.F.; Rahmanifar, M.S.; Kaner, R.B.; Mousavi, M.F. Designing 3D Highly Ordered Nanoporous CuO Electrodes for High-Performance Asymmetric Supercapacitors. *ACS Appl. Mater. Interfaces* **2015**, *7*, 4851–4860. [CrossRef]
413. Du, X.; Wang, C.; Chen, M.; Jiao, Y.; Wang, J. Electrochemical Performances of Nanoparticle Fe_3O_4/Activated Carbon Supercapacitor Using KOH Electrolyte Solution. *J. Phys. Chem. C* **2009**, *113*, 2643–2646. [CrossRef]
414. Cheng, X.; Gui, X.; Lin, Z.; Zheng, Y.; Liu, M.; Zhan, R.; Zhu, Y.; Tang, Z. Three-dimensional a-Fe_2O_3/carbon nanotube sponges as flexible supercapacitor electrodes. *J. Mater. Chem. A* **2015**, *3*, 20927–20934. [CrossRef]
415. Nithya, V.D.; Arul, N.S. Review on α-Fe_2O_3 based negative electrode for high performance supercapacitors. *J. Power Sources* **2016**, *327*, 297–318. [CrossRef]
416. Chu, J.; Lu, D.; Wang, X.; Wang, X.; Xiong, S. WO_3 nanoflower coated with graphene nanosheet: Synergetic energy storage composite electrode for supercapacitor application. *J. Alloys Compd.* **2017**, *702*, 568–572. [CrossRef]
417. Sun, P.; Deng, Z.; Yang, P.; Yu, X.; Chen, Y.; Liang, Z.; Meng, H.; Xie, W.; Tan, S.; Mai, W. Freestanding CNT-WO_3 hybrid electrodes for flexible asymmetric supercapacitors. *J. Mater. Chem. A* **2015**, *3*, 12076–12080. [CrossRef]
418. Yang, Y.; Li, L.; Ruan, G.; Fei, H.; Xiang, C.; Fan, X.; Tour, J.M. Hydrothermally Formed Three-Dimensional Nanoporous $Ni(OH)_2$ Thin-Film Supercapacitors. *ACS Nano* **2014**, *8*, 9622–9628. [CrossRef] [PubMed]
419. Zhang, L.; Ding, Q.; Huang, Y.; Gu, H.; Miao, Y.-E.; Liu, T. Flexible Hybrid Membranes with $Ni(OH)_2$ Nanoplatelets Vertically Grown on Electrospun Carbon Nanofibers for High-Performance Supercapacitors. *ACS Appl. Mater. Interfaces* **2015**, *7*, 22669–22677. [CrossRef]
420. Sun, W.; Rui, X.; Ulaganathan, M.; Madhavi, S.; Yan, Q. Few-layered $Ni(OH)_2$ nanosheets for high-performance supercapacitors. *J. Power Sources* **2015**, *295*, 323–328. [CrossRef]
421. Sun, Y.; Wu, Q.; Shi, G. Graphene based new energy materials. *Energy Environ. Sci.* **2011**, *4*, 1113–1132. [CrossRef]
422. Amade, R.; Jover, E.; Caglar, B.; Mutlu, T.; Bertran, E. Optimization of MnO_2/vertically aligned carbon nanotube composite for supercapacitor application. *J. Power Sources* **2011**, *196*, 5779–5783. [CrossRef]
423. Lu, Z.; Chao, Y.; Ge, Y.; Foroughi, J.; Zhao, Y.; Wang, C.; Long, H.; Wallace, G.G. High-performance hybrid carbon nanotube fibers for wearable energy storage. *Nanoscale* **2017**, *9*, 5063–5071. [CrossRef]
424. Zhang, Y.; Bai, W.; Cheng, X.; Ren, J.; Weng, W.; Chen, P.; Fang, X.; Zhang, Z.; Peng, H. Flexible and Stretchable Lithium-Ion Batteries and Supercapacitors Based on Electrically Conducting Carbon Nanotube Fiber Springs. *Angew. Chem. Int. Ed.* **2014**, *53*, 14564–14568. [CrossRef] [PubMed]
425. Choi, C.; Kim, S.H.; Sim, H.J.; Lee, J.A.; Choi, A.Y.; Kim, Y.T.; Lepró, X.; Spinks, G.M.; Baughman, R.H.; Kim, S.J. Stretchable, Weavable Coiled Carbon Nanotube/MnO_2/Polymer Fiber Solid-State Supercapacitors. *Sci. Rep.* **2015**, *5*, 9387. [CrossRef]
426. Global Supercapacitor Market—By Type (Double-layer Capacitor, Pseudo-capacitor, Hybrid-capacitor), End-user Vertical (Consumer Electronics, Industrial, Utilities, Healthcare, Aerospace & Defense, and Transportation), Geography, Trends, Forecast (2017–2022). 2017. Available online: https://www.mordorintelligence.com/industry-reports/supercapacitor-market (accessed on 1 June 2022).
427. Yang, C.; Shen, J.; Wang, C.; Fei, H.; Bao, H.; Wang, G. All-solid-state asymmetric supercapacitor based on reduced graphene oxide/carbon nanotube and carbon fiber paper/polypyrrole electrodes. *J. Mater. Chem. A* **2014**, *2*, 1458–1464. [CrossRef]
428. Supercapacitors Market: Global Industry Analysis and Opportunity Assessment 2016–2026. 2018. Available online: https://www.futuremarketinsights.com/reports/supercapacitors-market (accessed on 1 October 2024).
429. Yassine, M.; Fabris, D. Performance of Commercially Available Supercapacitors. *Energies* **2017**, *10*, 1340. [CrossRef]
430. Despite Initial Reports, MIT-Lamborghini Supercapacitor to Be Based on MOFs and Not Graphene. 2017. Available online: https://www.graphene-info.com/despite-initial-reports-mit-lamborghini-supercapacitor-be-based-mofs-and-not-graphene (accessed on 14 November 2017).
431. Blomgren, G.E. The Development and Future of Lithium Ion Batteries. *J. Electrochem. Soc.* **2017**, *164*, A5019–A5025. [CrossRef]
432. Ramoni, M.O.; Zhang, H.C. End-of-life (EOL) issues and options for electric vehicle batteries. *Clean Technol. Environ. Policy* **2013**, *15*, 881–891. [CrossRef]
433. Endo, M.; Kim, C.; Nishimura, K.; Fujino, T.; Miyashita, K. Recent development of carbon materials for Li ion batteries. *Carbon* **2000**, *38*, 183–197. [CrossRef]
434. Frackowiak, E.; Beguin, F. Electrochemical storage of energy in carbon nanotubes and nanostructured carbons. *Carbon* **2002**, *40*, 1775–1787. [CrossRef]
435. Nishidate, K.; Hasegawa, M. Energetics of lithium ion adsorption on defective carbon nanotubes. *Phys. Rev. B* **2005**, *71*, 245418. [CrossRef]
436. Meunier, V.; Kephart, J.; Roland, C.; Bernholc, J. Ab Initio Investigations of Lithium Diffusion in Carbon Nanotube Systems. *Phys. Rev. Lett.* **2002**, *88*, 075506. [CrossRef] [PubMed]

437. Wang, X.X.; Wang, J.N.; Su, L.F. Preparation and electrochemical performance of ultra-short carbon nanotubes. *J. Power Sources* **2009**, *186*, 194–200. [CrossRef]
438. Prem Kumar, T.; Ramesh, R.; Lin, Y.Y.; Fey, G.T.-K. Tin-filled carbon nanotubes as insertion anode materials for lithium-ion batteries. *Electrochem. Commun.* **2004**, *6*, 520–525. [CrossRef]
439. Behabtu, N.; Young, C.C.; Tsentalovich, D.E.; Kleinerman, O.; Wang, X.; Ma, A.W.K.; Bengio, E.A.; ter Waarbeek, R.F.; de Jong, J.J.; Hoogerwerf, R.E.; et al. Strong, Light, Multifunctional Fibers of Carbon Nanotubes with Ultrahigh Conductivity. *Science* **2013**, *339*, 182–186. [CrossRef] [PubMed]
440. Wang, J.N.; Luo, X.G.; Wu, T.; Chen, Y. High-strength carbon nanotube fibre-like ribbon with high ductility and high electrical conductivity. *Nat. Commun.* **2014**, *5*, 3848. [CrossRef] [PubMed]
441. Mukhopadhyay, I.; Kawasaki, S.; Okino, F.; Govindaraj, A.; Rao, C.N.R.; Touhara, H. Electrochemical Li insertion into single-walled carbon nanotubes prepared by graphite arc-discharge method. *Phys. B Condens. Matter* **2002**, *323*, 130–132. [CrossRef]
442. Shimoda, H.; Gao, B.; Tang, X.P.; Kleinhammes, A.; Fleming, L.; Wu, Y.; Zhou, O. Lithium Intercalation into Opened Single-Wall Carbon Nanotubes: Storage Capacity and Electronic Properties. *Phys. Rev. Lett.* **2001**, *88*, 015502. [CrossRef] [PubMed]
443. Kawasaki, S.; Hara, T.; Iwai, Y.; Suzuki, Y. Metallic and semiconducting single-walled carbon nanotubes as the anode material of Li ion secondary battery. *Mater. Lett.* **2008**, *62*, 2917–2920. [CrossRef]
444. Landi, B.J.; Ganter, M.J.; Schauerman, C.M.; Cress, C.D.; Raffaelle, R.P. Lithium Ion Capacity of Single Wall Carbon Nanotube Paper Electrodes. *J. Phys. Chem. C* **2008**, *112*, 7509–7515. [CrossRef]
445. Landi, B.J.; Ganter, M.J.; Schauerman, C.M.; DiLeo, R.A.; Cress, C.D.; Raffaelle, R.P.C.T. Single Wall Carbon Nanotube-$LiCoO_2$ Lithium Ion Batteries. *MRS Proc.* **2008**, *1127*, 1127-T03. [CrossRef]
446. Landi, B.J.; Dileo, R.A.; Schauerman, C.M.; Cress, C.D.; Ganter, M.J.; Raffaelle, R.P. Multi-Walled Carbon Nanotube Paper Anodes for Lithium Ion Batteries. *J. Nanosci. Nanotechnol.* **2009**, *9*, 3406–3410. [CrossRef]
447. Eom, J.Y.; Kwon, H.S.; Liu, J.; Zhou, O. Lithium insertion into purified and etched multi-walled carbon nanotubes synthesized on supported catalysts by thermal CVD. *Carbon* **2004**, *42*, 2589–2596. [CrossRef]
448. Eom, J.; Kim, D.; Kwon, H. Effects of ball-milling on lithium insertion into multi-walled carbon nanotubes synthesized by thermal chemical vapour deposition. *J. Power Sources* **2006**, *157*, 507–514. [CrossRef]
449. Gao, B.; Bower, C.; Lorentzen, J.D.; Fleming, L.; Kleinhammes, A.; Tang, X.P.; McNeil, L.E.; Wu, Y.; Zhou, O. Enhanced saturation lithium composition in ball-milled single-walled carbon nanotubes. *Chem. Phys. Lett.* **2000**, *327*, 69–75. [CrossRef]
450. Fang, S.; Shen, L.; Zhang, X. Chapter 9—Application of Carbon Nanotubes in Lithium-Ion Batteries A2—Peng, Huisheng. In *Industrial Applications of Carbon Nanotubes*; Elsevier: Boston, MA, USA, 2017; pp. 251–276.
451. Yang, S.; Huo, J.; Song, H.; Chen, X. A comparative study of electrochemical properties of two kinds of carbon nanotubes as anode materials for lithium ion batteries. *Electrochim. Acta* **2008**, *53*, 2238–2244. [CrossRef]
452. Klink, S.; Ventosa, E.; Xia, W.; La Mantia, F.; Muhler, M.; Schuhmann, W. Tailoring of CNT surface oxygen groups by gas-phase oxidation and its implications for lithium ion batteries. *Electrochem. Commun.* **2012**, *15*, 10–13. [CrossRef]
453. Huang, H.; Zhang, W.K.; Gan, X.P. Improved electrochemical storage of lithium into multi-walled carbon nanotubes by light irradiation. *Mater. Chem. Phys.* **2007**, *104*, 271–275. [CrossRef]
454. Wang, X.X.; Wang, J.N.; Chang, H.; Zhang, Y.F. Preparation of Short Carbon Nanotubes and Application as an Electrode Material in Li-Ion Batteries. *Adv. Funct. Mater.* **2007**, *17*, 3613–3618. [CrossRef]
455. Lahiri, I.; Oh, S.-W.; Hwang, J.Y.; Cho, S.; Sun, Y.-K.; Banerjee, R.; Choi, W. High Capacity and Excellent Stability of Lithium Ion Battery Anode Using Interface-Controlled Binder-Free Multiwall Carbon Nanotubes Grown on Copper. *ACS Nano* **2010**, *4*, 3440–3446. [CrossRef]
456. Evanoff, K.; Khan, J.; Balandin, A.A.; Magasinski, A.; Ready, W.J.; Fuller, T.F.; Yushin, G. Towards Ultrathick Battery Electrodes: Aligned Carbon Nanotube—Enabled Architecture. *Adv. Mater.* **2012**, *24*, 533–537. [CrossRef]
457. Du, F.; Dai, Q.; Dai, L.; Zhang, Q.; Reitz, T.; Elston, L. Vertically-Aligned Carbon Nanotubes for Electrochemical Energy Conversion and Storage. In *Nanomaterials for Sustainable Energy*; Springer: Berlin/Heidelberg, Germany, 2016; pp. 253–270.
458. Welna, D.T.; Qu, L.; Taylor, B.E.; Dai, L.; Durstock, M.F. Vertically aligned carbon nanotube electrodes for lithium-ion batteries. *J. Power Sources* **2011**, *196*, 1455–1460. [CrossRef]
459. Udomvech, A.; Kerdcharoen, T.; Osotchan, T. First principles study of Li and Li+ adsorbed on carbon nanotube: Variation of tubule diameter and length. *Chem. Phys. Lett.* **2005**, *406*, 161–166. [CrossRef]
460. Zhao, M.; Xia, Y.; Liu, X.; Tan, Z.; Huang, B.; Li, F.; Ji, Y.; Song, C. Curvature-induced condensation of lithium confined inside single-walled carbon nanotubes: First-principles calculations. *Phys. Lett. A* **2005**, *340*, 434–439. [CrossRef]
461. Zhang, Y.; Chen, T.; Wang, J.; Min, G.; Pan, L.; Song, Z.; Sun, Z.; Zhou, W.; Zhang, J. The study of multi-walled carbon nanotubes with different diameter as anodes for lithium-ion batteries. *Appl. Surf. Sci.* **2012**, *258*, 4729–4732. [CrossRef]
462. Zhou, Z.; Gao, X.; Yan, J.; Song, D.; Morinaga, M. Enhanced Lithium Absorption in Single-Walled Carbon Nanotubes by Boron Doping. *J. Phys. Chem. B* **2004**, *108*, 9023–9026. [CrossRef]

463. Zhou, Z.; Gao, X.; Yan, J.; Song, D.; Morinaga, M. A first-principles study of lithium absorption in boron- or nitrogen-doped single-walled carbon nanotubes. *Carbon* **2004**, *42*, 2677–2682. [CrossRef]
464. Li, X.; Liu, J.; Zhang, Y.; Li, Y.; Liu, H.; Meng, X.; Yang, J.; Geng, D.; Wang, D.; Li, R.; et al. High concentration nitrogen doped carbon nanotube anodes with superior Li^+ storage performance for lithium rechargeable battery application. *J. Power Sources* **2012**, *197*, 238–245. [CrossRef]
465. Mukhopadhyay, I.; Hoshino, N.; Kawasaki, S.; Okino, F.; Hsu, W.K.; Touhara, H. Electrochemical Li Insertion in B-Doped Multiwall Carbon Nanotubes. *J. Electrochem. Soc.* **2002**, *149*, A39–A44. [CrossRef]
466. Hsu, W.K.; Firth, S.; Redlich, P.; Terrones, M.; Terrones, H.; Zhu, Y.Q.; Grobert, N.; Schilder, A.; Clark, R.J.; Kroto, H.W.; et al. Boron-doping effects in carbon nanotubes. *J. Mater. Chem.* **2000**, *10*, 1425–1429. [CrossRef]
467. Zhang, L.; Xia, G.; Guo, Z.; Li, X.; Sun, D.; Yu, X. Boron and nitrogen co-doped porous carbon nanotubes webs as a high-performance anode material for lithium ion batteries. *Int. J. Hydrogen Energy* **2016**, *41*, 14252–14260. [CrossRef]
468. Yang, Z.; Li, Z.; Wu, H.; Simard, B. Effects of doped copper on electrochemical performance of the raw carbon nanotubes anode. *Mater. Lett.* **2003**, *57*, 3160–3166. [CrossRef]
469. Yang, Z.H.; Zhou, Y.H.; Sang, S.B.; Feng, Y.; Wu, H.Q. Lithium insertion into multi-walled raw carbon nanotubes pre-doped with lithium. *Mater. Chem. Phys.* **2005**, *89*, 295–299. [CrossRef]
470. Lahiri, I.; Oh, S.-M.; Hwang, J.Y.; Kang, C.; Choi, M.; Jeon, H.; Banerjee, R.; Sun, Y.-K.; Choi, W. Ultrathin alumina-coated carbon nanotubes as an anode for high capacity Li-ion batteries. *J. Mater. Chem.* **2011**, *21*, 13621–13626. [CrossRef]
471. Sahoo, M.; Ramaprabhu, S. Solar synthesized tin oxide nanoparticles dispersed on graphene wrapped carbon nanotubes as a Li ion battery anode material with improved stability. *RSC Adv.* **2017**, *7*, 13789–13797. [CrossRef]
472. Wang, Z.; Chen, G.; Xia, D. Coating of multi-walled carbon nanotube with SnO_2 films of controlled thickness and its application for Li-ion battery. *J. Power Sources* **2008**, *184*, 432–436. [CrossRef]
473. Natarajan, T.S.; Lee, J.Y.; Bajaj, H.C.; Jo, W.-K.; Tayade, R.J. Synthesis of multiwall carbon nanotubes/TiO_2 nanotube composites with enhanced photocatalytic decomposition efficiency. *Catal. Today* **2017**, *282*, 13–23. [CrossRef]
474. Madian, M.; Ummethala, R.; Naga, A.O.A.E.; Ismail, N.; Rümmeli, M.H.; Eychmüller, A.; Giebeler, L. Ternary CNTs@TiO_2/CoO Nanotube Composites: Improved Anode Materials for High Performance Lithium Ion Batteries. *Materials* **2017**, *10*, 678. [CrossRef]
475. Sehrawat, P.; Julien, C.; Islam, S.S. Carbon nanotubes in Li-ion batteries: A review. *Mater. Sci. Eng. B* **2016**, *213*, 12–40. [CrossRef]
476. Weng, W.; Lin, H.; Chen, X.; Ren, J.; Zhang, Z.; Qiu, L.; Guan, G.; Peng, H. Flexible and stable lithium ion batteries based on three-dimensional aligned carbon nanotube/silicon hybrid electrodes. *J. Mater. Chem. A* **2014**, *2*, 9306–9312. [CrossRef]
477. Qin, J.; Liu, D.; Zhao, N.; Shi, C.; Liu, E.-Z.; He, F.; Ma, L.; Li, Q.; Li, J.; He, C. Fabrication of Sn-core/CNT-shell nanocable anchored interconnected carbon networks as anode material for lithium ion batteries. *Mater. Lett.* **2018**, *212*, 94–97. [CrossRef]
478. Sun, X.; Zhu, X.; Yang, X.; Sun, J.; Xia, Y.; Yang, D. $CoFe_2O_4$/carbon nanotube aerogels as high performance anodes for lithium ion batteries. *Green Energy Environ.* **2017**, *2*, 160–167. [CrossRef]
479. Hays, K.A.; Banek, N.A.; Wagner, M.J. High Performance Arsenic: Multiwall Carbon Nanotube Composite Anodes for Li-Ion Batteries. *J. Electrochem. Soc.* **2017**, *164*, A1635–A1643. [CrossRef]
480. Tojo, T.; Yamaguchi, S.; Furukawa, Y.; Inada, R.; Sakurai, Y. Electrochemical Characterization of Phosphorus Encapsulated in Drilled Carbon Nanotubes as Anode Material for Lithium Ion Batteries. *ECS Trans.* **2017**, *75*, 39–44. [CrossRef]
481. Ishii, Y.; Sakamoto, Y.; Song, H.; Tashiro, K.; Nishiwaki, Y.; Al-zubaidi, A.; Kawasaki, S. Alkali metal ion storage properties of sulphur and phosphorous molecules encapsulated in nanometer size carbon cylindrical pores. *AIP Adv.* **2016**, *6*, 035112. [CrossRef]
482. Liang, H.; Chen, W.; Yao, Y.; Wang, Z.; Yang, Y. Hydrothermal synthesis, self-assembly and electrochemical performance of a-Fe_2O_3 microspheres for lithium ion batteries. *Ceram. Int.* **2014**, *40*, 10283–10290. [CrossRef]
483. Penki, T.R.; Shivakumara, S.; Minakshi, M.; Munichandraiah, N. Porous Flower-like a-Fe_2O_3 Nanostructure: A High Performance Anode Material for Lithium-ion Batteries. *Electrochim. Acta* **2015**, *167*, 330–339. [CrossRef]
484. Wang, J.; Wang, G.; Wang, H. Flexible free-standing Fe_2O_3/graphene/carbon nanotubes hybrid films as anode materials for high performance lithium-ion batteries. *Electrochim. Acta* **2015**, *182*, 192–201. [CrossRef]
485. Xu, X.; Cao, R.; Jeong, S.; Cho, J. Spindle-like Mesoporous a-Fe_2O_3 Anode Material Prepared from MOF Template for High-Rate Lithium Batteries. *Nano Lett.* **2012**, *12*, 4988–4991. [CrossRef]
486. Ye, J.; An, Y.; Montalvo, E.; Campbell, P.G.; Worsley, M.A.; Tran, I.C.; Liu, Y.; Wood, B.C.; Biener, J.; Jiang, H.; et al. Solvent-directed sol-gel assembly of 3-dimensional graphene-tented metal oxides and strong synergistic disparities in lithium storage. *J. Mater. Chem. A* **2016**, *4*, 4032–4043. [CrossRef]
487. Zhou, G.-W.; Wang, J.; Gao, P.; Yang, X.; He, Y.-S.; Liao, X.-Z.; Yang, J.; Ma, Z.-F. Facile Spray Drying Route for the Three-Dimensional Graphene-Encapsulated Fe_2O_3 Nanoparticles for Lithium Ion Battery Anodes. *Ind. Eng. Chem. Res.* **2013**, *52*, 1197–1204. [CrossRef]
488. Xia, C.; Yuqiao, W.; Qingyu, X.; Pingping, S.; Xiuzhen, W.; Tao, W.; Yueming, S. Carbon nanotube entangled Mn_3O_4 octahedron as anode materials for lithium-ion batteries. *Nanotechnology* **2017**, *28*, 255402.

489. Park, J.; Moon, W.G.; Kim, G.-P.; Nam, I.; Park, S.; Kim, Y.; Yi, J. Three-dimensional aligned mesoporous carbon nanotubes filled with Co_3O_4 nanoparticles for Li-ion battery anode applications. *Electrochim. Acta* **2013**, *105*, 110–114. [CrossRef]
490. Huang, J.; Jiang, Z. The preparation and characterization of $Li_4Ti_5O_{12}$/carbon nano-tubes for lithium ion battery. *Electrochim. Acta* **2008**, *53*, 7756–7759. [CrossRef]
491. Li, X.; Qu, M.; Huai, Y.; Yu, Z. Preparation and electrochemical performance of $Li_4Ti_5O_{12}$/carbon/carbon nano-tubes for lithium ion battery. *Electrochim. Acta* **2010**, *55*, 2978–2982. [CrossRef]
492. Shen, L.; Yuan, C.; Luo, H.; Zhang, X.; Xu, K.; Zhang, F. In situ growth of $Li_4Ti_5O_{12}$ on multi-walled carbon nanotubes: Novel coaxial nanocables for high rate lithium ion batteries. *J. Mater. Chem.* **2011**, *21*, 761–767. [CrossRef]
493. Kim, H.-K.; Roh, K.C.; Kang, K.; Kim, K.-B. Synthesis of nano-$Li_4Ti_5O_{12}$ decorated on non-oxidized carbon nanotubes with enhanced rate capability for lithium-ion batteries. *RSC Adv.* **2013**, *3*, 14267–14272. [CrossRef]
494. Jia, X.; Kan, Y.; Zhu, X.; Ning, G.; Lu, Y.; Wei, F. Building flexible $Li_4Ti_5O_{12}$/CNT lithium-ion battery anodes with superior rate performance and ultralong cycling stability. *Nano Energy* **2014**, *10*, 344–352. [CrossRef]
495. Pawlitzek, F.; Pampel, J.; Schmuck, M.; Althues, H.; Schumm, B.; Kaskel, S. High-power lithium ion batteries based on preorganized necklace type $Li_4Ti_5O_{12}$/VACNT nano-composites. *J. Power Sources* **2016**, *325*, 1–6. [CrossRef]
496. Chen, Y.; Zhang, H.; Li, Y.; Chen, Y.; Luo, T. Electrochemical performance of $Li_4Ti_5O_{12}$/carbon nanotubes/graphene composite as an anode material in lithium-ion batteries. *Int. J. Hydrogen Energy* **2017**, *42*, 7195–7201. [CrossRef]
497. Sun, L.; Kong, W.; Wu, H.; Wu, Y.; Wang, D.; Zhao, F.; Jiang, K.; Li, Q.; Wang, J.; Fan, S. Mesoporous $Li_4Ti_5O_{12}$ nanoclusters anchored on super-aligned carbon nanotubes as high performance electrodes for lithium ion batteries. *Nanoscale* **2016**, *8*, 617–625. [CrossRef]
498. Feng, W.; Cao, Y.; Zhao, X.; Gang, J.; Su, W. Effect of Carbon Nanotubes on the Electrochemical Performance of $LiFePO_4$ Particles in Lithium Ion Batteries. *Int. J. Electrochem. Sci.* **2017**, *12*, 5199–5207. [CrossRef]
499. Hosono, E.; Wang, Y.; Kida, N.; Enomoto, M.; Kojima, N.; Okubo, M.; Matsuda, H.; Saito, Y.; Kudo, T.; Honma, I.; et al. Synthesis of Triaxial $LiFePO_4$ Nanowire with a VGCF Core Column and a Carbon Shell through the Electrospinning Method. *ACS Appl. Mater. Interfaces* **2010**, *2*, 212–218. [CrossRef] [PubMed]
500. Qiao, Y.Q.; Feng, W.L.; Li, J.; Shen, T.D. Ultralong cycling stability of carbon-nanotube/$LiFePO_4$ nanocomposites as electrode materials for lithium-ion batteries. *Electrochim. Acta* **2017**, *232*, 323–331. [CrossRef]
501. Tan, L.; Tang, Q.; Chen, X.; Hu, A.; Deng, W.; Yang, Y.; Xu, L. Mesoporous $LiFePO_4$ Microspheres Embedded Homogeneously with 3D CNT Conductive Networks for Enhanced Electrochemical Performance. *Electrochim. Acta* **2014**, *137*, 344–351. [CrossRef]
502. Toprakci, O.; Toprakci, H.A.K.; Ji, L.; Xu, G.; Lin, Z.; Zhang, X. Carbon Nanotube-Loaded Electrospun $LiFePO_4$/Carbon Composite Nanofibers As Stable and Binder-Free Cathodes for Rechargeable Lithium-Ion Batteries. *ACS Appl. Mater. Interfaces* **2012**, *4*, 1273–1280. [CrossRef] [PubMed]
503. Wang, G.; Ma, Z.; Shao, G.; Kong, L.; Gao, W. Synthesis of $LiFePO_4$@carbon nanotube core-shell nanowires with a high-energy efficient method for superior lithium ion battery cathodes. *J. Power Sources* **2015**, *291*, 209–214. [CrossRef]
504. Wu, G.; Zhou, Y.; Gao, X.; Shao, Z. Facile low-temperature polyol process for $LiFePO_4$ nanoplate and carbon nanotube composite. *Solid State Sci.* **2013**, *24*, 15–20. [CrossRef]
505. Wu, G.; Ran, R.; Zhao, B.; Sha, Y.; Su, C.; Zhou, Y.; Shao, Z. 3D amorphous carbon and graphene co-modified $LiFePO_4$ composite derived from polyol process as electrode for high power lithium-ion batteries. *J. Energy Chem.* **2014**, *23*, 363–375. [CrossRef]
506. Cheng, J.; Gu, G.; Guan, Q.; Razal, J.M.; Wang, Z.; Li, X.; Wang, B. Synthesis of a porous sheet-like V_2O_5-CNT nanocomposite using an ice-templating 'bricks-and-mortar' assembly approach as a high-capacity, long cyclelife cathode material for lithium-ion batteries. *J. Mater. Chem. A* **2016**, *4*, 2729–2737. [CrossRef]
507. Sathiya, M.; Prakash, A.S.; Ramesha, K.; Tarascon, J.-M.; Shukla, A.K. V_2O_5-Anchored Carbon Nanotubes for Enhanced Electrochemical Energy Storage. *J. Am. Chem. Soc.* **2011**, *133*, 16291–16299. [CrossRef] [PubMed]
508. Zhou, X.; Wu, G.; Gao, G.; Cui, C.; Yang, H.; Shen, J.; Zhou, B.; Zhang, Z. The synthesis, characterization and electrochemical properties of Multi-Wall Carbon Nanotube-induced vanadium oxide nanosheet composite as a novel cathode material for lithium ion batteries. *Electrochim. Acta* **2012**, *74*, 32–38. [CrossRef]
509. Cao, Z.; Wei, B. V_2O_5/single-walled carbon nanotube hybrid mesoporous films as cathodes with high-rate capacities for rechargeable lithium ion batteries. *Nano Energy* **2013**, *2*, 481–490. [CrossRef]
510. Zhang, L.; Fu, J.; Zhang, C. Mechanical Composite of LiNi(0.8)Co(0.15)Al(0.05)O(2)/Carbon Nanotubes with Enhanced Electrochemical Performance for Lithium-Ion Batteries. *Nanoscale Res. Lett.* **2017**, *12*, 376. [CrossRef]
511. Luo, S.; Wang, K.; Wang, J.; Jiang, K.; Li, Q.; Fan, S. Binder-Free $LiCoO_2$/Carbon Nanotube Cathodes for High-Performance Lithium Ion Batteries. *Adv. Mater.* **2017**, *24*, 2294–2298. [CrossRef]
512. Yan, L.; Wang, K.; Luo, S.; Wu, H.; Luo, Y.; Yu, Y.; Jiang, K.; Li, Q.; Fan, S.; Wang, J. Sandwich-structured cathodes with cross-stacked carbon nanotube films as conductive layers for high-performance lithium-ion batteries. *J. Mater. Chem. A* **2017**, *5*, 4047–4057. [CrossRef]

513. Xia, H.; Ragavendran, K.R.; Xie, J.; Lu, L. Ultrafine $LiMn_2O_4$/carbon nanotube nanocomposite with excellent rate capability and cycling stability for lithium-ion batteries. *J. Power Sources* **2012**, *212*, 28–34. [CrossRef]
514. Tang, M.; Yuan, A.; Zhao, H.; Xu, J. High-performance $LiMn_2O_4$ with enwrapped segmented carbon nanotubes as cathode material for energy storage. *J. Power Sources* **2013**, *235*, 5–13. [CrossRef]
515. Tang, M.; Yuan, A.; Xu, J. Synthesis of highly crystalline $LiMn_2O_4$/multiwalled carbon nanotube composite material with high performance as lithium-ion battery cathode via an improved two-step approach. *Electrochim. Acta* **2015**, *166*, 244–252. [CrossRef]
516. Liu, X.-M.; Huang, Z.-D.; Oh, S.; Ma, P.-C.; Chan, P.C.H.; Vedam, G.K.; Kang, K.; Kim, J.-K. Sol-gel synthesis of multiwalled carbon nanotube-$LiMn_2O_4$ nanocomposites as cathode materials for Li-ion batteries. *J. Power Sources* **2010**, *195*, 4290–4296. [CrossRef]
517. Wang, W.; Liang, H.; Zhang, L.; Savilov, S.V.; Ni, J.; Li, L. Carbon nanotube directed three-dimensional porous Li_2FeSiO_4 composite for lithium batteries. *Nano Res.* **2017**, *10*, 229–237. [CrossRef]
518. Kim, S.-J.; Lee, A.Y.; Park, H.-C.; Kim, S.-Y.; Kim, M.-C.; Lee, J.-M.; Kim, S.-B.; Kim, W.-S.; Jeong, Y.; Park, K.-W. Carbon nanotube web-based current collectors for high-performance lithium ion batteries. *Mater. Today Commun.* **2015**, *4*, 149–155. [CrossRef]
519. Seo, M.-H.; Park, M.; Lee, K.T.; Kim, K.; Kim, J.; Cho, J. High performance Ge nanowire anode sheathed with carbon for lithium rechargeable batteries. *Energy Environ. Sci.* **2011**, *4*, 425–428. [CrossRef]
520. Hao, J.; Li, N.; Ma, X.; Liu, X.; Liu, X.; Li, Y.; Xu, H.; Zhao, J. Ionic liquid electrodeposition of germanium/carbon nanotube composite anode material for lithium ion batteries. *Mater. Lett.* **2015**, *144*, 50–53. [CrossRef]
521. Jahel, A.; Ghimbeu, C.M.; Monconduit, L.; Vix-Guterl, C. Confined Ultrasmall SnO_2 Particles in Micro/Mesoporous Carbon as an Extremely Long Cycle-Life Anode Material for Li-Ion Batteries. *Adv. Energy Mater.* **2014**, *4*, 1400025. [CrossRef]
522. Bazin, L.; Mitra, S.; Taberna, P.L.; Poizot, P.; Gressier, M.; Menu, M.J.; Barnabé, A.; Simon, P.; Tarascon, J.M. High rate capability pure Sn-based nano-architectured electrode assembly for rechargeable lithium batteries. *J. Power Sources* **2009**, *188*, 578–582. [CrossRef]
523. Fullenwarth, J.; Darwiche, A.; Soares, A.; Donnadieu, B.; Monconduit, L. NiP_3: A promising negative electrode for Li− and Na− ion batteries. *J. Mater. Chem. A* **2014**, *2*, 2050–2059. [CrossRef]
524. Marino, C.; Debenedetti, A.; Fraisse, B.; Favier, F.; Monconduit, L. Activated-phosphorus as new electrode material for Li-ion batteries. *Electrochem. Commun.* **2011**, *13*, 346–349. [CrossRef]
525. Nitta, N.; Yushin, G. High-Capacity Anode Materials for Lithium-Ion Batteries: Choice of Elements and Structures for Active Particles. *Part. Part. Syst. Charact.* **2014**, *31*, 317–336. [CrossRef]
526. Park, C.-M. Electrochemical lithium quasi-intercalation with arsenic. *J. Solid State Electrochem.* **2016**, *20*, 517–523. [CrossRef]
527. Poizot, P.; Laruelle, S.; Grugeon, S.; Dupont, L.; Tarascon, J.M. Nano-sized transition-metal oxides as negative-electrode materials for lithium-ion batteries. *Nature* **2000**, *407*, 496. [CrossRef]
528. Li, J.; Tang, S.; Lu, L.; Zeng, H.C. Preparation of Nanocomposites of Metals, Metal Oxides, and Carbon Nanotubes via Self-Assembly. *J. Am. Chem. Soc.* **2007**, *129*, 9401–9409. [CrossRef] [PubMed]
529. Gao, G.; Jin, Y.; Zeng, Q.; Wang, D.; Shen, C. Carbon nanotube-wrapped Fe(2)O(3) anode with improved performance for lithium-ion batteries. *Beilstein J. Nanotechnol.* **2017**, *8*, 649–656. [CrossRef]
530. Gao, J.; Lowe, M.A.; Abruna, H.D. Spongelike Nanosized Mn_3O_4 as a High-Capacity Anode Material for Rechargeable Lithium Batteries. *Chem. Mater.* **2011**, *23*, 3223–3227. [CrossRef]
531. Cui, X.; Wang, Y.; Chen, Z.; Zhou, H.; Xu, Q.; Sun, P.; Zhou, J.; Xia, L.; Sun, Y.; Lu, Y. Preparation of pompon-like MnO/carbon nanotube composite microspheres as anodes for lithium ion batteries. *Electrochim. Acta* **2015**, *180*, 858–865. [CrossRef]
532. Xia, H.; Zhu, D.; Fu, Y.; Wang, X. $CoFe_2O_4$-graphene nanocomposite as a high-capacity anode material for lithium-ion batteries. *Electrochim. Acta* **2012**, *83*, 166–174. [CrossRef]
533. Rai, A.K.; Gim, J.; Thi, T.V.; Ahn, D.; Cho, S.J.; Kim, J. High Rate Capability and Long Cycle Stability of Co_3O_4/$CoFe_2O_4$ Nanocomposite as an Anode Material for High-Performance Secondary Lithium Ion Batteries. *J. Phys. Chem. C* **2014**, *118*, 11234–11243. [CrossRef]
534. Wang, L.; Zhuo, L.; Cheng, H.; Zhang, C.; Zhao, F. Porous carbon nanotubes decorated with nanosized cobalt ferrite as anode materials for high-performance lithium-ion batteries. *J. Power Sources* **2015**, *283*, 289–299. [CrossRef]
535. Wang, B.; Liu, T.; Liu, A.; Liu, G.; Wang, L.; Gao, T.; Wang, D.; Zhao, X.S.C. A Hierarchical Porous C@$LiFePO_4$/Carbon Nanotubes Microsphere Composite for High-Rate Lithium-Ion Batteries: Combined Experimental and Theoretical Study. *Adv. Energy Mater.* **2016**, *6*, 1600426. [CrossRef]
536. Jiang, K.; Li, Q.; Fan, S. Spinning continuous carbon nanotube yarns. *Nature* **2002**, *419*, 801. [CrossRef] [PubMed]
537. Liu, K.; Sun, Y.; Chen, L.; Feng, C.; Feng, X.; Jiang, K.; Zhao, Y.; Fan, S. Controlled Growth of Super-Aligned Carbon Nanotube Arrays for Spinning Continuous Unidirectional Sheets with Tunable Physical Properties. *Nano Lett.* **2008**, *8*, 700–705. [CrossRef] [PubMed]
538. Jiang, K.; Wang, J.; Li, Q.; Liu, L.; Liu, C.; Fan, S. Superaligned Carbon Nanotube Arrays, Films, and Yarns: A Road to Applications. *Adv. Mater.* **2011**, *23*, 1154–1161. [CrossRef]

539. Chen, G.; Futaba, D.N.; Hata, K. Catalysts for the growth of carbon nanotube forests and superaligned arrays. *MRS Bull.* **2017**, *42*, 802–808. [CrossRef]
540. Shaijumon, M.M.; Perre, E.; Daffos, B.; Taberna, P.L.; Tarascon, J.M.; Simon, P. Nanoarchitectured 3D Cathodes for Li-Ion Microbatteries. *Adv. Mater.* **2010**, *22*, 4978–4981. [CrossRef] [PubMed]
541. Dai, X.; Zhou, A.; Xu, J.; Yang, B.; Wang, L.; Li, J. Superior electrochemical performance of $LiCoO_2$ electrodes enabled by conductive Al_2O_3-doped ZnO coating via magnetron sputtering. *J. Power Sources* **2015**, *298*, 114–122. [CrossRef]
542. Liu, L.; Zhang, H.; Yang, J.; Mu, Y.; Wang, Y. Fabrication of Fe-Doped $LiCoO_2$ Sandwich-Like Nanocomposites as Excellent Performance Cathode Materials for Lithium-Ion Batteries. *Chem.—A Eur. J.* **2015**, *21*, 19104–19111. [CrossRef]
543. Jiang, R.; Cui, C.; Ma, H. Using graphene nanosheets as a conductive additive to enhance the rate performance of spinel $LiMn_2O_4$ cathode material. *Phys. Chem. Chem. Phys.* **2013**, *15*, 6406–6415. [CrossRef] [PubMed]
544. Zhao, J.; Wang, Y. Atomic layer deposition of epitaxial ZrO_2 coating on $LiMn_2O_4$ nanoparticles for high-rate lithium ion batteries at elevated temperature. *Nano Energy* **2013**, *2*, 882–889. [CrossRef]
545. Cao, H.; Xia, B.; Xu, N.; Zhang, C. Structural and electrochemical characteristics of Co and Al co-doped lithium nickelate cathode materials for lithium-ion batteries. *J. Alloys Compd.* **2004**, *376*, 282–286. [CrossRef]
546. Lee, M.J.; Noh, M.; Park, M.H.; Jo, M.; Kim, H.; Nam, H.; Cho, J. The role of nanoscale-range vanadium treatment in LiNi0.8Co0.15Al0.05O2 cathode materials for Li-ion batteries at elevated temperatures. *J. Mater. Chem. A* **2015**, *3*, 13453–13460.
547. Kleiner, K.; Melke, J.; Merz, M.; Jakes, P.; Nagel, P.; Schuppler, S.; Liebau, V.; Ehrenberg, H. Unraveling the Degradation Process of LiNi0.8Co0.15Al0.05O2 Electrodes in Commercial Lithium Ion Batteries by Electronic Structure Investigations. *ACS Appl. Mater. Interfaces* **2015**, *7*, 19589–19600. [CrossRef]
548. Yoon, S.; Jung, K.N.; Yeon, S.H.; Jin, C.S.; Shin, K.H. Electrochemical properties of LiNi0.8Co0.15Al0.05O2 graphene composite as cathode materials for lithium-ion batteries. *J. Electroanal. Chem.* **2012**, *683*, 88–93.
549. Winter, M.; Besenhard, J.O.; Spahr, M.E.; Novak, P. Insertion Electrode Materials for Rechargeable Lithium Batteries. *Adv. Mater.* **1998**, *10*, 725–763. [CrossRef]
550. Liu, Q.; Li, Z.-F.; Liu, Y.; Zhang, H.; Ren, Y.; Sun, C.-J.; Lu, W.; Zhou, Y.; Stanciu, L.; Stach, E.A.; et al. Graphene-modified nanostructured vanadium pentoxide hybrids with extraordinary electrochemical performance for Li-ion batteries. *Nat. Commun.* **2015**, *6*, 6127. [CrossRef]
551. Pan, A.; Zhu, T.; Wu, H.B.; Lou, X.W. Template-Free Synthesis of Hierarchical Vanadium-Glycolate Hollow Microspheres and Their Conversion to V_2O_5 with Improved Lithium Storage Capability. *Chem. A Eur. J.* **2013**, *19*, 494–500. [CrossRef] [PubMed]
552. Zhao, H.; Yuan, A.; Liu, B.; Xing, S.; Wu, X.; Xu, J. High cyclic performance of V_2O_5@PPy composite as cathode of recharged lithium batteries. *J. Appl. Electrochem.* **2012**, *42*, 139–144. [CrossRef]
553. Wu, H.B.; Pan, A.; Hng, H.H.; Lou, X.W. Template-Assisted Formation of Rattle-type V_2O_5 Hollow Microspheres with Enhanced Lithium Storage Properties. *Adv. Funct. Mater.* **2013**, *23*, 5669–5674. [CrossRef]
554. Rui, X.; Zhu, J.; Sim, D.; Xu, C.; Zeng, Y.; Hng, H.H.; Lim, T.M.; Yan, Q. Reduced graphene oxide supported highly porous V_2O_5 spheres as a high-power cathode material for lithium ion batteries. *Nanoscale* **2011**, *3*, 4752–4758. [CrossRef] [PubMed]
555. Cheng, J.; Wang, B.; Xin, H.L.; Yang, G.; Cai, H.; Nie, F.; Huang, H. Self-assembled V_2O_5 nanosheets/reduced graphene oxide hierarchical nanocomposite as a high-performance cathode material for lithium ion batteries. *J. Mater. Chem. A* **2013**, *1*, 10814–10820. [CrossRef]
556. Yu, R.; Zhang, C.; Meng, Q.; Chen, Z.; Liu, H.; Guo, Z. Facile Synthesis of Hierarchical Networks Composed of Highly Interconnected V_2O_5 Nanosheets Assembled on Carbon Nanotubes and Their Superior Lithium Storage Properties. *ACS Appl. Mater. Interfaces* **2013**, *5*, 12394–12399. [CrossRef]
557. Li, Y.; Yao, J.; Uchaker, E.; Yang, J.; Huang, Y.; Zhang, M.; Cao, G. Leaf-Like V_2O_5 Nanosheets Fabricated by a Facile Green Approach as High Energy Cathode Material for Lithium-Ion Batteries. *Adv. Energy Mater.* **2013**, *3*, 1171–1175. [CrossRef]
558. Yang, Y.; Li, L.; Fei, H.; Peng, Z.; Ruan, G.; Tour, J.M. Graphene Nanoribbon/V_2O_5 Cathodes in Lithium-Ion Batteries. *ACS Appl. Mater. Interfaces* **2014**, *6*, 9590–9594. [CrossRef] [PubMed]
559. Ihsan, M.; Meng, Q.; Li, L.; Li, D.; Wang, H.; Seng, K.H.; Chen, Z.; Kennedy, S.J.; Guo, Z.; Liu, H.K. V_2O_5/Mesoporous Carbon Composite as a Cathode Material for Lithium-ion Batteries. *Electrochim. Acta* **2015**, *173*, 172–177. [CrossRef]
560. Nytén, A.; Abouimrane, A.; Armand, M.; Gustafsson, T.; Thomas, J.O. Electrochemical performance of Li_2FeSiO_4 as a new Li-battery cathode material. *Electrochem. Commun.* **2005**, *7*, 156–160. [CrossRef]
561. Chu, H.; Wei, L.; Cui, R.; Wang, J.; Li, Y. Carbon nanotubes combined with inorganic nanomaterials: Preparations and applications. *Coord. Chem. Rev.* **2010**, *254*, 1117–1134. [CrossRef]
562. Zhang, L.L.; Duan, S.; Yang, X.L.; Peng, G.; Liang, G.; Huang, Y.H.; Jiang, Y.; Ni, S.B.; Li, M. Reduced Graphene Oxide Modified Li_2FeSiO_4/C Composite with Enhanced Electrochemical Performance as Cathode Material for Lithium Ion Batteries. *ACS Appl. Mater. Interfaces* **2013**, *5*, 12304–12309. [CrossRef] [PubMed]
563. Li, Y.; Cheng, X.; Zhang, Y. Achieving High Capacity by Vanadium Substitution into Li_2FeSiO_4 for Li-Ion Battery. *ECS Trans.* **2012**, *41*, 87–95. [CrossRef]

564. Gao, H.; Hu, Z.; Zhang, K.; Cheng, F.; Chen, J. Intergrown Li_2FeSiO_4.$LiFePO_4$-C nanocomposites as high-capacity cathode materials for lithium-ion batteries. *Chem. Commun.* **2013**, *49*, 3040–3042. [CrossRef] [PubMed]
565. Ni, J.; Li, Y.C. Carbon Nanomaterials in Different Dimensions for Electrochemical Energy Storage. *Adv. Energy Mater.* **2016**, *6*, 1600278. [CrossRef]
566. Bruce, P.G.; Freunberger, S.A.; Hardwick, L.J.; Tarascon, J.M. Li-O_2 and Li-S batteries with high energy storage. *Nat. Mater.* **2012**, *11*, 19. [CrossRef] [PubMed]
567. Jung, H.G.; Hassoun, J.; Park, J.B.; Sun, Y.K.; Scrosati, B. An improved high-performance lithium-air battery. *Nat. Chem.* **2012**, *4*, 579–585. [CrossRef]
568. Manthiram, A.; Fu, Y.; Chung, S.H.; Zu, C.; Su, Y.S. Rechargeable Lithium-Sulfur Batteries. *Chem. Rev.* **2014**, *114*, 11751–11787. [CrossRef]
569. Peng, H.J.; Huang, J.Q.; Zhao, M.Q.; Zhang, Q.; Cheng, X.B.; Liu, X.Y.; Qian, W.Z.; Wei, F. Nanoarchitectured Graphene/CNT@Porous Carbon with Extraordinary Electrical Conductivity and Interconnected Micro/Mesopores for Lithium-Sulfur Batteries. *Adv. Funct. Mater.* **2014**, *24*, 2772–2781. [CrossRef]
570. Su, Y.-S.; Fu, Y. Manthiram, Self-weaving sulfur-carbon composite cathodes for high rate lithium-sulfur batteries. *Phys. Chem. Chem. Phys.* **2012**, *14*, 14495–14499. [CrossRef] [PubMed]
571. Shen, C.; Xie, J.; Zhang, M.; Hendrickson, M.A.; Plichta, E.J.; Zheng, J.P. Carbon Nanotube (CNT) Foams as Sulfur Hosts for High Performance Lithium Sulfur Battery. *ECS Trans.* **2017**, *77*, 457–465. [CrossRef]
572. Liu, B.; Wu, X.; Wang, S.; Tang, Z.; Yang, Q.; Hu, G.H.; Xiong, C. Flexible Carbon Nanotube Modified Separator for High-Performance Lithium-Sulfur Batteries. *Nanomaterials* **2017**, *7*, 196. [CrossRef] [PubMed]
573. Guo, J.; Xu, Y.; Wang, C. Sulfur-Impregnated Disordered Carbon Nanotubes Cathode for Lithium-Sulfur Batteries. *Nano Lett.* **2011**, *11*, 4288–4294. [CrossRef]
574. Zheng, W.; Liu, Y.W.; Hu, X.G.; Zhang, C.F. Novel nanosized adsorbing sulfur composite cathode materials for the advanced secondary lithium batteries. *Electrochim. Acta* **2006**, *51*, 1330–1335. [CrossRef]
575. Kazazi, M.; Ghadami, F.; Dadfar, M.R.; Sobhani, M.; Mohammadi, A.H. Effect of synthesis method on the morphological and electrochemical characteristics of sulfur/MWCNT composite cathode. *Solid State Ion.* **2016**, *290*, 40–46. [CrossRef]
576. Han, S.C.; Song, M.S.; Lee, H.; Kim, H.S.; Ahn, H.J.; Lee, J.Y. Effect of Multiwalled Carbon Nanotubes on Electrochemical Properties of Lithium/Sulfur Rechargeable Batteries. *J. Electrochem. Soc.* **2003**, *150*, A889–A893. [CrossRef]
577. Patel, M.D.; Cha, E.; Choi, W. A Binder Free and High Sulfur Loaded Three-Dimensional Carbon Nanotubes Electrode for High Performance Li-S Batteries. *ECS Trans.* **2017**, *77*, 437–445. [CrossRef]
578. Zhao, Y.; Zhang, X.; He, Y.; Liu, N.; Tan, T.; Liang, C. Biomass Derived Nitrogen-Doped Highly Porous Carbon Material with a Hierarchical Porous Structure for High-Performance Lithium/Sulfur Batteries. *Materials* **2017**, *10*, 1158. [CrossRef] [PubMed]
579. Bai, S.; Liu, X.; Zhu, K.; Wu, S.; Zhou, H. Metal-organic framework-based separator for lithium-sulfur batteries. *Nat. Energy* **2016**, *1*, 16094. [CrossRef]
580. Song, R.; Fang, R.; Wen, L.; Shi, Y.; Wang, S.; Li, F. A trilayer separator with dual function for high performance lithium-sulfur batteries. *J. Power Sources* **2016**, *301*, 179–186. [CrossRef]
581. Chung, S.-H.; Manthiram, A. High-Performance Li-S Batteries with an Ultra-lightweight MWCNT-Coated Separator. *J. Phys. Chem. Lett.* **2014**, *5*, 1978–1983. [CrossRef] [PubMed]
582. Xu, J.J.; Wang, Z.L.; Xu, D.; Zhang, L.L.; Zhang, X.B. Tailoring deposition and morphology of discharge products towards high-rate and long-life lithium-oxygen batteries. *Nat. Commun.* **2013**, *4*, 2438. [CrossRef]
583. Shen, C.; Liu, T.; Zhang, M.; Hendrickson, M.A.; Plichta, E.J.; Zheng, J.P. Macroporous Carbon Nanotube (CNT) Foams as Li-Air Battery Cathodes. *ECS Trans.* **2017**, *77*, 239–248. [CrossRef]
584. Nomura, A.; Ito, K.; Kubo, Y. CNT Sheet Air Electrode for the Development of Ultra-High Cell Capacity in Lithium-Air Batteries. *Sci. Rep.* **2017**, *7*, 45596. [CrossRef] [PubMed]
585. Ionescu, M.I. Direct synthesis of carbon nanotubes on metallic foams as a cathode material with high mass load for lithium-air batteries. *RSC Adv.* **2017**, *7*, 30365–30369. [CrossRef]
586. Huang, X.; Yu, H.; Tan, H.; Zhu, J.; Zhang, W.; Wang, C.; Zhang, J.; Wang, Y.; Lv, Y.; Zeng, Z.; et al. Carbon Nanotube-Encapsulated Noble Metal Nanoparticle Hybrid as a Cathode Material for Li-Oxygen Batteries. *Adv. Funct. Mater.* **2014**, *24*, 6516–6523. [CrossRef]
587. Kwak, W.J.; Lau, K.C.; Shin, C.D.; Amine, K.; Curtiss, L.A.; Sun, Y.K. A Mo_2C/Carbon Nanotube Composite Cathode for Lithium-Oxygen Batteries with High Energy Efficiency and Long Cycle Life. *ACS Nano* **2017**, *9*, 4129–4137. [CrossRef] [PubMed]
588. González, I.Z.; Valenzuela-Muñiz, A.M.; Alonso-Nuñez, G.; Farías, M.H.; Gomez, Y.V. Influence of the Synthesis Parameters in Carbon Nanotubes Doped with Nitrogen for Oxygen Electroreduction. *ECS J. Solid State Sci. Technol.* **2017**, *6*, M3135–M3139. [CrossRef]
589. Wu, Q.; Yang, L.; Wang, X.; Hu, Z. From Carbon-Based Nanotubes to Nanocages for Advanced Energy Conversion and Storage. *Acc. Chem. Res.* **2017**, *50*, 435–444. [CrossRef]

590. Mi, R.; Li, S.; Liu, X.; Liu, L.; Li, Y.; Mei, J.; Chen, Y.; Liu, H.; Wang, H.; Yan, H.; et al. Electrochemical performance of binder-free carbon nanotubes with different nitrogen amounts grown on the nickel foam as cathodes in Li-O_2 batteries. *J. Mater. Chem. A* **2014**, *2*, 18746–18753. [CrossRef]
591. Wu, X.; Layla, M.B.; Edwin, T.; Priyanka, B.; Meng, G.; Wendy, B.; Zimin, N.; Chongmin, W.; Ji-Guang, Z. Formation of Interfacial Layer and Long-Term Cyclability of Li-O_2 Batteries. *ACS Appl. Mater. Interfaces* **2012**, *6*, 14141–14151.
592. Lim, H.D.; Park, K.Y.; Song, H.; Jang, E.Y.; Gwon, H.; Kim, J.; Kim, Y.H.; Lima, M.D.; Robles, R.O.; Lepró, X.; et al. Enhanced Power and Rechargeability of a Li−O_2 Battery Based on a Hierarchical-Fibril CNT Electrode. *Adv. Mater.* **2013**, *25*, 1348–1352. [CrossRef] [PubMed]
593. Chen, Y.; Li, F.; Tang, D.M.; Jian, Z.; Liu, C.; Golberg, D.; Yamada, A.; Zhou, H. Multi-walled carbon nanotube papers as binder-free cathodes for large capacity and reversible non-aqueous Li–O_2 batteries. *J. Mater. Chem. A* **2013**, *1*, 13076–13081. [CrossRef]
594. Mitchell, R.R.; Gallant, B.M.; Shao-Horn, Y.; Thompson, C.V. Mechanisms of Morphological Evolution of Li_2O_2 Particles during Electrochemical Growth. *J. Phys. Chem. Lett.* **2013**, *4*, 1060–1064. [CrossRef] [PubMed]
595. Zhang, Y.; Wang, L.; Guo, Z.; Xu, Y.; Wang, Y.; Peng, H. High-Performance Lithium–Air Battery with a Coaxial-Fiber Architecture. *Angew. Chem. Int. Ed.* **2016**, *55*, 4487–4491. [CrossRef] [PubMed]
596. He, P.; Zhang, T.; Jiang, J.; Zhou, H. Lithium-Air Batteries with Hybrid Electrolytes. *J. Phys. Chem. Lett.* **2016**, *7*, 1267–1280. [CrossRef] [PubMed]
597. Le, H.T.T.; Ngo, D.T.; Park, C.-J. High Performance All-Solid State Lithium-Air Batteries Employing Aluminum-Substituted Lithium Lanthanum Titanate Solid Electrolyte. *Meet. Abstr.* **2017**, *MA2017-01*, 435. [CrossRef]
598. Sun, J.; Zhao, N.; Li, Y.; Guo, X.; Feng, X.; Liu, X.; Liu, Z.; Cui, G.; Zheng, H.; Gu, L.; et al. A Rechargeable Li-Air Fuel Cell Battery Based on Garnet Solid Electrolytes. *Sci. Rep.* **2017**, *7*, 41217. [CrossRef] [PubMed]
599. Yi, J.; Guo, S.; He, P.; Zhou, H. Status and prospects of polymer electrolytes for solid-state Li-O_2 (air) batteries. *Energy Environ. Sci.* **2016**, *10*, 860–884. [CrossRef]
600. Zhao, Y.; Kamiya, K.; Hashimoto, K.; Nakanishi, S. Efficient Bifunctional Fe/C/N Electrocatalysts for Oxygen Reduction and Evolution Reaction. *J. Phys. Chem. C* **2015**, *119*, 2583–2588. [CrossRef]
601. Chen, P.; Zhou, T.; Xing, L.; Xu, K.; Tong, Y.; Xie, H.; Zhang, L.; Yan, W.; Chu, W.; Wu, C.; et al. Atomically Dispersed Iron–Nitrogen Species as Electrocatalysts for Bifunctional Oxygen Evolution and Reduction Reactions. *Angew. Chem.* **2017**, *56*, 625–629. [CrossRef]
602. Ji, D.; Peng, S.; Safanama, D.; Yu, H.; Li, L.; Yang, G.; Qin, X.; Srinivasan, M.; Adams, S.; Ramakrishna, S. Design of 3-Dimensional Hierarchical Architectures of Carbon and Highly Active Transition Metals (Fe, Co, Ni) as Bifunctional Oxygen Catalysts for Hybrid Lithium–Air Batteries. *Chem. Mater.* **2017**, *29*, 1665–1675. [CrossRef]

Disclaimer/Publisher's Note: The statements, opinions and data contained in all publications are solely those of the individual author(s) and contributor(s) and not of MDPI and/or the editor(s). MDPI and/or the editor(s) disclaim responsibility for any injury to people or property resulting from any ideas, methods, instructions or products referred to in the content.